Max-Planck-Institut
für Meteorologie

REPORT No. 236

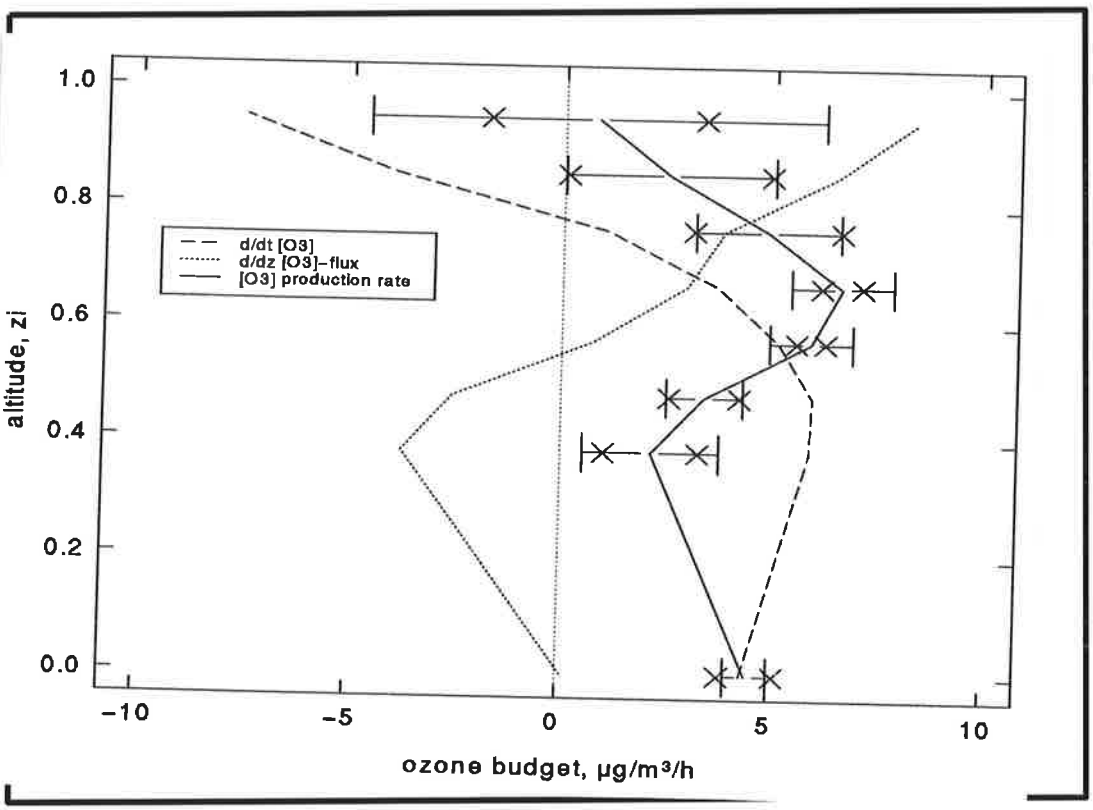

REMOTE SENSING OF THE TROPOSPHERE USING DIFFERENTIAL ABSORPTION LIDAR

by

Jens Bösenberg

HAMBURG, April 1997

AUTHOR:

Jens Bösenberg

Max-Planck-Institut
für Meteorologie

Titel-Figure:

Ozone budget in the boundary layer on June 30, 1993, 11:34-13:14 UT. The temporal rate of change, the vertical flux divergence of the ozone concentration, and the calculated ozone production rate are shown. For the latter error estimates are included, both for the instrumental errors (x) and for the sampling errors (⊣).

MAX-PLANCK-INSTITUT
FÜR METEOROLOGIE
BUNDESSTRASSE 55
D - 20146 HAMBURG
GERMANY

Tel.: +49-(0)40-4 11 73-0
Telefax: +49-(0)40-4 11 73-298
E-Mail: <name> @ dkrz.de

Remote Sensing of the Troposphere Using Differential Absorption Lidar

Jens Bösenberg
Max-Planck-Institut für Meteorologie
Hamburg, Germany

ISSN 0937–1060

Contents

Abstract

The methodology of laser remote sensing of the atmosphere using the **Di**fferential **A**bsorption **L**idar (DIAL) technique is reviewed in detail. A full treatment including the details of the spectral distribution before and after scattering is presented, and approximations for the application of the technique to water vapor, temperature, and ozone measurements are derived. The general methodology is used in conjunction with experimental data sets to identify possible sources of error and to provide quantitative estimates of the accuracy which can be achieved in the measurements.

Experimental data are presented for profiles of water vapor, temperature, and ozone in order to demonstrate the capability of providing accurate measurements of the space-time distribution of important atmospheric constituents, for both detailed process studies and routine observations. As a special application measurements of vertical flux profiles of water vapor and ozone in the boundary layer are presented, introducing the use of high resolution remote sensing data for eddy correlation measurements of the turbulent transport. Advantages and limits of this method are discussed.

A. Introduction

Progress in the understanding of atmospheric processes often requires experimental data describing the important features. While measurements at ground level can usually be performed with the required accuracy, resolution, and area coverage, the determination of the vertical distribution of many important parameters is still difficult. For in-situ measurements the applications are strongly limited by the available platforms: free flying balloons typically cannot be launched as frequent as necessary, and only rather cheap and small instruments can be deployed because they will generally get lost; tethered balloons mostly can be launched only under light-wind conditions, and in most regions are not permitted at all because of air traffic regulations; the use of aircraft is rather restricted because of their relatively high costs, in addition they do not allow direct acquisition of truly vertical profiles.Therefore the use of remote sensing techniques has become increasingly important for the acquisition of data necessary for detailed atmospheric process studies. In particular active remote sensing systems, using the backscatter from waves which are transmitted by the system itself, offer the high spatial and temporal resolution which is necessary to study many tropospheric processes. For determination of trace gas concentrations the method of Differential Absorption and Scattering Lidar, usually called DIAL (Differential Absorption Lidar) has been developed, which can be used in many applications.

In this paper three particular applications of this method shall be discussed in detail: measurements of the vertical distribution of water vapor, temperature, and ozone. All these applications are important topics in atmospheric research, at least in principle the same methodology is used, but with marked differences in the details, and they serve well as examples to demonstrate the broad range of applications of the DIAL technique.

Water vapor Investigation of the water cycle in the atmosphere is one of the primary goals of atmospheric and climate research, as stated in the „World Climate Research Programme“ (WCRP) of the World Meteorological Organization (WMO). These studies are organized world wide in the „Global Energy and Water Cycle Experiment“ (GEWEX) [WCRP-5, 1988]. The main reasons for the importance of the atmospheric water cycle are:

- Water is present in the atmosphere in all three phases: gaseous, liquid, and solid. It's phase transitions are associated with rather large energy transfers.

- Water has a major impact on the radiation budget in all three phases, but the spectral properties differ widely between the phases.

- Water vapor is the most important greenhouse gas, and it shows the largest variability both temporally and spatially of all important greenhouse gases.

- Water plays an important role in the feedback mechanisms of the climate system.

- The direct effect of atmospheric water vapor is mainly related to changes in the vertical distribution of radiation, and to the major contribution of latent heat to the overall transport of energy.

- Indirectly water vapor has a major impact on the radiation field by determining the distribution of clouds. Clouds have a large influence on the radiation field, which is quite complex because of the strong interaction between dynamic, thermodynamic and radiative processes associated with them.

- The local heating due to the condensation of water vapor and the heat transport associated with latent heat lead to a dual role of water in the atmosphere. It can enhance the energetics of individual weather systems (e.g. hurricanes), while allowing the large-scale motions to transport heat more effectively with smaller density anomalies than would be possible in a dry atmosphere.

In spite of it's long recognized importance the individual components of the water cycle are still not very well known. In the concept for GEWEX [WCRP-5, 1988] this is summarized as follows: *„Present uncertainties in the geographical and temporal distributions of the components of the water cycle are still shockingly large. Typical discrepancies between published budgets are a factor of 2 or more for net precipitation minus evaporation over whole continents"*.

Obviously, there is a desperate need for improved determination of both evaporation and precipitation rates, which are representative for extended areas. The remaining components of the water cycle are not sufficiently well known either. Particularly for measuring the vertical distribution suitable instruments are lacking, which achieve simultaneously high accuracy, high resolution, and continuous operation. Improved knowledge of the water vapor distribution is essential for an improved understanding of the water cycle. Especially, the GEWEX observing system development programme includes the suggestion of determining the global water vapor distribution using a space-borne Differential Absorption Lidar (DIAL). This method has been regarded as most promising for making significant contributions to determining the vertical distribution of water vapor, including ground-based, airborne, and space-borne applications [Schotland, 1966; Remsberg and Gordley, 1978].

It is quite clear that a complex remote sensing technique like water vapor DIAL has to be fully understood in all details of it's methodology before it can be used in extended applications, in particular space-borne applications. The fundamentals of the methodology have been summarized by Schotland (1974), and Measures (1984). Important aspects of the influence of the spectral distribution have been published by Mégie (1980), Cahen and Mégie (1981), Zuev at al. (1983a), Ansmann (1985), Bösenberg (1985), Ansmann and Bösenberg (1987). In this paper a comprehensive and detailed analysis of the DIAL-method including all details of the spectral distribution of the transmitted and the received light shall be presented. Considering the Doppler-broadening of the

molecular backscatter appears to be very important, because this effect can seriously limit the attainable accuracy. The possible errors due to this effect in cases of spatially inhomogeneous aerosol distribution will be studied extensively, and their magnitude will be estimated on the basis of extended experimental data sets.

The DIAL technique was first proposed for water vapor measurements [Schotland, 1966] and has since then been used for measurements of numerous trace gases [Measures, 1984]. Many water vapor measurements have been reported using the near infrared spectral region (690 - 730 nm) [Browell et al., 1979; Werner and Herrmann, 1981; Cahen et al., 1982; Browell, 1983; Zuev et al., 1983b; Browell et al., 1984; Ansmann, 1984; Bösenberg, 1987; Bösenberg, 1991; Senff, 1993; Ehret et al., 1993; Senff et al., 1994; Wulfmeyer, 1995]. In addition several systems have been developed and tested using CO_2-lasers at 10 μm, using both direct [Murray, 1978; Rothe, 1980; Baker, 1983] and heterodyne detection [Hardesty, 1984; Fukuda et al., 1984; Grant et al., 1987]. In spite of the great importance of water vapor measurements and of the large effort spent for the development of systems none of them has so far been used continuously in extended field measurements. This clearly indicates that in spite of the efforts (and in spite of some claims) the necessary accuracy had not been reached, at least not for routine operation. The main reason for this is the fact, that the water vapor absorption lines which can be used for such measurements are very narrow, so that all measurements performed with these lines fall within the scope of high resolution spectroscopy. Applications in atmospheric research are very demanding with respect to the required laser system properties as well as to accounting for atmospheric effects in the evaluation process. The laser system requirements have so far been a major obstacle for all water vapor DIAL measurements, only recently such systems have been developed which have demonstrated the required performance characteristics [Bruneau et al., 1994; Ponsardin et al., 1994; Wulfmeyer et al., 1995).

In this report it will be demonstrated by both theoretical studies and test measurements, that the DIAL technique is capable of providing very accurate measurements of the vertical distribution of water vapor throughout the troposphere. It will also be demonstrated, that such measurements are very well suited for studying vertical transport processes. Routine application appears feasible, and technical improvements are suggested which simplify the evaluation procedure.

Temperature The importance of measurements of the vertical atmospheric temperature distribution is obvious, they are absolutely necessary for all kinds of atmospheric process studies. Numerous methods have been suggested and explored, use of the DIAL technique can only be of advantage if good accuracy and high resolution in space and time can be reached. Suitable absorption lines for the application of the DIAL technique in this context are rotational-vibrational transitions of oxygen, which are even narrower than the water vapor lines. In addition, the required accuracy of the determination of the absorption coefficient is very high. Hence the details of the spectral distribution before and after the scattering process are even more important than for water vapor profiling. The requirements for attaining this accuracy will be studied in detail in this work.

Ozone Tropospheric ozone levels have been recognized to present a major environmental problem. High ozone concentrations during so-called summer smog episodes have already led to legislative actions attempting to limit the peak concentrations. Tropospheric ozone formation is part of a highly complex system of processes, where many trace substances, solar radiation, and meteorological transport processes are involved. This complex system of processes was studied in detail in the frame of the European cooperative research project EUROTRAC, and, with in this frame, particularly in the sub-projects „Tropospheric Ozone Research (TOR)" and „Tropospheric Environmental Studies by Laser Sounding (TESLAS)".

TOR was dealing mainly with the complex chemical processes which are important for the formation and destruction of ozone. To a large extent this was performed using a network of surface stations measuring a number of key species. The main objectives of TOR were to find out:

- How much ozone is exchanged within the troposphere?
- How much ozone is produced in the troposphere?
- How much of the ozone production is caused by anthropogenic precursor gases?
- How much ozone is destroyed by photochemical reactions in the troposphere, and how much by deposition at the surface?

The treatment of these problems is made particularly difficult by the facts, that the sources of precursors are inhomogeneously distributed, many substances having widely varying lifetimes are involved, and different mechanisms of destruction exist. The surface, where most of the measurements are performed, acts as the strongest sink in the system. Due to the long lifetimes of at least some of the substances, long range transport can cause major redistributions. Given that in all transport mechanisms the vertical component is important, it appears to be very important to measure the vertical distribution of at least the key substance, namely ozone.

At the present it is not possible to predict the tropospheric ozone distribution with sufficient accuracy using coupled chemistry-transport-models, see e.g. Langmann (1995). It could be shown by comparison of a series of measured ozone profiles with model results, that at least one reason for this is the inadequate treatment of vertical exchange processes in the model (Grabbe, 1995).

Methods for the experimental investigation of turbulent exchange processes in the lower troposphere have been developed in the frame of the EUROTRAC sub-project TESLAS, which was focused at the development of the DIAL technique for measuring vertical profiles of zone within the troposphere. Main topics were the studies of the accuracy, which can be reached under a broad range of meteorological conditions, and the optimization of the measurement systems with respect to reliability and ease of operation in routine applications. Important contributions to these goals are summarized in the present work. It will be shown, that the DIAL technique yields excellent accuracy as well as high spatial and temporal resolution. The latter is particularly important for studies of turbulent exchange processes. The importance of these processes for the resulting ozone distribution during summer smog episodes has been demonstrated (Senff et al., 1996).

In the previous paragraphs it has been shown that laser remote sensing using the differential absorption technique can contribute substantially to experimental studies of atmospheric processes. In this work a comprehensive treatment of the DIAL methodology is attempted. This will be amended by a number of selected examples of actual applications, demonstrating both the potential and the limits of this method. The results will also be compared to those obtained with other methods.

B. Basic Methodology of Laser Remote Sensing (Lidar and DIAL)

All lidar techniques which will be treated here have in common that light is analyzed which is backscattered in the atmosphere from a short light pulse transmitted from the lidar system. Scattering processes are thus key elements of these methods. A full treatment of all details of the relevant scattering processes is clearly beyond the scope of this paper, the reader is referred to the literature (e.g. van de Hulst, 1981; Bohren and Huffman, 1983). However, the most important facts shall be presented which will be used subsequently for the detailed treatment of the lidar methodology.

B.1. Scattering Processes

In the wavelength range of about 0.25 - 10 μm, which is generally used for lidar measurements, the following scattering processes are important:

1. Elastic scattering by molecules (Rayleigh scattering).
2. Elastic scattering by aerosol particles (Mie scattering).
3. Inelastic scattering by molecules (Raman and Brillouin scattering).
4. Fluorescence.

In this work only those scattering properties will be used which describe the intensity of the scattered light. Hence phase and polarization need not be considered in the following.

The scattering of a plane wave at a single particle is described as follows:
At large distance from the scattering particles the scattered radiation which propagates in a direction defined by the scattering angles Θ and Φ can be treated to good approximation as a spherical wave. The intensity of the scattered light at distances R is then given by

$$I(\Theta,\Phi,R) = I_0 \cdot p(\Theta,\Phi) \cdot C_{sca} \cdot \frac{1}{R^2} \quad . \tag{B.1}$$

Here Θ is the angle between $\vec{k}_0$ and $\vec{k}_s$ in the scattering plane, which is defined by the wave vectors of the incident and scattered waves, $\vec{k}_0$ and $\vec{k}_s$, respectively. Φ is the azimuthal angle in the plane perpendicular to $\vec{k}_0$. $p(\Theta,\Phi)$ is called phase function, and it describes the angular distribution of the scattered intensity. The azimuthal angle Φ is important only if the scattering particle does not have spherical symmetry. C_{sca} is called the scattering cross section, and is equal to the area which receives as much energy from the incident radiation as is scattered, integrated over all directions, by the particle. This is in analogy to the usual definition of the absorption cross section C_{abs}, and with these the extinction cross section C_{ext} is defined as

$$C_{ext} = C_{sca} + C_{abs}$$

Thus the extinction describes all that radiation which is removed from the incident beam.

For the present work the scattering by an ensemble of many particles is of particular importance. If the scattering at the individual particles is independent, the total scattered intensity is given simply by the sum of the scattered intensities from the individual particles. Introducing the density of the particles N (number of particles per unit volume), the extinction-, scattering-, and absorption-coefficients can be defined, respectively, as:

$$\begin{aligned} \alpha &= N \cdot C_{ext} \\ \alpha_{sca} &= N \cdot C_{sca} \\ \alpha_{abs} &= N \cdot C_{abs} \end{aligned} \tag{B.2}$$

This definition is for a single type of scatterers, e.g. the molecules of a homogeneous gas. For an aerosol the scattering properties depend on the radius of the particles only (for given chemical composition and wavelength of incident radiation), and the aerosol contains many particles with different radii a. Given the size distribution N(a), e.g. eq. (B.2) can be written as

$$\alpha = \int_{a_{min}}^{a_{max}} N(a) \cdot C_{ext}(a) da \tag{B.3}$$

In the context of this work scattering at the individual particles can be considered independent. As a rule of thumb, this is possible if the distance between the scatterers is larger than three times the radius of the particles (van de Hulst, 1981). This holds for all atmospheric conditions where lidar measurements can be performed. However, when coherent detection of the scattered radiation is used, e.g. in Doppler lidar applications, it has to be considered that the phases of the waves scattered at different particles have a fixed relation, which leads to interference effects (speckle). This requires an extremely narrow-band laser emission, and detection in a way that the diffuse scattering at a distributed target can be considered at least partially coherent. The size of the area for which this is true is given by the van Cittert-Zernike theorem (see e.g. Born and Wolf, 1993). For most lidar systems both the laser bandwidth and the detector area are too large to observe coherent signals. Only in specially designed systems, e.g. Doppler lidars, the partial coherence of the backscatter from a distributed target can be detected. These systems shall not be treated in detail in the frame of this work.

An important quantity in lidar applications is the backscatter coefficient β, because almost all lidar systems collect light which propagates in the backward direction with respect to the transmitted beam. The backscatter coefficient is defined as the product of the total scattering coefficient and the phase functions for $\Theta = \pi$,

$$\beta = p(\pi) \cdot \alpha_{sca} \tag{B.4}$$

Further the so-called lidar ratio is introduced as

$$S_L = \frac{\alpha}{\beta} \tag{B.5}$$

where α is the extinction coefficient.

B.1.1. Elastic scattering by molecules

The scattering of electromagnetic waves by molecules is usually described by a theory first developed by Lord Rayleigh (Strutt, 1871). The classical treatment of the problem assumes, that a dipole moment is induced in the molecules by the incident wave, which in turn is the source of a radiative field. Hence, the total scattered radiation is calculated as the sum of dipole radiation fields from statistically distributed molecules.

The quantities which are required for simple lidar applications are described briefly in the following. This presentation is mainly a summary of those given by Bohren and Huffman (1983), Long (1977), Wandinger (1994). For a gas with particle density N the backscatter and extinction coefficients are given by

$$\beta_m = k^4 \cdot N \frac{45a_m^2 + 7\gamma_m^2}{45} \tag{B.6}$$

$$\alpha_m = \frac{8\pi}{3} k^4 \cdot N \frac{45a_m^2 + 7\gamma_m^2}{45} \cdot K_\delta \tag{B.7}$$

respectively. Here the polarizability a_m^2 and the anisotropy γ_m^2 are molecular constants of the gas. K_δ takes into account the depolarization of the scattered radiation for anisotropic molecules, we have

$$K_\delta = \frac{45a_m^2 + 10\gamma_m^2}{45a_m^2 + 7\gamma_m^2} \tag{B.8}$$

Hence the lidar ratio for Rayleigh scattering is

$$S_{L,m} = \frac{8\pi}{3} \frac{45a_m^2 + 10\gamma_m^2}{45a_m^2 + 7\gamma_m^2} \tag{B.9}$$

For nitrogen and oxygen and hence for air the anisotropy is small, approximately we have

$$\frac{45a_m^2 + 10\gamma_m^2}{45a_m^2 + 7\gamma_m^2} \approx 1 + \frac{\gamma_m^2}{15a_m^2} \tag{B.10}$$

and hence

$$S_{L,m} \approx \frac{8\pi}{3}\left(1 + \frac{\gamma_m^2}{15a_m^2}\right) \tag{B.11}$$

A compilation of scattering matrices for the complete calculation of all scattered components for arbitrary state of polarization was given by Wandinger (1994).

Although the Rayleigh scattering process is elastic, the backscattered radiation differs in frequency from the incident radiation due to the Doppler-shift caused by the thermal motion of the molecules (velocity v_{th})

$$\frac{\Delta\nu}{\nu_0} = \frac{2v_{th}}{c} \tag{B.12}$$

For monochromatic incident radiation at wavenumber ν_0 the Rayleigh-backscatter has the spectral distribution described by

$$g_R(\nu) = \frac{1}{b_R\sqrt{2\pi}} e^{-(\nu - \nu_0)^2/2b_R^2} \tag{B.13}$$

with the halfwidth (HWHM) given by

$$b_R = \frac{2\nu_0}{c}\left(\frac{2k_B T \ln 2}{M_L}\right)^{1/2} \tag{B.14}$$

where k_B is Boltzmann's constant, T absolute temperature, and M_L the averaged molecular mass for air.

This distribution is slightly modified by the existence of Brillouin-scattering, i.e. scattering from longitudinal density waves. Brillouin-scattering causes two additional maxima in the spectrum of the backscattered light at $\nu_0 \pm \frac{2v_s}{c}$, where v_s is the velocity of sound in the scattering medium. A complete theory of Brillouin-scattering in air has not yet been presented, the model of Yip and Nelkin (1964) is regarded as rather good approximation. Since Brillouin-scattering causes only a minor modification of the Doppler-spectrum under standard atmospheric conditions, this can be

accounted for to sufficiently good approximation by just increasing the width of the Doppler-spectrum, $b_R^* = b_R \cdot c_B$. For the US standard atmosphere we have $c_B \approx 1.2$ at sea level, and $c_B \approx 1.1$ at 10 km height. Hence, the correction factors are rather small.

B.1.2. Scattering by aerosol particles

Scattering of electromagnetic waves by particles having dimensions on the order of the wavelength of the radiation has first been dealt with comprehensively by Mie (1908). This treatment was restricted to spherical particles with complex index of refraction n*. Later this theory has been extended, solutions in closed form are possible for scattering by ellipsoids with rotational symmetry. For more complex shapes closed form solutions do not exist. So not all of actually existing atmospheric aerosols can be described by this theory, e.g. crystalline particles like ice and mineral dust. But for most of the atmospheric aerosols the Mie theory for spherical particles provides for a sufficiently good approximation, therefore aerosol scattering is often called Mie-scattering.

For the calculation of the phase function $p(\Theta, \Phi)$ and the scattering, absorption, and extinction coefficients using the Mie theory it is necessary to provide the parameters $\frac{2\pi a}{\lambda}$, where a is the particle radius, the complex index of refraction n*, and the particle size distribution N(a). Because the general solution shows a pronounced oscillatory behaviour, the calculation even for a single particle is rather time consuming. For this reason a number of approximations have been developed for certain ranges of the parameters. The details of these calculations shall not be presented here, they are described in the standard literature, e.g. van de Hulst (1981).

The treatment of particles having a more complex shape than rotational ellipsoids is much more difficult, since no closed form solutions are possible. For particles much larger than the wavelength methods of geometrical optics can be applied, i.e. single rays are traced and the intensity distribution of externally and internally reflected as well as for the internally reflected rays is calculated. This method is called ray-tracing-technique. By adding the intensity of the scattered field, at least for sufficiently simple crystal forms like hexagonal ice crystals a rather good approximative solution for the scattering properties including polarization can be calculated (Wendling et al., 1979; Takano and Liou, 1989): Such calculations have now been extended to the treatment of more complex shapes (Macke, 1993; Takano and Liou, 1995).

For actual calculations using the ray-tracing-technique the exact particle shape, it's orientation with respect to the incident radiation, and it's complex index of refraction have to be provided. Since this is not really feasible for most of atmospheric aerosols, all solutions will be approximate only.

For the application of the DIAL technique most of the details of the scattering process are not really important, since scattering is quite similar at the two wavelengths used. If the frequency of

the incident wave remains unchanged, the results of DIAL measurements will not depend on the details of the scattering processes, at least to first approximation.

B.1.3. Raman-scattering

Regarding inelastic scattering processes only Raman-scattering shall be treated briefly here. Molecular scattering processes where the initial and final states of rotation or vibration are different are called rotational and vibrational Raman-scattering, respectively. If the energy of the final state is lower than that of the initial state, the rotational or vibrational energy is transferred to the scattered radiation. This case is called Anti-Stokes-scattering. If the energy of the final state is larger than that of the initial state, the extra energy is extracted from the incident radiation. This process is called Stokes-scattering. Between the wavenumbers ν_s of the Raman-transition we have the relation

$$\nu_s = \nu_0 \pm \nu_R \tag{B.15}$$

The plus sign designates Anti-Stokes-scattering, the minus sign designates Stokes-scattering. For the Raman-transition we have the selection rules

$$\Delta J = 0,\pm 2 \qquad \Delta v = 0,\pm 1 \tag{B.16}$$

where J is the rotational and v the vibrational quantum number.

The calculation of scattering cross sections for Raman-scattering is formally the same as for Rayleigh-scattering. Molecular constants a_m and γ_m are replaced by corresponding constants a_R and γ_R, which describe the change in polarizability associated with the Raman-transition. The wave vector $k = 2\,\pi\nu$ is replaced by $k_R = 2\,\pi\,(\nu_0 \pm \nu_R)$, and an additional factor $h/8\,\pi^2\,c\,\nu_R$ is introduced. Hence we have

$$\beta_R = \frac{h}{8\pi^2 c \nu_R} k_R^4 \cdot N \cdot \frac{45a_R^2 + 7\gamma_R^2}{45} \tag{B.17}$$

$$\alpha_R = \frac{h}{8\pi^2 c \nu_R} \frac{8\pi}{3} k_R^4 \cdot N \cdot \frac{45a_R^2 + 7\gamma_R^2}{45} \tag{B.18}$$

Due to the much larger anisotropy for Raman-scattering as compared to Rayleigh-scattering the depolarization is generally much larger. Therefore the exact formulae should be used (Wandinger, 1994).

The shift in wavenumber due to vibrational Raman-scattering amounts to $\nu_R = 2331$ cm^{-1} in nitrogen, $\nu_R = 1556$ cm^{-1} in oxygen, and $\nu_R = 3652$ cm^{-1} in water vapor. Obviously, these components of Raman-scattering in air, which are those which can actually be detected, are clearly separated in the spectrum and hence can easily be isolated. Because of the much smaller intensity of Raman-scattering as compared to the elastic scattering (about three orders of magnitude), the latter has to be suppressed very well when precise measurements of the Raman-scattered intensities are attempted.

Rotational Raman-scattering is caused by a change in polarizability due to a change of the rotational state of a molecule. The selection rule for the transition is $\Delta J = 0, \pm 2$, the resulting spectrum consists of a series of equidistant lines to each side of the unshifted line, with the distance given by $\Delta\nu = 4B\,(J + 3/2)$, with B a constant specific for each molecule. For N_2 we have $B = 2.01$ cm^{-1}, for O_2 we have $B = 1.45$ cm^{-1} (Herzberg, 1950). The intensity, in analogy to vibrational Raman-scattering, is a function of the polarizability and the anisotropy, for the exact formulae the reader is referred to Long (1977).

B.1.4. Other scattering processes

Another important atmospheric scattering process is fluorescence. This process can be viewed as an absorption of light by a molecule, followed by a mostly radiation less internal transition, and finally re-radiation at a different frequency. The lifetime for the intermediate state can be quite long, therefore, the condition of instantaneous scattering is often not true. This fact has to be considered when calculating the scattered intensity as a function of time. Fluorescence is used in some special lidar applications, e.g. for temperature measurements in the mesosphere, measurements of OH-concentration, or measurements of oil spills on the sea surface. These applications will not be treated in this paper. For the applications actually dealt with fluorescence is not important, since it is generally small in the spectral regions under consideration, and because re-emission occurs at substantially different wavelengths than the excitation. Hence it can be easily suppressed in the receiver optics.

B.2. Absorption by gas molecules

For all lidar techniques described in this paper it is assumed, that gaseous absorption is governed by an exponential law

$$P(R) = P(R_0) \cdot \exp\left(-\int_{R_0}^{R} \alpha_g(r) \cdot \; dr\right) \tag{B.19}$$

where α_g is the absorption coefficient of the gas. P(R) is the intensity of light at range R, R_0 is an arbitrary starting range. The absorption coefficient is the product of the number density ρ_n and the absorption cross section σ

$$\alpha_g = \rho_n \cdot \sigma . \tag{B.20}$$

Equation (B.19) holds if the intensity of light is sufficiently small so that the transition is not saturated. In the lower atmosphere this condition is true up to very large intensities because of the fast relaxation due to collisions.

B.2.1. Isolated absorption lines

The pressure and temperature dependence of isolated absorption lines of the rotational-vibrational spectrum results from the corresponding dependence of the three governing factors number density, absorption line strength, and absorption line form:

$$\alpha_g(\nu) = \rho_n(p,T) \cdot S(p,T) \cdot \Lambda(\nu,p,T) \quad . \tag{B.21}$$

For the number density we have the perfect gas law

$$\rho_n(p,T) = \frac{p}{k_B \cdot T} \quad . \tag{B.22}$$

The absorption line strength is to good approximation given by:

$$S = S_0\left(\frac{T}{T_0}\right)^{l} \exp\left[-\frac{\varepsilon}{k_B}\left(\frac{1}{T} - \frac{1}{T_0}\right)\right] \tag{B.23}$$

where S_0 is the line strength for standard conditions, ε the initial state energy of the transition under consideration, and k_B is Boltzmann's constant. The exponent l is l = 1 for diatomic molecules, for water vapor it is l = 1.5. For other species the value of this constant can be found in

spectroscopic data bases.

The absorption line form results from Doppler-broadening due to the thermal motion of the absorbing molecules and from collision broadening. For most applications the resulting line form is well approximated by the Voigt function

$$\Lambda_V = f_V \cdot \Re w(\xi_V + i a_V) \tag{B.24}$$

where

$$f_V = b_d^{-1} \cdot \sqrt{\ln 2/\pi}, \tag{B.25}$$

$$a_V = b_c \cdot b_d^{-1} \cdot \sqrt{\ln 2}, \tag{B.26}$$

$$\xi_V = (\nu - \nu_0) \cdot b_d^{-1} \cdot \sqrt{\ln 2}\,. \tag{B.27}$$

Here $\Re w$ denotes the real part of the complex error function. The halfwidths b_d of Doppler-broadening and b_c of collision broadening are given by:

$$b_d = \nu_0 \cdot \sqrt{2 \cdot k_B \cdot T \cdot \ln 2/(M \cdot c^2)} \tag{B.28}$$

$$b_c = b_c^0 \cdot \frac{p}{p_0} \cdot \left(\frac{T_0}{T}\right)^m. \tag{B.29}$$

Here M is the mass of the absorbing molecule, c the velocity of light, and b_c^0 the halfwidth of collision broadening at standard conditions. By a simplified theory the exponent m is calculated as m = 0.5 for linear molecules, but in practice it is different for different transitions and should be taken from spectroscopic measurements. With respect to the water vapor and oxygen lines used in this paper the reader is referred to Grossmann and Browell (1989) and to Ritter (1986) and Ritter and Wilkerson (1987), respectively.

In addition to broadening by collisions a small shift of the line center occurs in dependence of pressure (Eng et al., 1973; Eng et al., 1974; Bösenberg, 1985; Grossmann and Browell, 1989). The constants needed for calculating this shift are also given in the literature cited above.

The Voigt line shape is the convolution of a Lorentz line shape representing the collision broaden-

ing and a Gaussian line shape representing the Doppler broadening. In details, and in special cases, deviations from this line shape have been detected. These are due to the details of the interaction between molecules during their collisions, refined models to account for this have been presented by e.g. Rautian, Galatry, Sobelman and Berman. The differences of the resulting line forms from the Voigt line shape is less than about 10^{-2}, so only in special cases this will have to be considered. One such example is the measurement of temperature using the temperature dependence of certain oxygen absorption lines, where the neglection of the actual line shape ca lead to an error of about 1K (Theopold, 1990).

B.2.2. Broad absorption bands

Broad absorption bands like the Hartley-Huggins absorption band of ozone in the UV are generated by overlapping of a large number of individual lines. For the temperature dependence of the absorption coefficient there is no simple formula, for actual applications, the results of spectroscopic measurements should be used (Molina and Molina, 1986; Malicet et al., 1995). In many spectral regions the change with temperature is rather small, due to the blending of lines having different temperature dependence. The pressure dependence of the absorption coefficient in such bands is always small, since it is a average over several lines, and the total line strength is not pressure dependent.

B.3. The lidar equation

B.3.1. The general lidar equation

The lidar equation describes the power received from a scattering volume of distance R as a function of system constants and atmospheric parameters. Mostly it is given in the following form (Collis and Russell, 1976):

$$P(\nu,R) = P_L \frac{c\tau_L}{2} \frac{A}{R^2} \eta(\nu,R) \cdot \beta(\nu,R) \cdot e^{-2\int_0^R \alpha(\nu,r)dr} \tag{B.30}$$

where we have

$P(\nu, R)$	the power of the signal received from distance R
ν	the wavenumber of the transmitted light
R	the distance from transmitter/receiver to the scattering volume
P_L	the transmitted power
c	the velocity of light
τ_L	the transmitted pulse duration
A	the active area of the receiving telescope
$\eta(\nu, R)$	the total system efficiency
$\beta(\nu, R)$	the total backscatter coefficient at distance R
$\alpha(\nu, R)$	the total atmospheric extinction coefficient, including molecular absorption, Mie- and Rayleigh-scattering.

Equation (B.30) is valid only under a number of conditions:

1. the scattering is incoherent
2. only single scattering contributes significantly to the received signal
3. the time constant of the scattering process is small compared to the laser pulse length
4. the laser radiation is monochromatic
5. the wavelength remains unchanged under the scattering process.

While conditions 1 to 3 are generally no serious restrictions for atmospheric studies, the conditions 4 and 5 are not always easy to meet. An extension of Eq. (B.30) is therefore absolutely necessary, this will be treated in the following. But before that will be done, some remarks regarding conditions 1 to 3.

Incoherent scattering For typical lidar applications this condition is practically always met, unless a special system design assures at least partially coherent detection. As already mentioned in section B.1, coherent lidar techniques shall not be treated here.

Single scattering It is not always easy to find good reasons to neglect multiple scattering in lidar applications, since a closed form solution for this problem which is generally applicable has not yet been presented. Speaking qualitatively, it can be stated that contribution of multiple scattering to the received signal increases with the density of the scattering medium, with increasing beam divergence and receiver field of view, and with distance between receiver and scattering volume. For typical lidar geometries with small beam divergence and a receiver field of view of about 1 mrad it is small angle scattering which contributes most to multiple scattering. Under these conditions a full treatment of the actual ray traces is not always required. In particular for DIAL applications the multiple scattering affects both wavelengths in the same way and hence cancel at least to good approximation. But in clouds, or for unusual geometry like satellite applications, a full treatment of multiple scattering has to be performed. An overview over analytical and numerical methods was presented by Bissonnette et al. (1995) and in the individual articles of the groups involved in the intercomparison exercise described in that paper.

Instantaneous scattering For the scattering processes described in B.1 the condition of instantaneous, unretarded scattering is always met. The time constants associated with Rayleigh-, Mie-, and Raman-scattering are much smaller than the pulse lengths of the lasers used for lidar measurements. Only in the case of fluorescence longer life times may occur. If this happens, the delay in the scattering has to be accounted for, leading to a different lidar equation. Again this case shall not be treated here.

Finite width of the transmitted spectrum The condition of monochromatic laser emission is never true in a strict sense. But Eq. (B.30) is easily generalized including arbitrary spectral distribution (Mégie, 1980). Let the spectral distribution of the transmitted radiation be given by $l(\nu)$ for $\nu \in \Delta\nu$, which is the wavenumber interval where $l(\nu)$ does not vanish. Also let the distribution be normalized, $\int_{\Delta\nu} l(\nu)d\nu = 1$. Then the generalized lidar equation is obtained by multiplying the monochromatic term with the spectral density and integrating over the interval $\Delta\nu$

$$P(R) = \frac{P_0}{R^2}\int_{\Delta\nu} l(\nu)\cdot\eta(\nu,R)\cdot\beta(\nu,R)\cdot T(\nu,R)^2 d\nu \qquad \text{(B.31)}$$

using the abbreviations

$$P_0 = P_L\cdot\frac{c\cdot\tau_L\cdot A}{2} \qquad T(\nu,R) = e^{-\int_0^R \alpha(\nu,r)dr} \,. \qquad \text{(B.32)}$$

Change of the spectral distribution by scattering It also has to be considered that the spectral distribution may be changed by the scattering process, e.g. by inelastic scattering or Doppler-broadening. For monochromatic excitation at wavenumber ν' the backscattered power at

wavenumber ν is given by

$$P(\nu,R) = \frac{P_0}{R^2} \cdot \eta(\nu,R) \cdot T(\nu',R) \cdot \beta(\nu',R) \cdot h(\nu - \nu',R) \cdot R(\nu,R) \qquad \text{(B.33)}$$

Here the term $\beta(\nu', R) \bullet h(\nu - \nu', R)$ describes the scattering process. $\beta(\nu', R)$ is the total backscatter coefficient for excitation at wavenumber ν', $h(\nu - \nu', R)$ is the normalized spectral distribution after scattering. The total backscattered power is obtained by integrating over the spectral distribution after scattering. If the incident radiation is not monochromatic, additionally an integration over the transmitted spectral distribution has to be performed. Hence the most general lidar equation for the case of incoherent, instantaneous single scattering reads:

$$P(R) = \frac{P_0}{R^2} \cdot \int_{\Delta\nu'} \int_{\Delta\nu} l(\nu') \cdot \eta(\nu,R) \cdot T(\nu',R) \cdot \beta(\nu',R) \cdot h(\nu - \nu',R) \cdot T(\nu,R) d\nu d\nu' \qquad \text{(B.34)}$$

This generalized lidar equation should be used whenever isolated narrow absorption lines like rotational and/or vibrational transitions in molecules are involved, or if inelastic scattering contributes significantly to the received signal. Eq. (B.34) has a rather simple formal appearance, but the double integration may require considerable efforts. Under realistic experimental conditions, however, some of the terms under the integrals are constant to a good approximation, and hence can be written just as factors. This makes the integration much easier to perform. Such approximate solutions which are of great practical importance will be derived and treated in some detail in the following.

B.3.2. Approximative lidar equations

Eq. (B.34) is considerably simplified when the laser line width is so small, that $\beta(\nu)$ can be assumed as constant for all wavenumbers which have to be considered. This can be reached for practically all actual lidar applications. Probably the most critical case is that of Rayleigh-scattering in the UV, where the ν^4-dependence of the scattering cross-section causes e.g. a 1% change over the interval of $\Delta\nu \approx 100\ cm^{-1}$, the natural line width of the KrF-laser. Generally this can be neglected, and if for special investigations this change appears to be critical, special lasers having much narrower line width are easily available.

Resonance scattering, however, showing narrow peaks in the spectral distribution of the backscattered radiation, e.g. resonance scattering from the mesospheric sodium layer, need the more general treatment and have to be excluded in this approximation.

The total extinction coefficient α is given by the sum of the extinction coefficients due to gaseous absorption α_g (see section B.2), to particle scattering α_p (section B.1.2) and molecular scattering α_m (section B.1.1), $\alpha = \alpha_g + \alpha_p + \alpha_m$.

Of these contributions only that from gaseous absorption has to be considered as strongly wavelength dependent, we have $\alpha_p \approx$ const and $\alpha_m \approx$ const for $\nu \in \Delta\nu$ for all lasers which are used for lidar work. Introducing the abbreviations

$$T_a(R) = \exp\left(-\int_0^R (\alpha_p(r) + \alpha_m(r))dr\right)$$

$$T_g(\nu,R) = \exp\left(-\int_0^R \alpha_g(\nu,r)dr\right)$$

we have

$$P(R) = \frac{P_0}{R^2} \cdot \beta(R) \cdot T_a^2(R) \cdot \int_{\Delta\nu'}\int_{\Delta\mu} (l(\nu') \cdot \eta(\nu,R) \cdot T_g(\nu,R) \cdot h(\nu-\nu') \cdot T_g(\nu',R)d\nu d\nu' \tag{B.35}$$

This equation becomes more transparent when the spectral distribution modified by transmission, $g(\nu, R)$, is introduced

$$g(\nu,R) = \frac{\int_{\Delta\nu} (l(\nu')T_g(\nu',R) \cdot h(\nu-\nu')d\nu'}{\int_{\Delta\nu} (l(\nu')T_g(\nu',R)d\nu'} \tag{B.36}$$

as well as abbreviations for the effective transmission factors for upward and downward propagation

$$T_u(R) = \int_{\Delta\nu'} l(\nu')T_g(\nu',R)d\nu'$$

$$T_d(R) = \int_{\Delta\nu} g(\nu,R)T_g(\nu,R)d\nu \quad .$$

Without losing generality it can also be assumed that the system efficiency $\eta(\nu, R)$ is constant $\eta(\nu, R) = \eta(\nu_s, R)$ for the interval where the backscattered signal is nonvanishing, where ν_s is the center frequency of the backscattered spectrum. Then we have

$$P(R) = \frac{P_0}{R^2} \cdot \eta(\nu_s,R) \cdot \beta(R) \cdot T_a^2(R) \cdot T_u(R) \cdot T_d(R) \tag{B.37}$$

So the backscattered power can be described formally as the product of seven terms with direct

physical meaning: the system constant P_0, the factor $1/R^2$ because the scattered waves are spherical, the total system efficiency $\eta(\nu_s, R)$, the backscatter coefficient $\beta(R)$, the transmission factor for wavelength independent contribution $T_a^2(R)$, the transmission factor $T_u(R)$ for upward propagation, and the transmission for downward propagation $T_d(R)$ for the strongly wavelength dependent contributions. The last two terms are effective transmissions, they are calculated as integrals over the respective spectral distribution.

A particularly useful formulation of the lidar equation is obtained by forming the logarithmic derivative of eq. (B.37):

$$\frac{d}{dR}\ln P(R)\cdot R^2 = \frac{d}{dR}\ln\eta + \frac{d}{dR}\ln\beta - 2\alpha_p - 2\alpha_m + \frac{1}{T_u}\frac{dT_u}{dR} + \frac{1}{T_d}\frac{dT_d}{dR} \tag{B.38}$$

A physical interpretation for the last two terms of eq. (B.38) is obtained by introducing

$$\begin{aligned}\frac{1}{T_u}\frac{dT_u}{dR} &= \frac{1}{T_u}\frac{d}{dR}\int_{\Delta\nu'} l(\nu')\cdot T_g(\nu',R)d\nu' \\ &= -\frac{\int_{\Delta\nu'}\alpha(\nu',R)\cdot l(\nu')\cdot T_g(\nu',R)d\nu'}{\int_{\Delta\nu'} l(\nu')\cdot T_g(\nu',R)d\nu'} \\ &\equiv -\alpha_{u,eff}(R)\end{aligned} \tag{B.39}$$

Here $\alpha_{u,\,eff}(R)$ is introduced formally as an effective extinction coefficient for upward propagation, where

$$l^*(\nu') = \frac{l(\nu')\cdot T_g(\nu',R)}{\int_{\Delta\nu'} l(\nu')\cdot T_g(\nu',R)}$$

is the normalized spectral distribution for upward propagation at distance R. Here the original spectral distribution of the laser emission, $l(\nu)$, is modified by the different transmission at the respective wavenumbers.

The term

$$\frac{1}{T_d}\frac{dT_d}{dR}$$

for downward propagation can be treated correspondingly, but it has to be considered that the spectral distribution of the backscattered light is height dependent, too. We have

$$\frac{1}{T_d}\frac{dT_d}{dR} = \frac{1}{T_d}\cdot\int_{\Delta\nu}\left(-g(\nu,R)\cdot T_g(\nu,R)+\frac{dg(\nu,R)}{dR}\cdot T_g(\nu,R)\right)d\nu \tag{B.40}$$

$$= -\alpha_{d,eff}(R)+\frac{\int_{\Delta\nu}\frac{dg(\nu,R)}{dR}\cdot T_g(\nu,R)d\nu}{\int_{\Delta\nu} g(\nu)\cdot T_g(\nu,R)d\nu}$$

with the effective extinction coefficient for downward propagation.

$$\alpha_{d,eff}(R)\equiv\frac{\int_{\Delta\nu}\alpha(\nu,R)\cdot g(\nu)\cdot T_g(\nu,R)d\nu}{\int_{\Delta\nu} g(\nu)\cdot T_g(\nu,R)d\nu} \tag{B.41}$$

Introducing

$$[G]\equiv\frac{\int_{\Delta\nu}\frac{dg(\nu,R)}{dR}\cdot T_g(\nu,R)d\nu}{\int_{\Delta\nu} g(\nu,R)\cdot T_g(\nu,R)d\nu} \tag{B.42}$$

the lidar equation in differential forms reads

$$\frac{d}{dR}\ln(P\cdot R^2) = \frac{d}{dR}\ln\eta+\frac{d}{dR}\ln\beta-2\alpha_p-2\alpha_m-\alpha_{u,eff}-\alpha_{d,eff}+[G] \tag{B.43}$$

Hence the logarithmic derivative of the range corrected signal is given by the logarithmic derivative of the system efficiency, the logarithmic derivative of the backscatter coefficient, the extinction coefficients due to molecular and particular scattering, the effective absorption coefficients for upward and downward propagation, and a correction term [G], which depends on the gradient of the spectral distribution of the backscattered signal and on the transmission up to the scattering volume, R.

Three special cases of general importance shall be treated in some more detail. If the halfwidths of the laser line, the backscattered lines, and the absorption lines of a gas under study are given by $\Delta\nu_L$, $\Delta\nu_s$, and $\Delta\nu_g$, respectively, we have to distinguish the cases:

1. $\Delta\nu_L$ and $\Delta\nu_s \ll \Delta\nu_g$, $\nu_s = \nu_L$ (broad absorption line, elastic scattering)
2. $\Delta\nu_L$ and $\Delta\nu_s \ll \Delta\nu_g$, $\nu_s \neq \nu_L$ (Raman-scattering)
3. $\Delta\nu_L \approx \Delta\nu_g$ and/or $\Delta\nu_s \approx \Delta\nu_g$, $\nu_s \approx \nu_L$ (narrow absorption line, quasi-elastic scattering)

B.3.2.1. Lidar equation for broad absorption lines

In the case of a broad absorption line and elastic scattering the spectral distributions of the transmitted and the backscattered light do not have to be taken into account explicitly. Eq. (B.37) is reduced to the standard lidar equation (B.30), and eq. (B.43) is reduced to:

$$\frac{d}{dR}\ln(P \cdot R^2) = \frac{d}{dR}\ln(\eta) + \frac{d}{dR}\ln\beta - 2\alpha_p - 2\alpha_m - 2\alpha_g \tag{B.44}$$

B.3.2.2. Lidar equation for Raman-scattering

In the case of Raman-scattering it is assumed, that the spectral distributions before and after scattering do not overlap, i.e. $l(\nu) \cdot g(\nu) = 0$, and that $\alpha_g(\nu) \approx$ const. for $\nu \approx \nu_L$ and for $\nu \approx \nu_s$ (ν_L and ν_s are the line centers of the transmitted and the inelastically scattered radiation, respectively). Then we have

$$P(R) = \frac{P_0 \cdot \eta(R)}{R^2}\beta_R(R) \cdot T_a^2(R) \cdot T_u(R) \cdot T_d(R) \tag{B.45}$$

where β_R is the Raman-backscatter coefficient, and the transmission factors are given by

$$T_u(R) = e^{-\int_0^R \alpha_g(\nu_L,r)dr}$$

$$T_d(R) = e^{-\int_0^R \alpha_g(\nu_S,r)dr} .$$

To account for the different extinction by molecular and particular scattering at ν_L and ν_s, the term $2(\alpha_p + \alpha_m)$ in the definition of T_a has to be replaced by $\alpha_m(\nu_L) + \alpha_p(\nu_s) + \alpha_m(\nu_L) + \alpha_p(\nu_s)$.

We then have the Raman-lidar equation

$$\frac{d}{dR}\ln(P \cdot R^2) = \frac{d}{dR}\ln\eta(\nu_s) + \frac{d}{dR}\ln\beta_R$$

$$-\alpha_p(\nu_L) - \alpha_p(\nu_s) - \alpha_m(\nu_L) - \alpha_m(\nu_s) - \alpha_g(\nu_L) - \alpha_g(\nu_s) \qquad \text{(B.46)}$$

This equation clearly shows the advantage of Raman-lidar-techniques when scattering by a gas of well known concentration is used, e.g. nitrogen or oxygen: Since $\frac{d}{dR}\ln\beta_R$ is known with rather good precision, and because $\frac{d}{dR}\ln\eta(\nu_s) = 0$ can be attained through proper system design at least for some extended measurement range, the total extinction coefficient can easily be determined from a single measurement, but as an average over the values at wavenumber ν_L and ν_s. This has been used to determine aerosol extinction coefficients (Ansmann et al., 1992b). Unfortunately, the backscatter cross section for Raman-scattering is very small, so that even for high power lasers the backscattered signals remain very weak.

B.3.2.3. Lidar equation for narrow absorption lines, including effects due to Doppler-broadening of molecular scattering

When narrow absorption lines like rotational-vibrational transitions of water vapor or oxygen in the infrared spectral region are used for humidity or temperature measurements, it has to be taken into account that generally two scattering mechanisms having different spectral distributions contribute to the lidar signal. While particle scattering leaves the incident spectrum unchanged to good approximation, for molecular scattering the Doppler-broadening has to be accounted for. The contribution of vibrational and rotational Raman-scattering, which is also present, is usually suppressed in the receiving optics by suitable filters.

In order to treat this case in more detail let us introduce

$$S_K = \frac{1}{K_S} = \frac{\beta_m}{\beta} = \frac{\beta_m}{\beta_m + \beta_p} \qquad \text{(B.47)}$$

the inverse of the widely used scattering ratio K_s (Measures, 1984). Then the spectral distribution of the backscattered radiation is given by

$$g(\nu,R) = (1 - S_K) \cdot l(\nu) + S_K \cdot h(\nu,R)$$

where h(ν, R) is the spectral distribution of Doppler-broadened Rayleigh-scattering according to eq. (B.13) from section B.1.

For this case the correction term

$$[G] = \frac{\int_{\Delta\nu} \frac{dg(\nu,R)}{dR} \cdot T_g(\nu,R)d\nu}{\int_{\Delta\nu} g(\nu,R) \cdot T_g(\nu,R)d\nu}$$

in eq. (B.43) can be estimated as follows. We have:

$$[G] = \frac{\int_{\Delta\nu} \left((h(\nu,R) - l(\nu)) \frac{dS_K}{dR} + S_K \frac{d}{dR} h(\nu,R) \right) \cdot T_g(\nu,R)d\nu}{S_K \cdot \int_{\Delta\nu} h(\nu,R) \cdot T_g(\nu,R)d\nu + (1 - S_K) \cdot \int_{\Delta\nu} l(\nu) \cdot T_g(\nu,R)d\nu} \tag{B.48}$$

The term [G] can be split up according to

$$[G] \equiv [G1] + [G2] \equiv [E1] \cdot \frac{dS_K}{dR} + [E2] \cdot S_K \tag{B.49}$$

The sensitivity factors [E1] and [E2] evaluate to

$$[E1] = \frac{\int_{\Delta\nu} h(\nu,R) \cdot T_g(\nu,R)d\nu - \int_{\Delta\nu} l(\nu) \cdot T_g(\nu,R)d\nu}{S_K \cdot \int_{\Delta\nu} h(\nu,R) \cdot T_g(\nu,R)d\nu + (1 - S_K) \cdot \int_{\Delta\nu} l(\nu) \cdot T_g(\nu,R)d\nu} \tag{B.50}$$

$$[E2] = \frac{\int_{\Delta\nu} \frac{dg(\nu,R)}{dR} h(\nu,R) \cdot T_g(\nu,R)d\nu}{S_K \cdot \int_{\Delta\nu} h(\nu,R) \cdot T_g(\nu,R)d\nu + (1 - S_K) \cdot \int_{\Delta\nu} l(\nu) \cdot T_g(\nu,R)d\nu} \tag{B.51}$$

Hence the correction term accounting for the change in spectral distribution due to Doppler-broadening Rayleigh-scattering consists of two contributions. [G1] is proportional to the gradient of the inverse scattering ratio, [G2] is proportional to the gradient of the spectral distribution of Rayleigh-scattering and to the inverse scattering ratio itself. The first term becomes important in regions of spatially inhomogeneous aerosol distribution, e.g. at the top of the planetary boundary layer. Since the spectral distribution changes only slowly with height the second term mostly is small. Only if the optical depth up to the measurement range is really large this term can become important, too. A precise calculation of the full correction term is possible only if the profile $S_K(R)$ is known. The „Rayleigh-Doppler-correction“, given by term [G], is important for measurements of humidity and temperature using the DIAL technique. Therefore, this technique shall be explained first, before having a closer look at [G] again.

B.4. DIAL-equations

The **Di**fferential **A**bsorption and **S**cattering lidar technique, called either DAS-lidar or, mostly, DIAL, is based on two lidar measurements at different wavenumbers. The parameter determined directly with this technique is a differential absorption coefficient. From this either a gas density can be calculated if the differential absorption cross section is known, or, if the gas density is known, the differential absorption cross section is retrieved, which can be a measure of e.g. temperature or pressure.

B.4.1. General DIAL equation

By combining two lidar equations, denoted by indices 1 and 2 for the wavenumber ν_1 and ν_2, the DIAL equation is obtained. We have

$$\frac{d}{dR}\ln\frac{P_1(R)}{P_2(R)} = \frac{1}{P_1}\frac{d}{dR}P_1 - \frac{1}{P_2}\frac{d}{dP}P_2 \tag{B.52}$$

In the most general case the backscatter signals are given by equation (B.34), but in most cases simpler approximations can be used.

B.4.1.1. DIAL equation for broad absorption lines

For the case that the lidar equation (B.30) can be applied, this is the case where the line widths of the transmitted and backscattered spectra are negligible compared wo the width of the absorption line, we have

$$\frac{d}{dR}\ln\frac{P_1(R)}{P_2(R)} = -2\Delta\alpha + \frac{d}{dR}\ln\frac{\eta_1}{\eta_2} + \frac{d}{dR}\ln\frac{\beta_1}{\beta_2} \tag{B.53}$$

with $\Delta\alpha = \alpha_1 - \alpha_2$.

By proper system design it can generally be achieved that the system efficiency is independent of range or at least shows the same range dependence for bothe wavenumbers, hence $\frac{d}{dr}\ln\frac{\eta_1}{\eta_2} = 0$. Deviations from this assumption shall not be treated here. Splitting the extinction coefficient according to $\alpha = \alpha_g + \alpha_p + \alpha_m$, we have

$$\frac{d}{dR}\ln\frac{P_1(R)}{P_2(R)} = -2\Delta\alpha_g - 2\Delta\alpha_p - 2\Delta\alpha_m + \frac{d}{dR}\ln\frac{\beta_1}{\beta_2} \tag{B.54}$$

In case that several gases absorb at either ν_1 or ν_2 the differential absorption $\Delta\alpha_g$ is the sum of all

contributions $\Delta\alpha_{g,\,i}$. Then equation (B.54) is the most general DIAL equation for broad poorly structured absorption bands like the Hartley-Huggins-band of ozone in the ultraviolet.

If in addition we have $\nu_1 \approx \nu_2$, so that we can assume $\Delta\alpha_p \approx 0$, $\Delta\alpha_m \approx 0$, and $\frac{d}{dR}\ln\frac{\beta_1}{\beta_2} \approx 0$, we obtain the „standard" DIAL equation

$$\frac{d}{dR}\ln\frac{P_1(R)}{P_2(R)} = -2\Delta\alpha_g \tag{B.55}$$

So in simple cases the determination of the differential absorption coefficient directly yields the density of a trace gas. From this the importance of the DIAL equation becomes evident.

B.4.1.2. DIAL equation for narrow absorption lines

In the case of narrow absorption lines where the spectral distributions of both the transmitted laser pulse and the backscattered light have to be considered, the lidar equation (B.43) has to be applied. Under these conditions generally a reference wavenumber can be chosen which is not located on an absorption line. For such reference measurement the influence of the laser and the backscattered line widths can be neglected, i.e.

$$T_{u,2}(\nu,R) = T_{d,2}(\nu,R) = \exp\left(-\int_0^R \alpha_2(r)dr\right)$$

In addition under these conditions the reference wavenumber may be chosen sufficiently close to the online wavenumber such that $\beta_1 \approx \beta_2$, $\alpha_{p,\,1} \approx \alpha_{p,\,2}$, and $\alpha_{m,\,1} \approx \alpha_{m,\,2}$. We then have

$$\frac{d}{dR}\ln\frac{P_1(R)}{P_2(R)} = -\alpha_{u,eff} - \alpha_{d,eff} + 2\alpha_2(R) + \frac{\int_{\Delta\nu}\frac{dg(\nu,R)}{dR}\cdot T_g(\nu,R)d\nu}{\int_{\Delta\nu} g(\nu,R)\cdot T_g(\nu,R)d\nu} \tag{B.56}$$

This DIAL equation differs from the „standard" DIAL equation (B.55) in that the absorption coefficient α_g is replaced by the sum of the *effective* absorption coefficients for up- and downward propagation, and that a correction term has to be included, namely the term [G] from the appropriate lidar equation (B.43). This term accounts for the change in spectral distribution caused by the scattering process. When the DIAL technique is applied to gases with narrow absorption lines the change in spectral distribution caused by scattering is mainly due to Doppler-broadening of the Rayleigh-scattered part. For this case the term [G] had already been calculated explicitly in section B. 3.2.3.

B.5. Importance of spectral distributions for measurements of water vapor and temperature

In this work three areas of application of the DIAL technique will be treated in detail: measurements of tropospheric ozone using the ultraviolet spectral region, water vapor retrievals using absorption lines in the near infrared, and temperature measurements using temperature dependent oxygen-lines, also in the near infrared. While the ozone measurements are performed in a broad absorption band, both water vapor and temperature measurements make use of narrow isolated lines of the rotational-vibrational spectrum, where all details of the spectral distributions have to be considered. Since the integrals in equation (B.56) are kind of involved some examples will be given to demonstrate the importance of including the details of the spectral distribution in the analysis. In particular it shall be demonstrated

- under which conditions the finite laser line width has to be considered,
- under which conditions the Doppler-broadening of the Rayleigh-scattered part has to be considered,
- under which conditions the change of spectral distribution with range due to stronger absorption in the line center as compared to the line wings has to be considered,
- how large the sensitivity is with respect to gradients in the spatial distribution of aerosols (factor [E1] in the correction term [G]),
- how large the sensitivity is with respect to gradients in the spectral distribution of the Rayleigh-scattering (factor [E2] in the correction term [G]).

For all these studies the width of the absorption line is most important, Figure B.1 shows the halfwidths (HWHM) of a typical water vapor and oxygen absorption line (according to equations (B.25) and (B.29)) as well as the width of the Rayleigh-line (according to equation (B.14)), as a function of altitude, assuming the US-standard-atmosphere.

At the ground the width of the water vapor line is about three times that of the Rayleigh-line, in the upper troposphere they have about the same width. For oxygen both lines have about the same widths over the complete height range, with the absorption line being narrower than the Rayleigh-line almost everywhere.

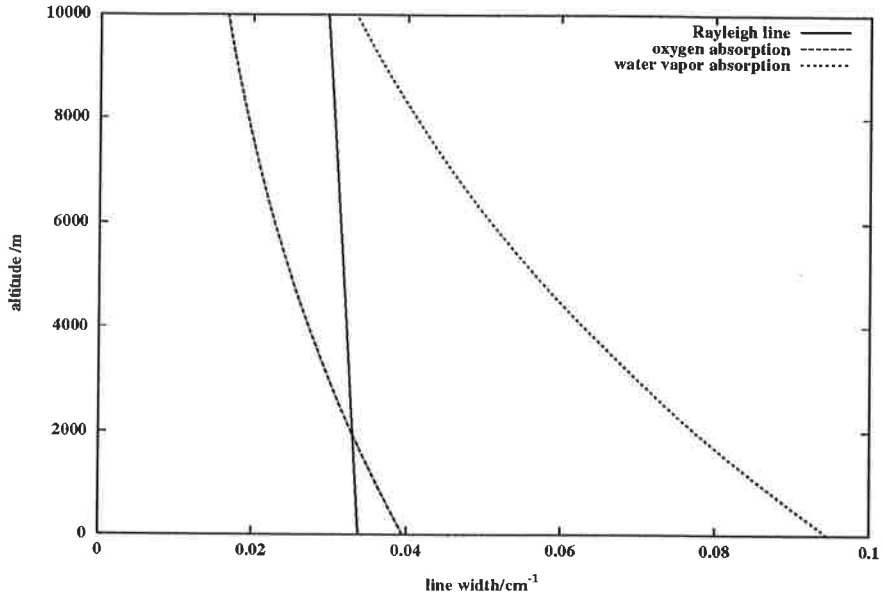

Figure B.1: Line widths of Rayleigh-scattering, the oxygen absorption line ${}^{P}P_{27,27}$ and the water vapor absorption line at ν_0 =13718.58 cm^{-1}.

The question, under which conditions the finite spectral width of the laser has to be considered, is addressed in Figure B.2. It shows the ratio of the absorption cross section in the line center and the effective absorption cross section as a function of the fractional laser line width compared to the absorption line width. If 5% accuracy is considered sufficient the laser line width can be neglected if it is less than 0.25 of the absorption line width, 2% accuracy are reached for $b_L/b_a = 0.15$. Hence for water vapor measurements a line width $b_L < 0.01$ cm^{-1} is required, for temperature measurements using oxygen lines we have $b_L < 0.003$ cm^{-1}. It requires considerable effort to achieve such narrow line widths for high power pulsed lasers (Wulfmeyer, 1995). In any case for the Rayleigh scattered part its spectral distribution has to be accounted for and an effective absorption coefficient has to be calculated. Figure B.3 addresses the question, under which conditions it has to be considered that the transmitted spectrum is changed due to stronger absorption in the line center as compared to the wings. It shows the ratio of the effective absorption cross section including this absorption effect to that one where this is neglected. This ratio is a function of optical depth, and of the relative line widths. An accuracy of better than 2% up to as optical depth of $\tau = 2$ is reached when the laser line is smaller than 0.3 of the absorption line width. Again, for the Rayleigh-scattered part this effect always has to be accounted for.

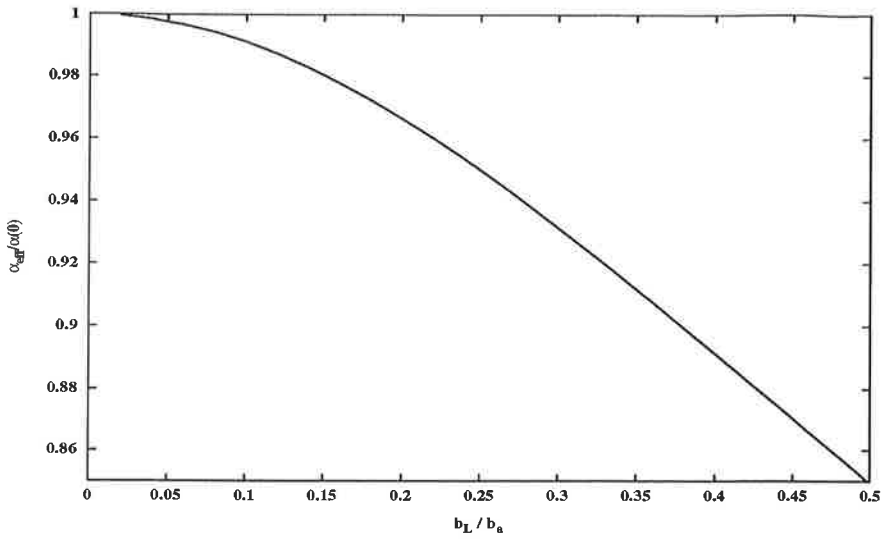

Figure B.2: Effective absorption cross section $\alpha_{eff}/\alpha(\nu_0)$ as a function of the ratio between laser and absorption line widths b_L/b_a.

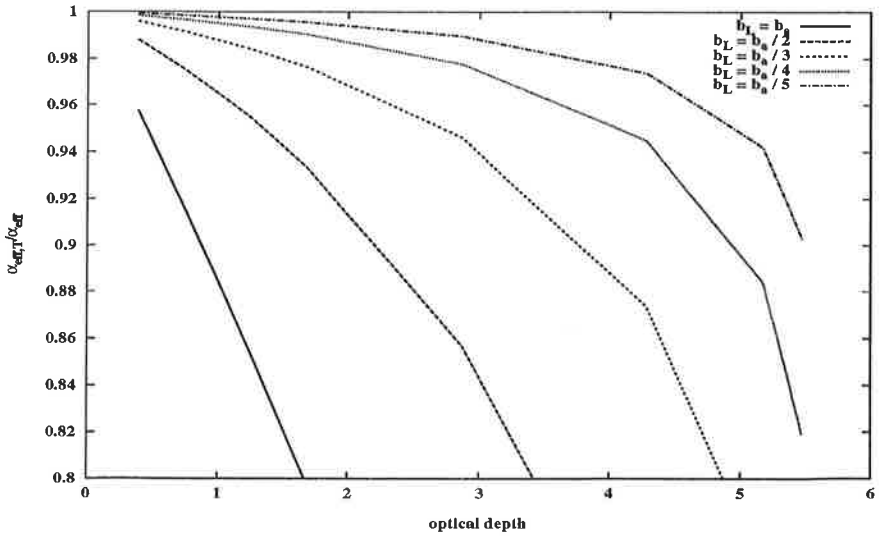

Figure B.3: Ratio of the effective absorption cross section including the effect of absorption on the path up to the scattering volume and that one calculated with constant spectrum $\frac{\alpha_{eff,T}}{\alpha_{eff}}$, as a function of the one-way optical depth. Parameter is the ratio of laser to absorption line width b_L/b_a.

B.5.1. Estimate of the Rayleigh-Doppler-correction

The two terms of the correction term [G] = [G1] + [G2] can only be calculated if the inverse scattering ratio S_K and its gradient dS_K/dR are known. In addition the spectral distributions of the laser and the Rayleigh-scattering have to be known, as well as the vertical distribution of the absorbing gas, e.g. water vapor or oxygen, below the scattering volume. To come to a kind of general estimate under which conditions the Rayleigh-Doppler-correction is important, in the following the sensitivity factors [E1] with respect to dS_K/dR and [E2] with respect to S_K will be estimated. This will be performed for atmospheric conditions corresponding to the US-standard atmosphere, and for a simple water vapor distribution. In the experimental part of this work a statistical distribution of dS_K/dR derived from a large number of lidar measurements in different regions of the atmosphere will be presented. This can then be used to estimate the probability of exceeding certain error limits.

Since the spectral distribution of the backscattered light is always broader than that of the incident light, for the denominators of the terms [E1] and [E2] of equation (B.51) we have

$$S_K \cdot \int_{\Delta\nu} h(\nu,R) \cdot T_g(\nu,R)d\nu + (1-S_K) \cdot \int_{\Delta\nu} l(\nu) \cdot T_g(\nu,R)d\nu \geq \int_{\Delta\nu} h(\nu,R) \cdot T_g(\nu,R)d\nu$$

$$S_K \cdot \int_{\Delta\nu} h(\nu,R) \cdot T_g(\nu,R)d\nu + (1-S_k) \cdot \int_{\Delta\nu} l(\nu) \cdot T_g(\nu,R)d\nu \leq \int_{\Delta\nu} l(\nu) \cdot T_g(\nu,R)d\nu \tag{B.57}$$

if the laser is tuned to the absorption maximum. From (B.57) if follows that

$$\left(\frac{\int_{\Delta\nu} h(\nu) \cdot T_g(\nu,R)d\nu}{\int_{\Delta\nu} l(\nu) \cdot T_g(\nu,R)d\nu} - 1 \right) \leq [E1] \leq \left(1 - \frac{\int_{\Delta\nu} l(\nu) \cdot T_g(\nu,R)d\nu}{\int_{\Delta\nu} h(\nu,R) \cdot T_g(\nu,R)d\nu} \right) \tag{B.58}$$

$$\frac{\int_{\Delta\nu} \frac{d}{dR} h(\nu,R) \cdot T_g(\nu,R)d\nu}{\int_{\Delta\nu} l(\nu,R) \cdot T_g(\nu,R)d\nu} \leq [E2] \leq \frac{\int_{\Delta\nu} \frac{d}{dR} h(\nu,R) \cdot T_g(\nu,R)d\nu}{\int_{\Delta\nu} h(\nu,R) \cdot T_g(\nu,R)d\nu} \tag{B.59}$$

The upper limit in equation (B.58) will be reached for large values of S_K, when molecular scattering dominates, the lower limit of (B.59) is approached for dominating particle scattering.

The upper and lower limits of the sensitivity factors have been estimated according to (B.58) and (B.59) for four examples. For all of them the US standard atmosphere has been assumed (USSA,

1976), and a water vapor vertical distribution according to $\rho_{H_2O}(h) = \rho_0 \cdot \exp(- h/a_{H_2O})$, where $\rho_0 = 6\ g \cdot m^{-3}$ and $a_{H_2O} = 2200$ m. Two different absorption lines for both water vapor and oxygen have been chosen, corresponding to measurements optimized for boundary layer studies and the upper troposphere, respectively.

From Figures B.4 and B.5 it is evident that [E1] increases with height up to values around 0.1 to 0.2 within the usable measurement range. To achieve an accuracy of better than 10% for the absorption coefficient, which is about 10^{-4} to 10^{-3} m^{-1}, we have to know dS_K/dR to an accuracy of 10^{-3} to 10^{-4} m^{-1}. Particularly for measurements with high resolution and in regions with small water vapor absorption this may be difficult to achieve.

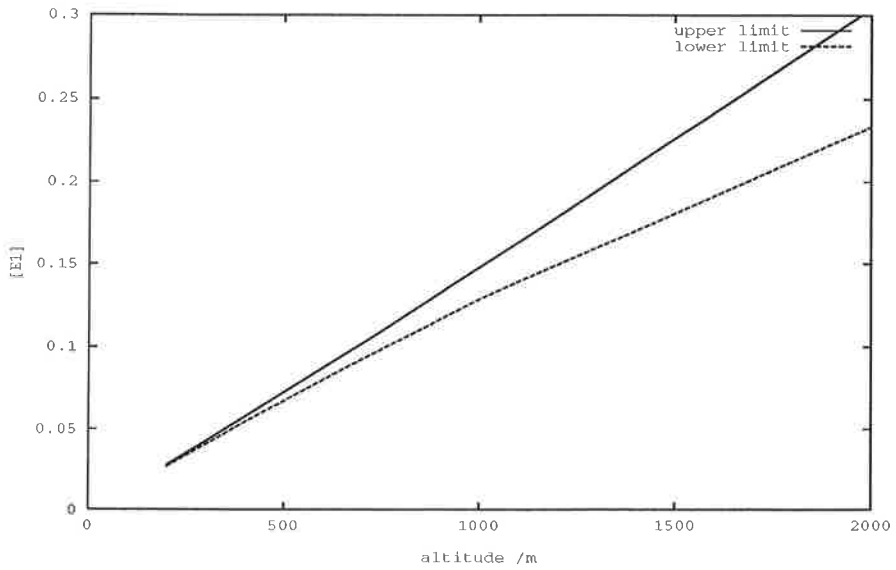

Figure B.4: Sensitivity [E1], calculated for the water vapor line at 13718.58 cm^{-1}.

The absolute value of the sensitivity with respect to changes in the spectral distribution of the Rayleigh-backscatter, [E2], remains smaller than $5 \cdot 10^{-5}$ m^{-1}, or even smaller than $5 \cdot 10^{-6}$ m^{-1} if a water vapor line suitable for upper tropospheric measurements is chosen. Since $S_K \leq 0.5$ in the lower troposphere and $S_K < 1$ everywhere, the correction term [G2] remains smaller than $2 \cdot 10^{-5}$ m^{-1} or $5 \cdot 10^{-6}$ m^{-1}, respectively. In most cases this will not have a major influence on the measurement accuracy.

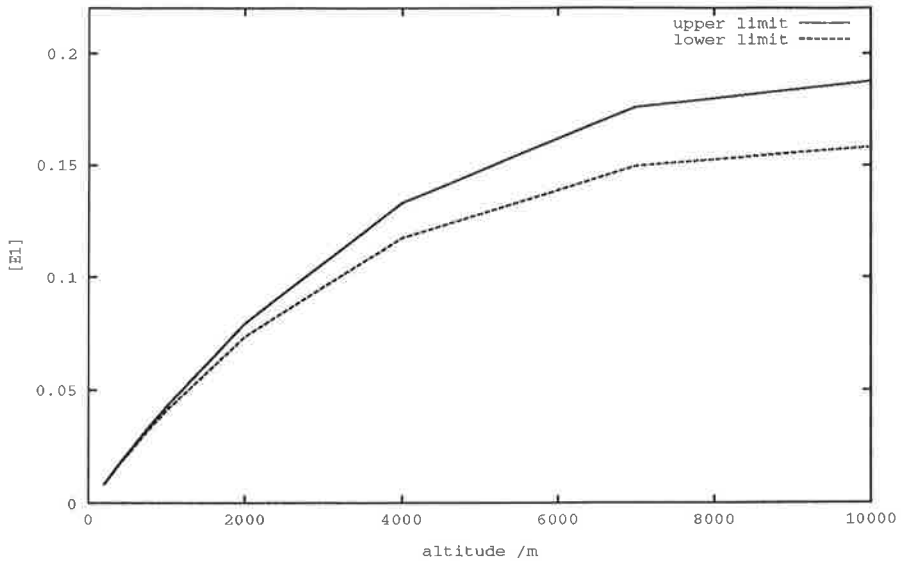

Figure B.5: Sensitivity [E1], calculated for the water vapor line at 13739.44 cm^{-1}.

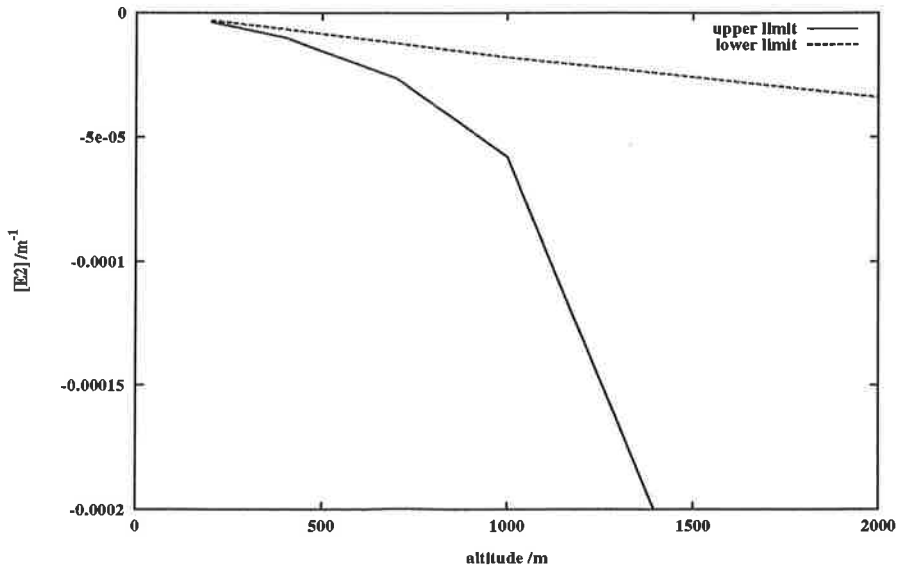

Figure B.6: Sensitivity [E2], calculated for the water vapor line at 13718.58 cm^{-1}.

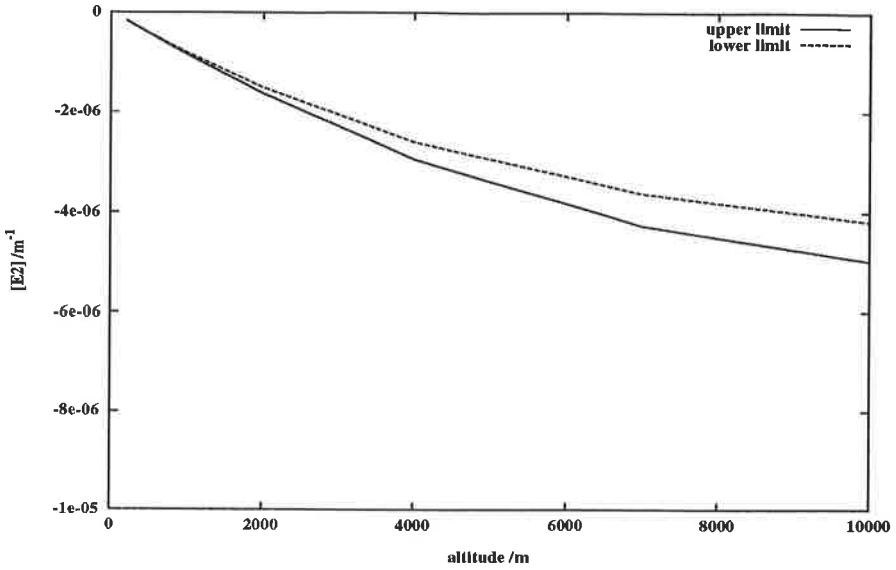

Figure B.7: Sensitivity [E2], calculated for the water vapor line at 13739.44 cm^{-1}.

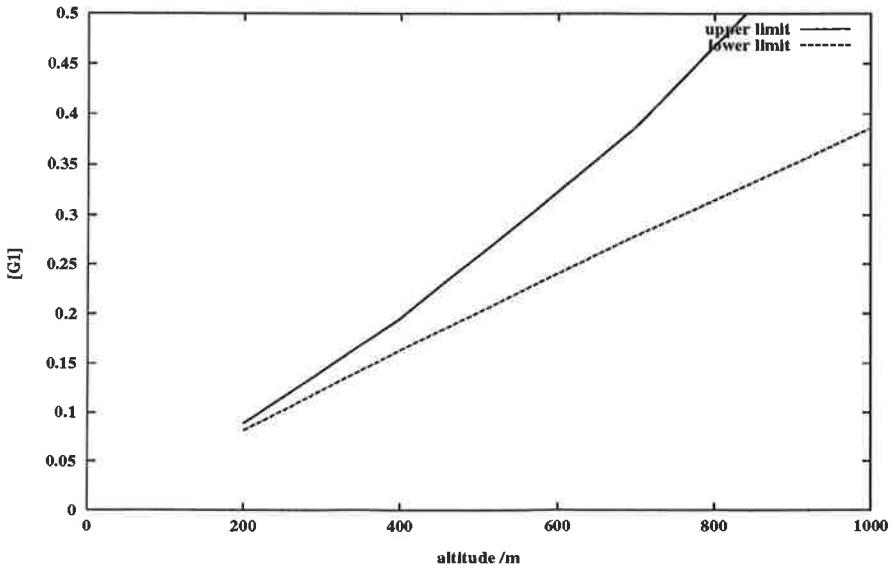

Figure B.8: Sensitivity [E1], calculated for the oxygen line $^{P}P_{27,27}$.

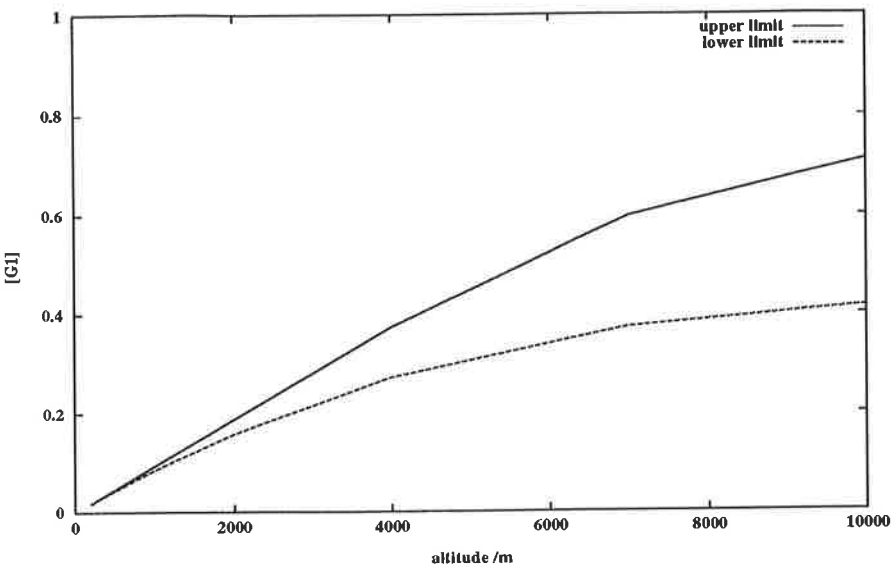

Figure B.9: Sensitivity [E1], calculated for oxygen line $^{P}P_{31,31}$.

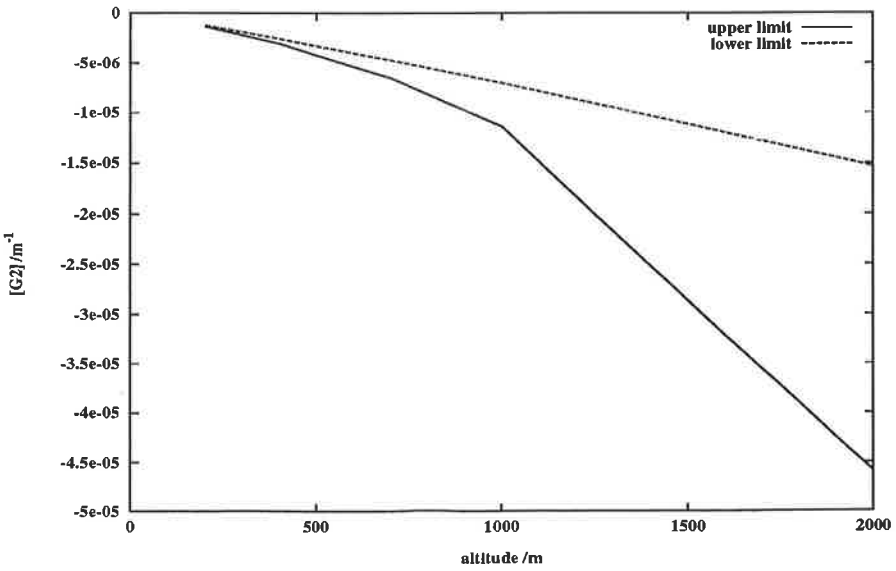

Figure B.10: Sensitivity [E2], calculated for oxygen line $^{P}P_{27,27}$.

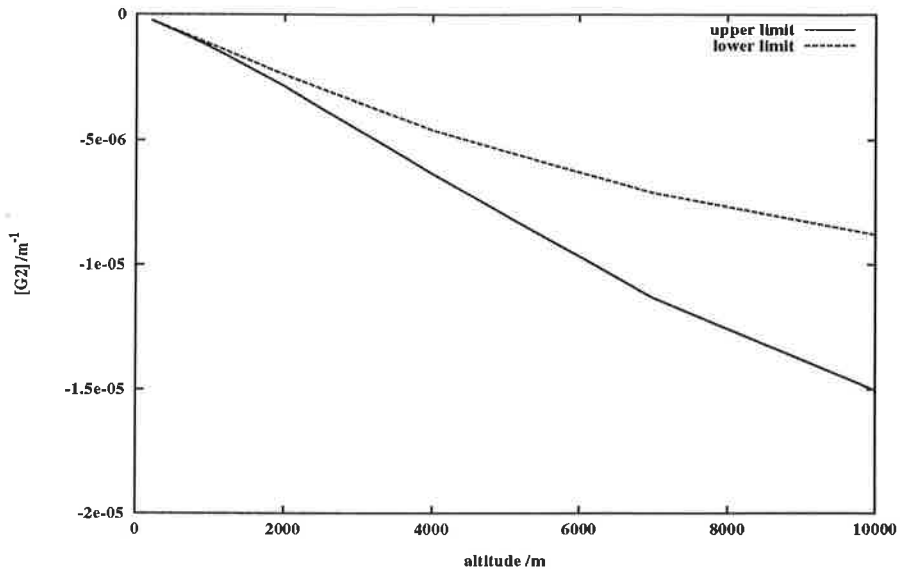

Figure B.11: Sensitivity [E2], calculated for the oxygen line ${}^{P}P_{31,31}$.

For oxygen absorption lines the problem of Rayleigh-Doppler-correction is much more serious because of their smaller widths. Figures B.8 to B.11 show that [E1] can be as large as 0.5, and [E2] a s large as $2 \cdot 10^{-5}$ m^{-1}. For useful temperature retrievals the error in the retrieved absorption coefficient has to be smaller than about $5 \cdot 10^{-6}$ m^{-1}, hence we need to know dS_K/dR to better than 10^{-5} m^{-1}. Only in cases with particularly homogeneous aerosol distribution this will be reached. The term [G2] mostly is negligible compared to [G1]. Its dependence on S_K is less critical, the required accuracy is only about 0.2, which is quite feasible.

B.6. Discussion of errors

B.6.1. Random errors

In retrievals of the differential absorption coefficient using the DIAL technique both systematic and random errors will occur.

The main source of random errors is the noise content of the measured backscatter signals. For the general error discussion it is sufficient to use the „standard"-DIAL equation (B.55). In more difficult cases involving additional correction terms their dependence on random errors has to be studied, too. This shall not be attempted here. Applying the error propagation law to the DIAL equation (B.55) yields:

$$\begin{aligned} \delta(\Delta\alpha_g) &= \delta\left(\frac{1}{2}\frac{d}{dR}\ln\frac{P_1(R)}{P_2(R)}\right) \\ &= \frac{1}{2\Delta R}\cdot\sqrt{2\cdot\left(\frac{\delta(P_1)}{P_1}\right)^2+2\cdot\left(\frac{\delta(P_2)}{P_2}\right)^2} \end{aligned} \tag{B.60}$$

$\delta(x)$ designates the standard deviation of the argument x, and ΔR is the range resolution used for the determination of gradients.

B.6.2. Systematic errors

The determination of differential absorption coefficients using the DIAL technique always includes the term

$$\frac{d}{dR}\ln\frac{P_1(R)}{P_2(R)},$$

which depends on the backscattered signals at both wavelengths. Systematic errors in the determination of this term depend on the details of the measurement setup, and hence can hardly be treated in general. To include these errors in the overall error budget, the general formula in analogy to (B.60) is

$$\delta(\Delta\alpha_g) = \frac{1}{\sqrt{2}\Delta R}\cdot\left(\frac{\delta(P_1)}{P_1}-\frac{\delta(P_2)}{P_2}\right) \tag{B.61}$$

where δ(x) now designates the systematic error of x rather than the standard deviation due to ran-

dom errors.

B.6.2.1. Errors due to temporal and spatial averaging

In the derivation of lidar and DIAL equations in section B it had been assumed that the backscattered signal power can be measured to the required accuracy in a time interval short enough to exclude changes of the remaining parameters like backscatter and extinction coefficients. In many cases this assumption does not hold since the backscattered signals tend to be rather weak in spite of the use of high power lasers. Since the backscattered intensity can be measured only in discrete quanta, the Poisson-distribution of received photons leads to rather large errors in the individual measurements. This uncertainty is further increased by detector and electronic noise. For repetition rates typical for present day systems, on the order of 10 Hz, the aerosol in the scattering volume will be exchanged completely between successive measurements. Therefore, it can not be assumed generally that the aerosol parameters remain constant. Since the DIAL equation establishes a nonlinear relation between the measured quantities and the remaining parameters it has to be investigated how the necessary averaging is performed best, and which errors may occur. For this purpose it suffices to use the most simple DIAL equation:

$$2\Delta\alpha = -\frac{d}{dR}(\ln P_1 - \ln P_2) + \frac{d}{dR}(\ln\beta_1 - \ln\beta_2) \tag{B.62}$$

The differentiation d/dR is a linear operator and hence may be applied in any order. This does not hold for calculating the logarithm, which is the only nonlinear operator in equation (B.62).

For the case where only the signals P_i vary during the averaging interval, but $\Delta\alpha$ and β_i are constant, we have

$$2\Delta\alpha = -\frac{d}{dR}(\ln\overline{P_1} - \ln\overline{P_2}) + \frac{d}{dR}(\ln\beta_1 - \ln\beta_2) \tag{B.63}$$

Averaging of the signals is performed here before applying the logarithm. In case that also β_i varies during the averaging interval, the same order of operations applies. If β_1 and β_2 are completely correlated, no error will be caused by the term including β_i. In DIAL systems this can often be reached by transmitting the pulses at both wavelengths either simultaneously or at least in such a short time interval that the aerosol properties can be considered unchanged. It has to be considered, however, that for a larger wavelength separation full correlation cannot be achieved. The resulting error has already been treated. If only $\Delta\alpha$ varies in the averaging interval (this is not a particularly realistic assumption), we have

$$2\Delta\alpha = -\frac{d}{dR}(\overline{\ln P_1(R) - \ln P_2(R)}) + \frac{d}{dR}(\overline{\ln\beta_1 - \ln\beta_2}) \tag{B.64}$$

Hence, we have to form the logarithm before averaging.

In the most general case all quantities will vary during the averaging interval, the rules for order of application of the operators are contradictory. Hence, it has to be studied what kind of error remains when the order of operations is changed. For the stochastic variables P_i and β_i we have to calculate $\ln(\overline{P_i}) - \overline{\ln(P_i)}$ and $\ln(\overline{\beta_i}) - \overline{\ln(\beta_i)}$. To this end first the distribution functions for P_i and β_i, have to be established. The true backscatter signals follow a Poisson distribution, but in fact what is measured is the sum of the true signals P_i, a contribution due to background light P_{bg}, and a noise contribution P_n.

$$P_m = P_i + P_{bg} + P_n \tag{B.65}$$

P_{bg} and P_n are stochastic variables, the actual values of which are unknown. Only their mean values $\overline{P_{bg}}$ and $\overline{P_n} = 0$, and possibly their variances, may be determined independently. In the most general case the distribution function of P_m is a mixture of Poisson distributions for P_i and P_{bg}, and a Gaussian distribution for P_n. The used quantity

$$P = P_m - \overline{P_{bg}} \tag{B.66}$$

also has a quite complicated distribution function. At his point it shall be emphasized, that in particular the signal calculated according to (B.66) may assume negative values. In this case the DIAL equation is not directly applicable since the logarithm of a negative argument is not defined. Hence, the signals have to be averaged until at least $P > 0$ before a calculation of an absorption coefficient may be performed. It is obvious that disregarding negative values of P leads to erroneous results. For sufficiently large signal to noise ratio we may assume P as a normally distributed stochastic variable with mean $\overline{P}$ and variance δ^2:

$$P = \overline{P} \cdot \left(1 + \frac{\delta}{\overline{P}} \cdot x\right) \tag{B.67}$$

where x is normally distributed with zero mean and variance 1.

For the case of $\delta/\overline{P} \ll 1$ we have

$$\begin{aligned} \overline{\ln(P)} &= \ln(\overline{P}) + \overline{\ln\left(1 + \frac{\delta}{\overline{P}} \cdot x\right)} \\ &\approx \ln(\overline{P}) + \frac{\delta}{\overline{P}} \cdot \bar{x} + \frac{\delta^2}{2 \cdot \overline{P}^2} \cdot \overline{x^2} \end{aligned} \tag{B.68}$$

Since x is normally distributed with zero mean and variance 1, x^2 follows a χ^2 distribution with one degree of freedom (see e.g. Davenport and Root, 1958). We then have

$$\overline{\ln(P)} \approx \ln(\bar{P}) + \frac{\delta^2}{2 \cdot \bar{P}^2} \tag{B.69}$$

According to this the systematic error caused by exchanging the order to applying the logarithm and averaging operators decreases with the square of the normalized standard deviation, while the statistical error of the mean decreases only linearly. E.g. a normalized standard deviation of 10% causes a systematic error of 0.5%, if ln(P) is averaged rather than P.

The second term in the DIAL equation (B.62) can be treated analogously, but here we can start directly by assuming at least a near normal distribution for β. It should also be safe to assume $\delta_\beta/\bar{\beta} \ll 1$, at least β is always positive.

For most DIAL applications we can assume that variations in $\Delta\alpha$ are much slower than those of P_i, the latter can vary from shot to shot. Then the best strategy is to average over the signals first until the error caused by exchanging the order of application for the operators according to equation (B.69) is sufficiently small. Then further averaging may be performed in the resulting $\Delta\alpha$, or $\overline{\ln(P)}$, without introducing additional errors.

In cases where such a separation of scales is not possible because $\Delta\alpha$ varies to fast it is generally not possible to obtain an unbiased result.

It is noteworthy that a special case exists due to the fact that $\Delta\alpha$ is determined from $\ln\overline{P_1} - \ln\overline{P_2}$. The systematic error due to exchange of operators has the same (positive) sign for both terms. In case that $\delta/\bar{P}$ is the same for P_1 and P_2, the errors cancel. But because of the quadratic dependence on the mean signal the height range is rather restricted for which such compensation of errors occurs.

The problem treated in this section has been dealt with in the literature mostly under the aspect whether or not averaging over N shots actually leads to an improvement of the retrieval of the absorption coefficient proportional to $\sqrt{N}$. While an extended set of measurements performed with a heterodyne lidar and hard targets showed considerable deviations (Killinger and Menyuk, 1987), measurements from atmospheric targets mostly showed the expected reduction in error proportional to $\sqrt{N}$ (Milton and Woods, 1987; Staehr et al., 1985; Grant et al., 1988). Grant et al. (1988) demonstrated by simulating a change of absorption within the averaging interval, that in this case the standard deviation of the ratio from on- to off-line signals does not decrease proportionally to $\sqrt{N}$. As has been explained above, this cannot be expected, since this corresponds exactly to the case where both β and $\Delta\alpha$ vary during the averaging interval. Further Grant et al. (1988) have pointed out that the deviations observed by Killinger and Menyuk (1987) had been

caused by their specific measurement setup. The signal statistics for heterodyne measurements using hard targets are to large extent determined by the speckle patterns due to interference. These patterns can have rather long correlation times (for hard targets). Under these very special conditions successive measurements cannot be assumed independent. Such effects are not to be expected for measurements using direct detection techniques.

B.6.2.2. Miscellaneous systematic errors

Inspection of the general DIAL equation (B.45) and the corresponding lidar equation (B.38) reveals the possibility of a number of additional systematic errors. Any error in the determination of differential correction terms for the gradient of the system efficiency, the gradient of the total backscatter coefficient, the extinction coefficients for both particle and molecular scattering, as well as that for the „Rayleigh-Doppler-correction" [G] directly enters the determination of the differential absorption coefficient. In addition any error in the determination of spectral distributions before and after the scattering process will cause an error of the retrieved absorption coefficient. These systematic errors shall not be treated here because they are quite specific for the individual application and can only be analyzed when the experimental details are known.

In the calculation of trace gas density from the retrieved differential absorption coefficient two sources of error have to be considered. First, other gases than that under study may absorb at the wavelengths used for the experiment. This may be quantified in terms of cross-sensitivities. When individual vibrational rotational transitions having narrow line widths such cross-sensitivities can generally be avoided. However, if broad absorption bands are used as in the case of ozone retrievals using the UV spectral range, cross-sensitivities to other gases generally cannot be avoided. Some values for the most important gases will be presented in section H.1, only in strongly polluted areas they will cause a considerable error in tropospheric ozone measurements.

Secondly, we have to consider errors in the values for the absorption cross sections involved in the calculation. For measurements using individual vibrational rotational transitions special attention has to be paid to the pressure and temperature dependence of the absorption cross section, described by equations (B.21) through (B.29). An extensive study of such errors has been performed by Ansmann (1984). If suitable temperature independent lines are selected the resulting error can be limited to $< 3\%$. In that study, however, it had not been considered that the pressure shift of absorption lines may cause additional errors. But this pressure shift can be experimentally determined, for many lines used in DIAL measurements this has already been done (Bösenberg, 1985; Grossmann and Browell, 1989). If the known shift is properly accounted for the remaining errors are negligibly small.

C. Determination of vertical transports

C.1. Basic principle

A new application area of laser remote sensing in combination with a system for vertical wind measurements (for the studies reported in this work a Radar/Rass system has been used, Rass = **R**adio **A**coustic **S**ounding **S**ystem) has been established with the determination of vertical trace gas transport by applying the eddy correlation method using remote sensing techniques. For in-situ measurements the eddy correlation method is **the** standard method for measurements of vertical transports, since it is a direct method not requiring any assumptions about the actual turbulence structure. A general overview over this technique may be found in Wyngaard (1991).

In this method the definition of the transport of a gas with density ρ and velocity $\vec{u}$ is applied directly:

$$\vec{F}_\rho = \overline{\vec{u} \cdot \rho} \tag{C.1}$$

The transport is a vector with the same direction as $\vec{u}$, it is calculated as the temporal average of the instantaneous transport. Averaging is indicated by the overbear.

The vertical flux simply is the vertical component of (C.1). Let w designate the vertical velocity, and separate all terms into a mean and a fluctuating part, then we have

$$\rho = \bar{\rho} + \rho'$$

$$w = \bar{w} + w'$$

and the vertical flux is given by

$$F_\rho = \overline{w'\rho'} + \bar{w} \cdot \bar{\rho} \tag{C.2}$$

Thus the method depends on simultaneous measurements of the gas concentration and the vertical wind. The mean transport is then calculated as the sum of the covariance of the fluctuating parts and the product of their mean values. Mostly it is assumed that $\bar{w} = 0$, where the small vertical velocities associated with large scale convergence or divergence are neglected. One reason for this neglection certainly is that these velocities are too small to be measured directly to any reasonable accuracy.

Webb et al. (1980) have pointed out that sensible and latent heat fluxes, which are associated with density fluctuations, lead to a violation of the continuity equation, if $\overline{w} = 0$ is assumed. To maintain the balance of the mass budget $\overline{w} \neq 0$ has to be assumed. The resulting mean vertical velocity is on the order of several mm/s only, and hence can hardly be determined experimentally. Therefore, it is calculated from the measured heat flux. The term $\overline{w} \cdot \overline{\rho}$ were $\overline{w}$ is calculated from the heat flux is called Webb-correction.

However, it has to be mentioned that the mean vertical velocity resulting from the heat flux is of the same order of magnitude as that one resulting from the large scale convergence or divergence of the flow field. Since this contribution to the mean vertical wind cannot be measured either, errors of the same size as the Webb-correction remain anyhow.

C.2. Requirements regarding the measurement system

For the determination of the local flux the measurements have to met two requirements:

1. The temporal and spatial resolution has to be sufficiently good to resolve all those eddy sizes contributing considerably to the overall transport.
2. The accuracy of the measurements has to be sufficiently high to guarantee a good estimate of the covariance, which for vertical transports generally results as the small difference of large numbers.

For the determination of fluxes which are supposed to be representative for a larger region of the atmosphere the measurements in principle should be performed at many locations simultaneously. Since this is mostly not feasible, measurements are typically performed at a single location but for an extended period of time. How long this time interval has to be depends on the details of the turbulence statistics. An extensive treatment of this problem may be found in Lenschow et al. (1994). Temporal averaging may be taken as a surrogate for ensemble averaging whenever the statistical properties of the turbulent flow are stationary and horizontally homogeneous, and if a mean horizontal wind provides for transporting a sufficiently large number of eddies across the location where the measurements are performed. It is obvious that these conditions can be met only for certain meteorological conditions, in many cases this will not be possible. The question which horizontal scales have to be included in the measurements had been discussed extensively in conjunction with airborne in-situ flux measurements, see e.g. Lenschow and Stankov (1986). Since the mean horizontal wind is typically a factor of 10 smaller than the aircraft speed the problem of poor spatial representativeness is much more serious for groundbased measurements. This may, however, be compensated by the possibility to perform repeated measurements on many days under similar conditions.

To meet the requirements of sufficient resolution at ground level typically resolutions of 1 to 10 Hz temporally and several decimeters vertically have to be achieved, for both the vertical wind and the trace gas concentration measurements. Of course this cannot be achieved with remote

sensing techniques, at least not for a larger range. But such high resolution is not required for measurements in greater heights, since the size of the eddies contributing most to the transport increases remarkably with height above ground. The resolution required in any particular case of course depends largely on the meteorological situation and the state of turbulence of the flow. However, several general statements can be made.

- Large eddies contribute most to the transport.
- Under convective conditions eddies with a diameter up to the height of the boundary layer actually occur.
- Eddy sizes decrease with decreasing distance to either boundary of the boundary layer, the maximal radius of the eddies is approximately given by the distance to the nearest boundary.
- Generally an inertial subrange exists, where mainly transformation of energy from larger to smaller eddies occurs. In this spectral region the variance of both the vertical wind and any passive tracer decreases proportional to $f^{-5/3}$, and the vertical transport decreases proportional to $f^{-7/3}$. If the resolution is sufficient to include at least the low frequency end of the inertial subrange, it is rather safe to assume that the main contribution to the transport is included in the measurement.

From that we can conclude that the vertical resolution has to be better than half of the distance between the measurement range and the nearest boundary of the boundary layer, either the ground or the capping inversion height. The required temporal resolution may be calculated from the vertical resolution and the vertical velocity, $\Delta t = \Delta z/w$. Under convective conditions vertical velocities reach up to several m/s, for shear driven turbulence 1/30 of the mean horizontal wind is predicted by a rule of thumb (Tennekes and Lumley, 1972). In order to include not only the largest eddies the actual resolution should be somewhat better, at least say by a factor of 3. To give an example, for a measurement height of 600 m a rough estimate yields 100 m vertical and 50 s temporal resolution ($\Delta t \approx 100$ m/2 m $\cdot$ $s^{-1} = 50$ s). Such performance is in fact within the reach of present active remote sensing instruments.

At this point it has to be stated clearly, that it cannot be expected that the method presented here will be applicable under all meteorological conditions, mainly because of the limited resolution of present remote sensing instruments. Therefore, for each individual application an analysis of the relevant length and time scales has to be performed. In this work examples will be presented in the chapters dealing with experimental determinations of the latent heat flux and the ozone flux, respectively.

D. Experimental basis

D.1. Measurement system

Lidar systems generally consist of several subsystems which are clearly separated in functionality. Figure D.1 shows a typical block diagram. Within the complete system the laser system is the component which has to be designed very specifically for each individual application. This also holds for the spectral separation and filtering of the backscattered light as part of the receiver optics especially of DIAL systems. The remaining subsystems, transmitter optics, telescope, detector, signal processing, and data acquisition are quite similar, at least in principle, for a broad range of applications. However, even in these systems there is some potential for fine tuning with respect to each individual application.

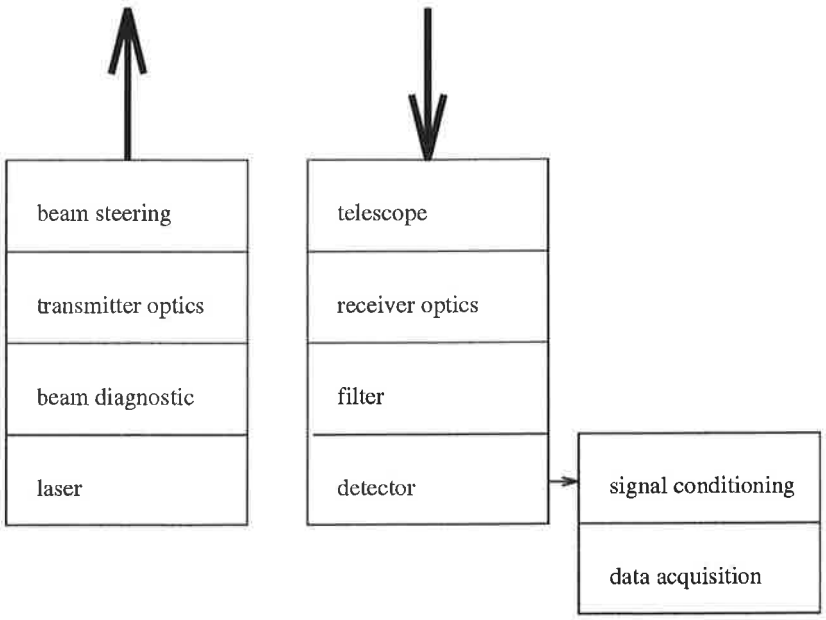

Figure D.1: Block diagram of a lidar or DIAL system.

Particularly for DIAL applications the requirements regarding the accuracy and performance of the different subsystems are rather demanding. This may best be demonstrated by giving a simple example: the differential absorption coefficient can best be determined when the optical depth up to the measurement range is about $\tau_0 = 1.1$ (Remsberg and Gordley, 1978). Since DIAL measurements are supposed to yield profiles of the absorption coefficient, let us assume that 10 layers have to be resolved, each with optical depth $\Delta\tau_0 \approx 0.1$. According to equation (B.60) the error of the retrieval of the optical depth $\tau_0 = \Delta\alpha \cdot \Delta R$ is

$$\sqrt{2}\delta\tau_o = \sqrt{\frac{\delta^2(P_1)}{P_1^2} + \frac{\delta^2(P_2)}{P_2^2}}$$

For simplicity we assume the same error in both signals P_1 and P_2. Then the absolute error of the retrieved differential optical depth is equal to the relative error of each signal. To achieve an accuracy of 5% for the retrieval of a differential optical depth of $\Delta\tau_0 \approx 0.1$, each signal has to be measured with a accuracy of better than 0.5%. This clearly demonstrates the necessity of outstanding performance of the signal acquisition subsystem. The requirements resulting for the different system components will be studied in detail in the following sections.

D.1.1. Laser

General requirements for laser transmitters used in lidar systems are short pulse length ($\tau_L \leq 100$ nsec), small beam divergence (generally not a critical point, since it can be much improved by beam expansion), excellent pointing stability, high reliability and ease of operation. The latter two properties are particularly important in applications requiring operation during field measurement campaigns. Other required properties depend on the individual application. It is obvious that high spatial and temporal resolution can only be achieved if the pulse energy and repetition rate are high (typical values are 50 mJ at 10 Hz).

Spectral properties are not critical in case of applications involving broad absorption bands (e.g. ozone measurements in the UV). On the other hand, when narrow vibrational rotational lines are involved (e.g. for H_2O, O_2) the requirements with respect to line width, frequency stability, and spectral purity are extremely demanding.

How to account for finite laser line width has been explained in section B.3. However, this requires the transmitted spectrum to be known. For lasers in which several resonator modes are excited in principle this has to be measured for each shot, since the distribution of energy on the different models varies from shot to shot. Therefore, one primary goal of the development of laser systems to be used for water vapor or temperature measurements has been to reduce the laser line width sufficiently so that the remaining uncertainties of the spectral distribution do not affect the results considerably. Table D.1 summarizes the requirements resulting from this request and typical absorption line widths of H_2O and O_2 for the altitude range up to the tropopause. From the requested accuracy of water vapor or temperature measurements and the known line widths also the requirements for the laser frequency stability are derived.

Another very important laser property is its spectral purity, which shall be defined here as that fraction of the transmitted energy which is contained in a well known line shape. The unknown fraction mostly occurs as a broadband emission with very low spectral density, and therefore is extremely difficult to determine experimentally. How the DIAL retrievals of the absorption coeffi-

cient are affected by spectral impurity has been discussed previously (Bösenberg, 1987; Ismail and Browell, 1989; Bösenberg, 1991). Figure D.2 shows as the main result the relative error in the retrieval of the absorption coefficient as a function of the optical depth up to the measurement range, with the spectral impurity as parameter. The results show that even a small spectral impurity can cause rather large errors, unless the optical depth is small. In principle this error can be corrected for, but Figure D.2 shows that rather precise knowledge of the spectral impurity is required to reach sufficiently accurate corrections. In most applications this will not be possible to achieve.

Table 1: Required laser properties in order to keep laser induced errors in water vapor retrievals smaller than 5% and in temperature retrievals smaller than 1K throughout the troposphere.

Parameter	demanded	
	H_2O	T
Wavelength λ / nm	720 - 730	767 - 771
line width (FWHM) / MHz	< 500	< 200
stability of frequency(1 σ) / MHz	± 210	± 50
spectral purity	> 0.995	> 0.999
pulse length	200	
divergence / mrad	≈ 1	
pulse energy / mJ	≈ 50	
repetition rate / Hz	> 10	
t_{on} - t_{off} / ms	≈ 1	

D.1.2. Transmitter optics

In the most simple case the transmitter optics can be omitted completely. However, often at least a beam expansion is recommended to reduce the beam divergence. The divergence of the transmitted beam should be somewhat smaller than the field of view of the receiving telescope (typically on the order of 1 mrad).

Another purpose of transmitter optics often is the adjustment of the beam pointing relative to the receiver optical axis. The pointing accuracy and stability should be much smaller than the field of view, about 10 µrad appears to be a good number for this. When high quality mounts are used for the deflecting mirror this requirement does not cause serious problems.

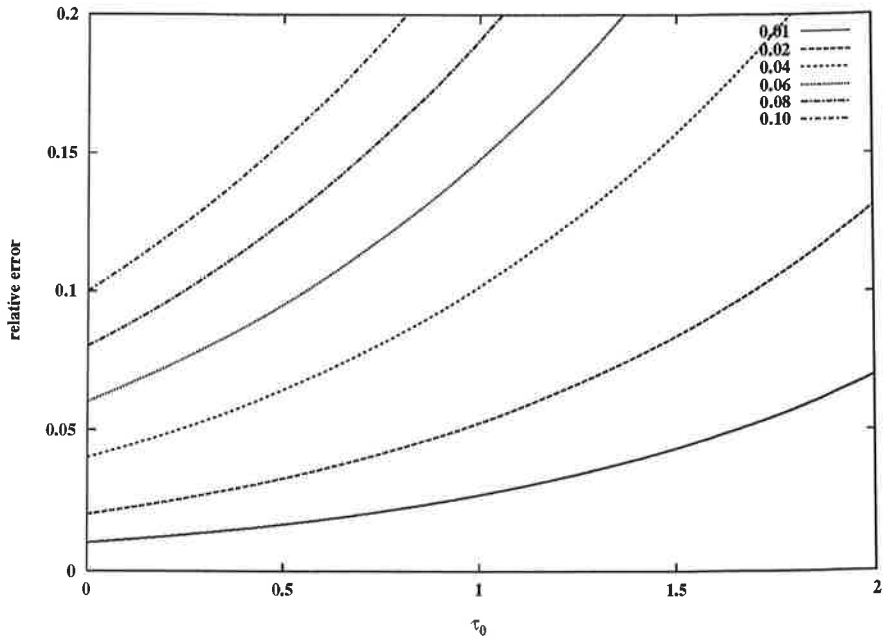
0.2
0.15
0.1
0.05
0
relative error
0
0.5
1
1.5
2
τ_0
0.01
0.02
0.04
0.06
0.08
0.10

Figure D.2: Relative error of the retrieved absorption coefficient due to spectral impurity as a function of optical depth τ_0 up to the measurement range. The spectral impurity is parameter of the set of curves.

D.1.3. Receiving telescope

The requirements for a receiving telescope for lidar applications are quite easy to meet. The most important parameter is the area of the primary mirror, and of course its reflectance. The requirement regarding resolution is rather poor even in comparison to simple telescopes used by hobby astronomers, further the required image area is very small. Consequently it is not necessary to install elements for correcting aberrations. In principle one parabolic mirror is sufficient, e.g. mounted in Newton-configuration. Even simpler than that is the direct coupling into an optical fiber right in the focal plane of the primary (and only) mirror. Such simple configuration has been used with good success in the ozone DIAL system designed at the Max-Planck-Institute for Meteorology (Bösenberg et al., 1993; Schaberl, 1995). The main point to observe in this design is that the f-number of the primary has to be adapted to the core diameter and the numerical aperture of the fiber, and to the desired field of view. The fiber also determines the product of beam diameter and divergence, all following optics has to match that product in order to avoid transmission losses and shadowing effects. The stability of the mounting has to meet the same requirements as the transmitter optics.

D.1.4. Spectral separation and filtering

All lidar systems require some spectral filtering to reduce unwanted background light. The bandwidth of this filter should be as narrow as possible, restrictions are caused by the wavelength separation in DIAL systems and in some cases by the temperature stability of the filter function. A bandwidth of $\Delta\lambda \approx 5$ nm is easy to achieve, and in many applications addressing only the lower troposphere this is already sufficient. To achieve larger measurement ranges with corresponding smaller signals the bandwidth may be reduced to $\Delta\lambda \approx 0.5$ nm, without intolerable losses in transmission. But particularly when narrowband filters are used attention has to be paid to the fact that the transmission depends on the angle between the received bundle and the optical axis of the filter. This effect may easily cause a dependence of transmission on range, since in a non-coaxial lidar system the angle depends on the distance from the lidar to the scattering volume. Beam expansion after the diaphragm in the receiver optics can help to avoid this problem.

If a DIAL system is designed such that both wavelength are generated sequentially (e.g. in the systems designed for water vapor and temperature measurements at the Max-Planck-Institute for Meteorology), both signals can be acquired using the same detector. In this case no spectral separation is required. If, however, those wavelengths are generated simultaneously, e.g. in the ozone DIAL, spectral separation has to be performed in the receiving optics. This can be achieved either by interference filters or through a spectrometer. Excellent performance has been demonstrated for a grating spectrometer which had been specifically designed for the use in our ozone DIAL system. A special design was necessary to adapt it to the diameter and numerical aperture of the optical fiber used for coupling with the receiving telescope. In this design the output is coupled into a fiber as well, making this spectrometer very flexible in use. As a side product excellent galvanic isolation is achieved of the detector from all mechanical structures supporting the bulky transmitter and receiver optics. This minimizes the electromagnetic interference between the excimer laser, where a high voltage of up to 30 kV is switched in a few ns, and the detector, where extremely small photo currents have to be measured to high precision. This spectrometer has been described in detail by Schaberl (1990).

An upgrade of this spectrometer as a double-spectrometer for the detection of Raman-scattering has been performed by Matthias (1993). A special feature of this spectrometer is that it is used in two planes simultaneously for two separate receiving telescopes, and both for direct detection of elastically scattered light and for detection of Raman-scattering through the use of an additional filter or spectrograph. In the latter application a suppression of scattered light of $3 \cdot 10^{-8}$ has been reached in conjunction with an overall transmission of about 5%, measured from input to the detector. This large suppression of straylight is necessary to avoid significant perturbation of the extremely small Raman-signals.

D.1.5. Detector

The most important detector property is as high a quantum efficiency as possible at the relevant wavelength in order to keep the noise due to the Poisson-distribution of detected photo electrons small. The detector bandwidth has to match the desired range resolution, typically about 10 MHz for a range resolution of 15 m in the lidar signals. A good selection of detectors is available for all wavelength regions.

The dynamic range of lidar signals, in particular for ground-based, vertically pointing systems, is extremely large. Due to the decrease according to $1/R^2$, multiplied by an exponential decrease caused by absorption and scattering, and an additional decrease of the aerosol backscatter with height the signals from the far range are generally several orders of magnitude smaller than those from close ranges.

For ozone lidar systems this factor is $> 10^8$ for ranges between 100 m and 10000 m. For measurements in the near infrared this factor is generally even larger because of the smaller contribution of molecular scattering at these wavelengths, and because of the strong decrease of aerosol backscatter with height. Since a very high accuracy of the acquired signals is requested, excellent detector linearity over a large dynamic range is mandatory. Great care has to be taken in the selection of detectors, amplifiers and all associated electronics regarding this point.

The complete range of the signal is covered in single returns, in about 100 µs. The photo-multipliers used almost exclusively for the measurements reported here are known to exhibit major signal distortions which may be caused by overloading the photocathode, excessive current in the final stages, or afterpulses induced by ion-feedback. These distortions show up as non-linearity and/or delayed ghost signals, usually called „signal induced bias“ or SIB. The details of the physical processes inside the photomultiplier and their effect on the output signal are not yet completely understood. However, experimental investigations show (Iikura et al., 1987; McDermid et al., 1990; Gast, 1991) that in particular the memory effects are dependent on both the height and the length of the signals, and that they can be described to a good approximation by an exponentially decreasing tail after the strong signal causing the distortion is switched off. If it is possible to determine this tail from actual measurements, e.g. from a region where it is known that the real signal vanishes, at least a partial correction is possible.

D.1.6. Signal processing and data acquisition

The requirements regarding the signal processing have already been discussed in conjunction with those for the detector. Linearity, large bandwidth, low memory effects, and low noise are standard requirements. However, in real systems these can only be used with some restrictions. But generally it can be stated that the data processing, if properly designed, does not make a major contribution to the overall error.

In contrast to that the limited accuracy of available data acquisition systems is a major source of error. Analog-to-digital converters which are used here at the required sampling rate of about 10 MHz cover a dynamic range of 12 bit corresponding to 1:4096, but the accuracy of a single measurement is typically a factor of 2 to 8 worse, depending on the signal frequency. The accuracy which can actually be achieved of course largely depends on both the individual converter and on the details of the signal. This shall not be treated in any detail here. Most important for DIAL measurements is the accuracy which can be achieved by averaging over many shots. This has not been covered extensively in the literature yet. We have deduced from actual lidar measurements that for the type we use (Pentek 4246) the resulting error remains as large as 0.2 LSB (LSB = least significant bit = step size of the converter), no matter how many signals are averaged. Apparently other high quality systems show similar behaviour. This limited accuracy of data acquisition systems represents a major limitation for the usable signal range in DIAL measurements.

D.1.7. Reduction of signal dynamic range

Since the required accuracy of the data acquisition system, including all errors of the detector, pre-amplifier, and AD-converter can be achieved for a limited range of signals only, in DIAL systems normally some kind of dynamic range reduction is performed. Mostly this is achieved by reducing the field of view of the receiving telescope and geometrically separating receiving and transmitting optics, thus suppressing the signals from close ranges almost completely (up to several 100 m in many cases). In this range of course no measurements can be made. Often a second much smaller receiving telescope is installed to cover the close ranges only. While this is very simple, it adds considerable complexity to the detector, signal processing, and data acquisition subsystem.

Up to now it has not been demonstrated convincingly that the region of incomplete overlap of receiver field of view and transmitted beam can actually be used for DIAL measurements, as suggested and discussed in detail by Harms (1979) and Zhao et al. (1992). This failure is probably due to the fact that even very small differences in the beam profile for the two wavelengths used will cause substantial errors in the DIAL measurement. Apparently it is not possible to generate sufficiently homogeneous beam profiles.

It has also been attempted to reduce the signal dynamics by modulating the gain of either the photomultiplier (Edner et al., 1987) or the pre-amplifier (Kempfer et al., 1994). Within certain limits this has been successful, but it does not reduce the problems caused by the detector itself, e.g. nonlinearity or memory effects.

These problems can be avoided when the optical signal is modulated before it reaches the detector. One possibility is the use of a mechanical chopper, which serves as a simple on-off switch. This technique is widely used for stratospheric measurements. For applications addressing the

lower troposphere the necessarily short switching time is hard to achieve. Therefore, a new technique has been developed using an electro-optic cell (Lehmann, 1994). In this technique a rapidly variable transmission is achieved by rotating the polarization plane of the received signal using a Pockels-cell between crossed polarizers. A dynamic range reduction by a factor of 1000 has been demonstrated with this device. The reproducibility of the attenuation was sufficiently good to guarantee an error in DIAL measurements of $\delta \ln P_1/P_2 < 0.01$ even at close ranges. In the far range the error is even smaller. This variable attenuator is now being used in the recently redesigned water vapor lidar of the Max-Planck-Institute. For ozone measurements the use of this technique appears feasible, but it has not yet been demonstrated experimentally that it works at the rather large wavelengths separations used in these applications.

E. Measurements of the water vapor distribution

E.1. Introduction

In the general introduction the importance of the water cycle for many atmospheric processes has already been emphasized. Improved retrievals of the spatial and temporal distribution of tropospheric water vapor has been identified as one of the most important goals in atmospheric research. An important partial goal in this connection is the improved determination of evaporation rates which are representative for a large area.

The importance of evaporation rates results from the fact that the evaporation at the surface, soil or water, is the only source for water (in gaseous, liquid, or solid state) in the atmosphere except for very small amounts produced chemically from other trace gases. While a large number of indirect methods are in use requiring the turbulence structure to meet certain conditions in order to yield reasonable results, the eddy correlation technique has become the preferred direct method for in-situ measurements of vertical water vapor fluxes, both at ground and on aircraft platforms. When this method is applied close to the ground the main difficulty is the inhomogeneity of evaporation over land surfaces, since it depends strongly on details of the soil structure, vegetation and turbulence structure influenced by the terrain profile. Due to this strong inhomogeneity it is difficult to derive evaporation estimates which are valid for a larger area from one or even a few ground level flux measurements.

This is different for measurements performed at greater heights within the boundary layer, since the small scale variations are already merged and have formed larger eddies, providing for some area averaging. This has been used in a number of aircraft experiments, but it should be emphasized here that in this height range the measurements can also be performed using active remote sensing techniques (Senff et al., 1994). The main advantage of remote sensing techniques is that they can be applied on a routine basis with relatively little effort, once the technique has been fully developed. Thus it is comparatively easy to collect a comprehensive data set covering a large range of atmospheric conditions. In addition the remote sensing of eddy correlation fluxes provides vertical flux profiles rather than values at isolated levels, which is most important for a number of process studies.

Measurements of turbulent transport using the eddy correlation technique require that the structure of all eddies contributing significantly to the flux are resolved. This size depends on the height of the measurement and on the stability of the stratification. The studies we have performed so far have shown, that a vertical resolution of 75 m and a temporal resolution of 60 s are already sufficient in a convectively mixed boundary layer. Of course an improvement of resolution is very desirable in order to extend the measurement capabilities to conditions where smaller eddy sizes are dominant, e.g. for shear driven turbulences.

The requirements regarding absolute accuracy are not very high, about 10% is sufficient in view of total errors in flux measurements. The crucial requirement is that for excellent relative accuracy, certainly better than about 3%, because in large parts of the boundary layer the vertical transport is associated with small variations of the water vapor density only. Another important requirement is that the measurements must be performed during daylight, too, in order to include all important contributions to the vertical latent heat flux.

If only the main structure of the vertical distribution of water vapor is to be determined the requirements regarding resolution are somewhat relaxed, because in most cases these structures have rather large scales. A vertical resolution of 100 m should be sufficient in almost all cases, in the upper troposphere a resolution of 1 km only would yield very valuable results. With respect to temporal resolution the requirements are much reduced, too. Measurements with even 1 hour averaging time are an important improvement over most of the conventional measurements. But for special process studies, e.g. in connection with cloud processes, every attempt should be made to provide high resolution measurements throughout the troposphere. Lidar measurements can make an important contribution to such studies.

The method of measuring water vapor concentration using the DIAL technique has already been discussed in detail in preceeding sections, where in particular the problems associated with accounting for the details of the spectral distribution of the transmitted laser pulse and the backscattered radiation have been addressed. In the following section some examples will be used to demonstrate the potential contribution of DIAL measurements to atmospheric process studies, to further explain some of the problems, and to suggest solutions for these problems.

E.2. Measurements of the vertical distribution of water vapor

E.2.1. Measurements using a system based on dye lasers

Already in 1985 a DIAL system for water vapor measurements was constructed, in which two narrow band dye lasers were used (Bösenberg and Hinzpeter, 1986; Bösenberg et al., 1989). This system was used to evidence that spatially and temporally high resolution measurements of humidity during both night and day can be performed. In the boundary layer a statistical error of 0.1 g/m^3 was reached at 75 m vertical and 50 sec temporal resolution.

Measurements have also been performed up to 8 km height. The achievable absolute accuracy was mainly restricted by the insufficient spectral purity of the dye lasers, the broadband emission due to ASE (amplified spontaneous emission) often exceeded 2%. This level of spectral impurity causes a strong height dependence of the measurement error. Another nasty feature was that the spectral impurity was time dependent, too, because the level of ASE generally increased during the measurements because of deterioration of the dye solution, and because of minor changes in the adjustments. This made the correction of errors due to spectral impurity rather difficult. Only

in special cases the correction could be performed reliably, e.g. when quasi-simultaneous measurements were performed using two absorption lines having different line strengths. Routine operation of this system was impossible.

However, the system was used for measurements in different parts of the atmosphere to illustrate the potential but also the limits of the technique. One example, measured during the approach of a warm front in the upper troposphere, gave clear evidence of the importance of the Rayleigh-Doppler-correction. Figure E.1 shows an example of the results described by Ansmann (1989).

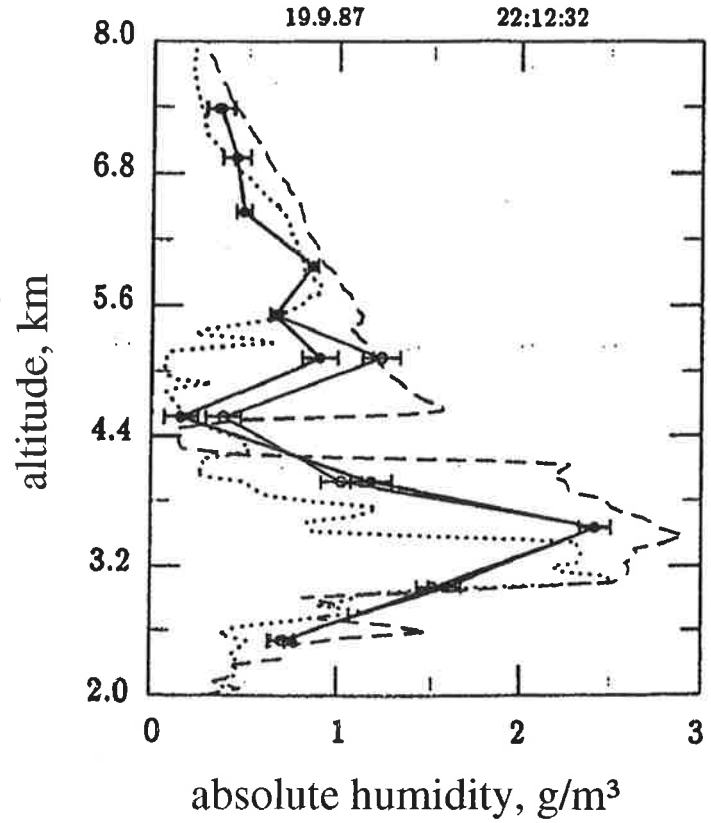

Figure E.1: DIAL water vapor measurements (solid lines) in comparison to radio soundings at 18:00 UT (dotted line) and at 21:00 UT (dashed line). Resolution ΔR = 500 m, ΔT = 5.5 min. Evaluation without (o) and with inclusion of the Rayleigh-Doppler-correction (•). Statistical errors are included for the lidar measurements.

In summary the most important results of this study were:

- Humidity measurements up to 7.5 km are possible with a resolution of 500 m vertically and 5.5. min temporally.
- For these conditions the statistical error remains less than 12% for an absolute humidity of 0.3 g m^{-3}.
- The Rayleigh-Doppler-correction can approach 50% of the actual measurement, even for this rather poor resolution.
- In this particular case it cannot be excluded that the error in the correction is as large as the

correction itself, because of the uncertainties associated with the parameters entering the aerosol retrieval. Hence, the error due to the Rayleigh-Doppler-broadening can exceed all other error terms, but only at the boundaries between different atmospheric layers.

- The agreement of the lidar measurements with those of two locally launched radiosondes is satisfactory, but the results of the two ascents performed with 3 hours separation show rather large differences in several regions of the atmosphere.
- Studies addressing processes associated with cloud formation require high resolution measurements, both vertically and temporally.

This example gave clear evidence that the uncertainties associated with the calculation of the Rayleigh-Doppler-correction can be the major limitation for the accuracy of DIAL measurements at boundaries between different layers of the atmosphere. But it also demonstrated that continuous lidar measurements are very suitable for studying processes in the free troposphere.

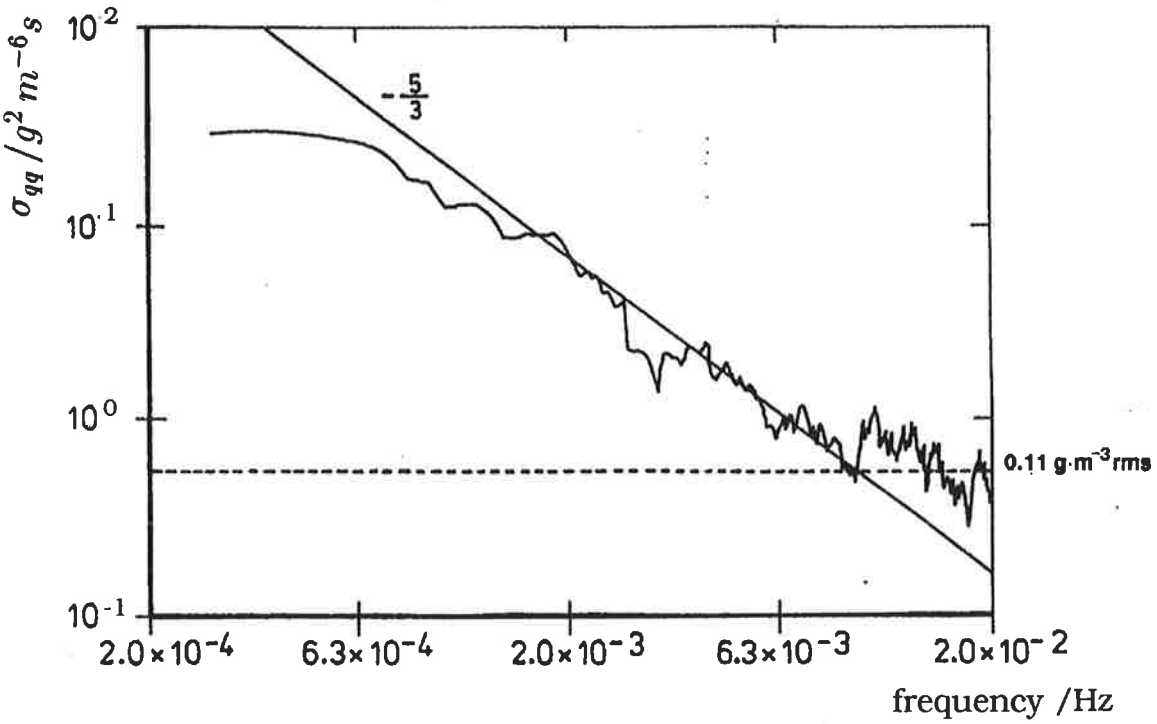

Figure E.2: Variance spectrum of a water vapor measurement performed on September 18, 1987 in Hamburg, 13 to 16 UT. Measurement height was 247 m, vertical resolution 75 m, temporal resolution 25 s.

For measurements in the boundary layer Figure E.2 illustrates what kind of resolution and relative accuracy can be achieved. It shows a variance spectrum calculated from a 3 hours humidity measurement, performed on September 18th, 1987, 13:00 to 16:00 UT in Hamburg at an altitude

of 247 m above ground. The signals were averaged over 75 m vertically and 25 s temporally, so the Nyquist-frequency is $2 \cdot 10^{-2}$ Hz.

The spectrum exhibits a strong decrease of power spectral density with increasing frequency, approximately proportional to $f^{-5/3}$. This decrease is predicted for the inertial subrange, where neither production nor dissipation of energy is observed. At the high frequency end of the measured spectrum a significant deviation from this decrease is observed, the spectrum approaches a constant value of about 0.6 g^2 m^{-6} s. This can be explained by the statistical error of the humidity retrieval, the spectrum of which is white for this kind of measurements. Hence, the values observed at the high frequency end of the spectrum yield an upper limit for the spectral density of the white noise contained in the measurements, when the atmospheric variability is neglected at these frequencies. In the example shown in Figure E.2 this noise corresponds to a standard deviation of 0.11 g m^{-3}, or about 1.5% of the mean value. This clearly demonstrates the potential of the DIAL technique to provide accurate high resolution measurements in the boundary layer.

The possibility of performing high resolution measurements was used to derive the turbulent transport of water vapor in a convective boundary layer using the eddy correlation technique with remote sensing instruments for the first time (Senff et al., 1994). For these measurements the DIAL system was combined with a Radar/Rass to measure the vertical wind component (Peters et al., 1988; Peters and Kirtzel, 1994). The main results of these very first measurements of the latent heat flux are:

- The resolution of the combined measurements of water vapor and vertical wind is 75 m vertically and 60 s temporally.
- In the middle of the boundary layer a relative accuracy of ≈ 0.1 g m^{-3} is achieved, which is determined by the signal noise and the background light.
- The corresponding accuracy of the wind measurement is ≈ 0.1 m/s.
- Variance spectra of both vertical wind and humidity exhibit a decrease proportional to $f^{-5/3}$, presumably because the inertial subranges has been reached. In this part of the flow spectrum the contribution to the covariance is supposed to decrease proportional to $f^{-7/3}$. Therefore it is justified to assume that only a minor contribution to the transport is made at frequencies larger than those resolved by the system.
- Measurements of the latent heat flux have been performed with averaging times between 30 and 180 min.
- Due to the short averaging times the representativeness of these measurements for a larger area is restricted, the sampling error is the largest contribution to the error budget.
- The magnitude and the observed diurnal variation of measured fluxes is very plausible, estimates using indirect methods yielded similar values.
- The actual range of 450 to 675 m where measurements could be performed was rather restricted due to technical problems in both the DIAL and the Radar/Rass systems.

It is concluded that the first measurements of turbulent fluxes of water vapor in the boundary layer using active remote sensing techniques showed satisfactory results. Due to the large difficulties in

adjusting and operating the DIAL system properly no further measurements have been completed successfully. But in order to make this technique valuable for flux measurements it is most important that they can be extended over long periods of time and be repeated under similar conditions, in order to reduce the sampling error. The latter point is a principal problem for measurements of rather large scale turbulence structures performed at a fixed location, because one has to rely on the mean horizontal wind to provide for transport of the atmospheric features across the measurement system. The necessity of performing long-term observations calls for a system which is easy to adjust and to operate reliably. This could in no way be achieved for the dye laser system, mainly because of problems with stability and proper adjustment. For this reason, and to achieve better absolute accuracy, a new laser system has been developed, for which high reliability and stability was a major design goal. This development has now been completed as far as the laser operation is concerned, but the lifetime for some of the components still has to be increased.

Further requests for improvements are mainly concerning resolution, in order to extend the measurements at atmospheric conditions where smaller eddy sizes prevail, e.g. for shear generated turbulence. Improvements of resolution are actually expected from an increase of laser power as well as from a telescope with larger aperture. In detailed studies it has to be found out which combination of vertical and temporal resolution is best suited for flux measurements. This is important because the statistical error of the water vapor retrieval has a much stronger dependence on vertical than on temporal resolution. It should be noted here that in the Rass measurements of the vertical wind a better resolution is achieved now.

The increase of altitude range is also desired in order to determine the entrainment flux at the top of the boundary layer from the height dependence of the latent heat flux.

Whether or not a direct flux determination at the top of the boundary layer is possible still has to be studied in detail. First attempts to measure the ozone flux across the peplopause gave evidence that serious problems occur due to particularly large sampling errors in this case. This restriction is not caused by the remote sensing technique we have applied, but rather by the special flow pattern which is found in this part of the troposphere.

E.2.2. Measurements performed with a newly developed solid state layer system

Because the measurements performed with the dye laser system had established that the main source of error was associated with the inadequate spectral properties of this laser, a new laser system was developed which meets all the stringent requirements regarding spectral purity, narrow bandwidth, and frequency stability. This laser system also provides sufficient pulse energy to facilitate both high resolution measurements in the boundary layer and long range measurements of mean profiles up to the upper troposphere. In Table E.1 the demonstrated laser properties are compared to the requirements for accurate water vapor and temperature measurements throughout the troposphere. This is the first laser system meeting all requirements for accurate DIAL meas-

urements involving narrow water vapor or oxygen lines, including the demand for excellent spectral purity.

To achieve the required spectral properties and the necessary output energy the following design features are deemed necessary and have proven successful:

- Separation of the laser system into two subsystems according to the so-called MOPA-concept (Master Oscillator - Power Amplifier).
  - master oscillator operating in the continuous wave (cw) mode at comparatively low power; tunable, frequency stabilized, single mode operation (both longitudinal and transversal), with high spectral purity
  - power amplifier operating in pulse mode, injection seeded by the master oscillator, operating on maximal 2, preferably only one longitudinal mode;
- use of tunable solid state laser material
  - Ti: sapphire in the master oscillator
  - Alexandrite in the power amplifier
- construction as a uni-directional ring resonator with optimized cavity design
- sufficient seed power
- coupling of the seeder into the power amplifier via a polarizer, matched to the Packels cell for Q-switching.

Table E.1: Requirements regarding the laser transmitters for a water vapor and a temperature lidar with an error caused by laser performance of less than 5% and 1K, respectively.

Parameter	Requirements		Laser performance
	H_2O	T	
Wavelength λ/ nm	720 - 730	767 - 771	720 - 780
line width (FWHM) / MHz	< 500	< 200	160 (26)
frequency stability (1 σ) / MHz	± 210	± 50	43 (15)
spectral purity	> 0.995	> 0.999	> .999
pulse length / ns	≤ 200		≤ 200
beam divergence / mrad	≈ 1		0.45
pulse energy / mJ	≈ 50		≈ 50
repetition rate / Hz	> 10		≈ 20
on-off-separation, t_{on} - t_{off} / ms	≈ 1		≈ 50

The separation of the laser system into two subsystems, master oscillator and power amplifier, has the advantage that the necessary narrowing of bandwidth, passive and active stabilization of wavelength and excellent spectral purity can be achieved relatively easy and reliably in a cw laser compared to a high power pulsed laser. The technique of injection seeding provides for maintaining these properties during amplification to the required peak power in the pulsed amplifier, if

both systems are carefully matched. Both lasers operate as uni-directional rings and use solid state laser materials only to provide wavelength, stability and spectral purity. Two different laser crystals are used, a titanium doped sapphire pumped by an Argon ion laser in the master, and a flash-lamp pumped Alexandrite rod in the power amplifier. The details of this design and an extensive study of possible variants are described by Wulfmeyer (1995).

To illustrate the accuracy which can be reached when this new laser system is used for DIAL measurements Table E.2 summarizes the results of two actual measurements (Wulfmeyer, 1995). For that one performed in the lower troposphere data from a locally launched radiosonde (Vaisala RS80) were available for intercomparison. Here the observed differences between lidar and radiosonde are smaller than the error margin of the sondes, so these values should not be interpreted as lidar measurement errors.

Table E.2: Maximum and mean random error $\max(\sigma_\rho)$ and $\overline{\sigma}_\rho$, and maximum and mean difference between lidar and sonde $\max(\Delta\rho)$ and $\overline{\Delta}_\rho$ for two test measurements performed with the new lidar system. R_{max} is the maximum Range, ΔR the range resolution, and Δt the temporal resolution of these measurements.

R_{max}	ΔR	Δt	$\max(\sigma_\rho)$	$\overline{\sigma}_\rho$	$\max(\Delta\rho)$	$\overline{\Delta}_\rho$
2 km	45 - 225 m	15 min	0.14 g • m^{-3}	0.04 g • m^{-3}	0.3 g • m^{-3}	0.1 g • m^{-3}
5.5 km	300 - 900 m	15 min	0.04 g • m^{-3}	0.02 g • m^{-3}	-----	-----

For the measurements in the upper troposphere up to now no suitable data for intercomparison were available. An assessment of accuracy for this range was made indirectly by determining the humidity within optically thin clouds.

The water vapor density within a thin altostratus of little more than 300 m depth at an altitude of 5 km was determined as 1.4 ± 0.2 g m^{-3}. The saturation vapor density at the cloud temperature estimated from a radio sonde ascent started in Kiel was 1.5 g m^{-3}, showing excellent agreement. A similar experiment for a cirrus extending from 8 to 10.5 km altitude gave a result of 0.054 ± 0.003 g m^{-3} for 9 km height. The saturation vapor density (over ice) averaged over the height range used for the lidar retrieval (18250 m to 9750 m) was calculated as 0.052 ± 0.004 g m^{-3}. The error margin was caused by the uncertainty of the temperature profile, which had not been measured at exactly the same location. Further details of these measurements may be found in Wulfmeyer (1995). The results clearly show that excellent accuracy can be reached with this lidar in upper tropospheric measurements, too.

The reason for these measurements being more accurate than all previously published water vapor DIAL results is attributed mainly to the fact, that the new laser system used here is the first one meeting all requirements which have been deduced from a rigorous treatment of the methodology.

E.3. Impact of the Rayleigh-Doppler-correction

From the rather few measurements of the water vapor distribution using the DIAL technique it cannot be derived how much the uncertainty of the Rayleigh-Doppler-correction affects the accuracy of the results in a statistical sense. Nevertheless, an estimate of the probability distribution of the error caused by Rayleigh-Doppler-broadening can be obtained by making use of a large number of backscatter lidar measurements which have been performed in this wavelength region. From this large data set the statistical distribution of the quantity dS_K/dR can be derived. This can then be used in conjunction with the sensitivity factors calculated in section B.5 to estimate a statistical distribution of the errors caused by Rayleigh-Doppler-broadening.

E.3.1. Investigation of typical aerosol distributions

The statistical distribution function for the gradient of the inverse scattering ratio dS_K/dR was derived from evaluations of a large set of backscatter lidar measurements obtained during the International Cirrus Experiment ICE '89 which was conducted in September/October 1989 on the island of Sylt. Twenty-one individual cases were analyzed, corresponding to 27 hours of observations or more than 3000 individual profiles. The meteorological conditions covered a broad range from persistent high pressure conditions with little cloud cover to cold air outbreaks associated with strong convection and heavy showers. The actual cloud regions were discarded for the evaluation.

For the purpose of this study four regions of the atmosphere were distinguished: planetary boundary layer (PBL), entrainment zone (EZ), lower (LFT) and upper (UFT) free troposphere. The heights of the different regions were deduced from the measured temporal-spatial distribution of the aerosol backscatter. Not in all cases this can be performed correctly, e.g. because not always an entrainment zone exists. But for the purpose of this study just a coarse division into certain atmospheric regions was attempted. In this context that region of the atmosphere was called entrainment zone where strong aerosol gradients occurred at the transition from the more or less well mixed boundary layer to the usually much cleaner free troposphere.

For the retrieval of the inverse scattering ratio S_K the analytical inversion as described by Fernald (1984) was applied, mostly in the backward integration mode because of the much better numerical stability. In some cases no homogeneous region suitable for calibration in the far range was existent, in those cases at least for part of the range forward integration was used. The lidar ratio was assumed as $S_L = 35\ sr^{-1}$ in the PBL and free troposphere, and $S_L = 10$ in cirrus. When forward integration was applied smaller values were used to stabilize the solution. The quantity dS_K/dR was calculated directly from the retrieved vertical distribution of S_K.

The raw data were acquired with a vertical resolution of 7.5 m and a temporal resolution of 10 s, for the evaluation this was mostly averaged to 90 m and 30 s. For most cases in the lower tropo-

sphere this was sufficient to suppress the noise to an acceptable level. For upper tropospheric measurements this kind of averaging is sufficient in cirrus only, in the remaining part where molecular scattering dominates much more averaging is necessary. Therefore, a homogeneous treatment of a scene containing both cirrus and cloud-free regions does not make much sense. In the cloud-free upper troposphere the aerosol backscatter coefficients could not be determined with sufficient accuracy, the result is strongly dependent on the assumptions to be made for the scattering ratio at the calibration height. But from the raw backscatter data it could be concluded that generally no large values of dS_K/dR can be expected, with the exception of occasionally observed aerosol layers. For these reasons no distribution of dS_K/dR was compiled for the upper troposphere.

The aerosol gradients observed in cirrus can best be illustrated using an example. Figure E.3 shows the range corrected lidar signal from more than 4 hours of measurements when a cirrus deck in the altitude range 7.5 to 11.5 km approached the site. In this figure the time resolution is 18 s and the vertical resolution 30 m.

Within the cloud many small-scale structures are clearly visible. Figure E.4 shows the gradient of the inverse scattering ratio dS_K/dR for the same case. The resolution was reduced to 90 m, corresponding to the interval used for calculating the gradient. At this high resolution in the cloud-free area only noise with very large variability is observed. With the exception of cloud boundaries, where extremely large values of dS_K/dR occur (in this case up to $1 \cdot 10^{-2}$ m^{-1}) which are still limited by the resolution, inside the cirrus only rather small values of less than $1 \cdot 10^{-4}$ m^{-1} are observed. This results in a Rayleigh-Doppler-correction of the retrieved absorption coefficient of less than $1 \cdot 10^{-5}$ m^{-1} inside the cirrus. The term [G2] is not important in the cirrus region, since $S_K < 1 \cdot 10^{-2}$. At the cloud boundaries [G1] assumes very large values, here it is not really feasible to obtain accurate measurements.

Figure E.5 shows as an example an evaluation of lower tropospheric measurements up to 3000 m altitude. the strong aerosol gradient at the top of the boundary layer is clearly visible, mostly around 2400 m height. During 20 to 80 min after the start of the measurements the PBL reaches much higher, up to about 2800 m. But also in the height region below the PBL top, beyond about 1400 m some persistent aerosol layer and associated boundaries can be distinguished. This region, where at least for some time mixing with free tropospheric air may have occurred, has been classified as entrainment zone for this study, although this does not correspond to the classical case of entrainment due to convective mixing at the top of the PBL. In the present study that region at the top of the PBL was generally classified as entrainment zone EZ, where particularly strong aerosol gradients occurred. Only the apparently well mixed region was classified as boundary layer PBL. The reason for this way of classification is that the Rayleigh-Doppler-correction assumes large values in a small region around layer boundaries only, while it is much smaller in the large regions which are much more homogeneous.

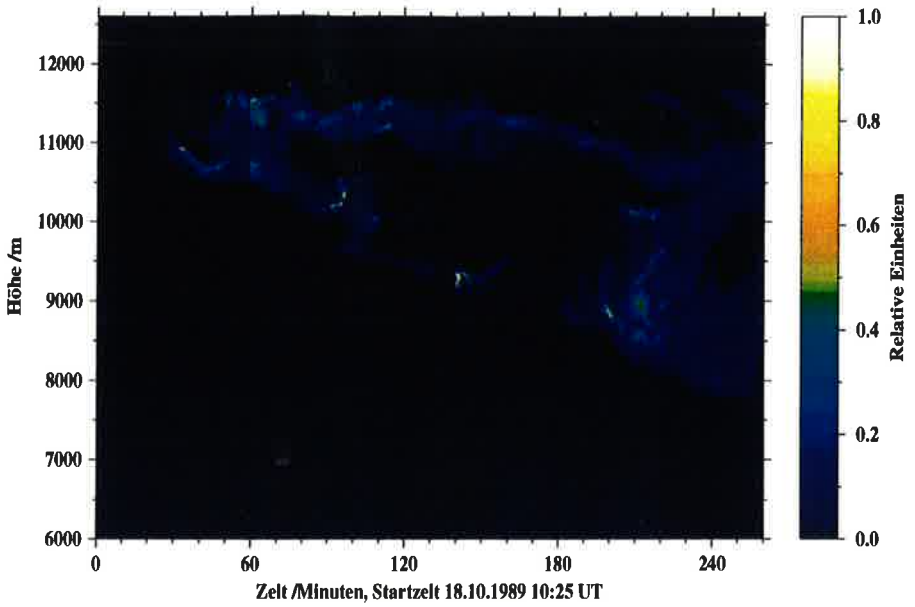

Figure E.3: Range corrected lidar signal, ln ($P \cdot R^2$). λ = 728 nm, ΔR = 30 m, ΔT = 18 s.

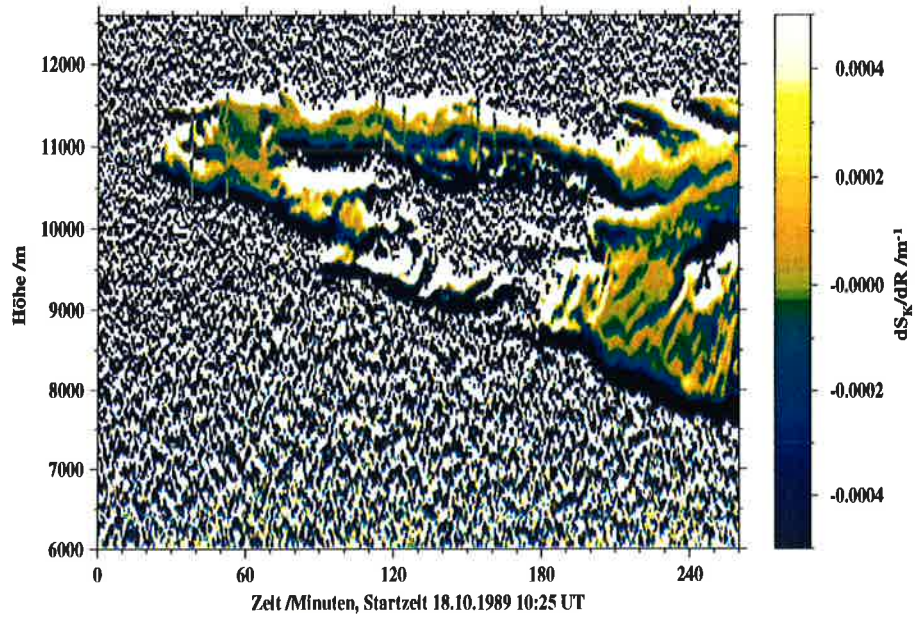

Figure E.4: Gradient of the inverse scattering ratio dS_K/dR. λ = 728 nm, ΔR = 30 m, ΔT = 18 s.

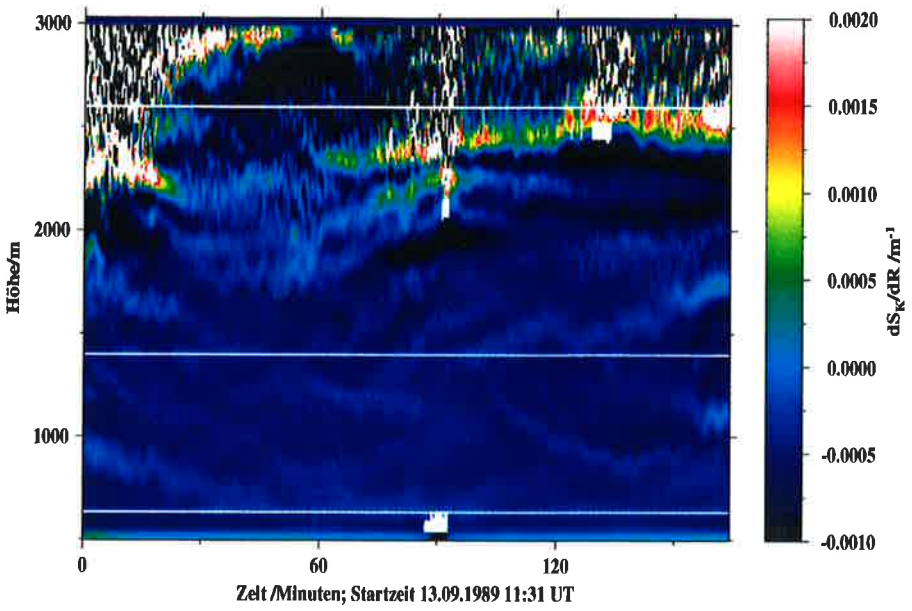

Figure E.5: Gradient of the inverse scattering ratio dS_K/dR. $\lambda = 728$ nm, $\Delta R = 30$ m, $\Delta T = 18$ s.

The distribution of dS_K/dR for the complete data set is presented in Figures E.6 and E.7 as cumulative distribution functions for each classified region. In the evaluation of so many data it could not be avoided that outliers were included in the analysis, caused by e.g. small clouds or short interruptions of the measurements. These outliers corresponding to much less than 3% of the measured points have been removed a posteriori from the distribution.

The distribution functions as shown in the figures clearly deviate from Gaussian distributions, obviously the wings are much more pronounced. The limits for 68% and 95% confidence are indicated in the figures, the observed values for these confidence levels are summarized in Table E.3.

Table E.3: Confidence intervals for dS_K/d_R, numbers in units of m^{-1}.

Atmospheric region	68% confidence interval		95% confidence interval	
boundary layer	$- 1.3 \cdot 10^{-4}$	$+ 1.7 \cdot 10^{-4}$	$- 5.4 \cdot 10^{-4}$	$+ 5.4 \cdot 10^{-4}$
entrainment zone	$- 2.2 \cdot 10^{-4}$	$+ 8.9 \cdot 10^{-4}$	$- 9.3 \cdot 10^{-4}$	$22.8 \cdot 10^{-4}$
lower free troposphere	$- 2.2 \cdot 10^{-4}$	$+ 2.0 \cdot 10^{-4}$	$- 12.0 \cdot 10^{-4}$	$+ 3.8 \cdot 10^{-4}$

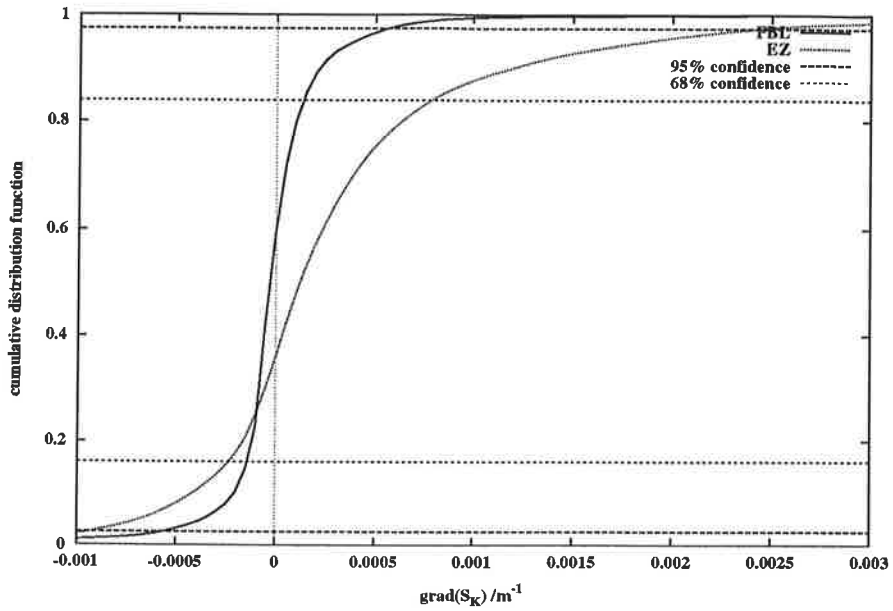

Figure E.6: Cumulative distribution function of dS_K/d_R for the boundary layer (PBL) and the entrainment zone (EZ)

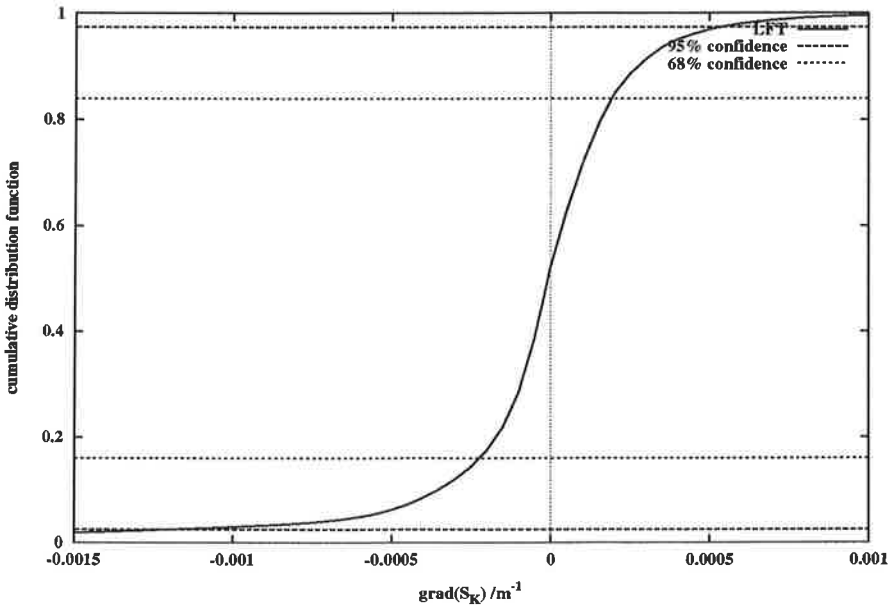

Figure E.7: Cumulative distribution function of dS_K/d_R for the lower free troposphere.

Apparently the gradients of the inverse scattering ratio are smallest in the well mixed boundary layer. For studies involving only mean profiles the 68% confidence intervals may be considered appropriate, where the gradients remain smaller than about $1.5 \cdot 10^{-4}$ m^{-1}. For studies in which the wings of the distribution can be important, e.g. those involving the cross-correlation with the vertical wind for deriving the latent heat flux, the 95% limits are certainly better suited. Within the PBL this interval of about $\pm 5.4 \cdot 10^{-4}$ m^{-1} is rather small, too. Applying the sensitivity factor [E1] derived in section B.5, [E1] $\approx$ 0.1, the correction term [G1] with 65% probability remains less than 1.5 ± 10^{-5} m^{-1} and with 95% probability smaller than $5.4 \cdot 10^{-5}$ m^{-1}. It is difficult to make a general assessment of error margins for the retrieval of S_K and dS_K/dR, because these errors largely depend on estimated aerosol properties needed as input parameters for the inversion. For many cases 30% error is probably a realistic assumption. If this value is adopted the resulting error in the retrieved absorption coefficient due to the incomplete Rayleigh-Doppler-correction is $< 0.5 \cdot 10^{-5}$ m^{-1} and $1.6 \cdot 10^{-5}$ m^{-1}, respectively. For boundary layer measurements an absorption line should be selected with an absorption coefficient of about $1 \cdot 10^{-3}$ m^{-1}, hence the error due to Rayleigh-Doppler-broadening may be neglected in most cases. Application of the correction, however, is advised at least for correlation studies, since errors of more than 5% in about 5% of the samples can have a large impact on correlation products.

The latter is particularly true when measurements in the entrainment zone at the top of the boundary layer are involved. Without correction the error will be larger than $9 \cdot 10^{-5}$ m^{-1} for 32% of the samples and with 5% probability greater than $22 \cdot 10^{-5}$ m^{-1}. For detailed process studies this level of error is not tolerable. When the correction is applied the errors can at least be kept below 10%.

In the lower free troposphere the error margins for 68% confidence are rather small again, about $0.7 \cdot 10^{-5}$ m^{-1}, but the 95% interval is much more extended in particular towards negative gradients. When the correction is applied errors should generally stay below $2 \cdot 10^{-5}$ m^{-1}, but considering the generally low humidity in this region this may already cause some noticeable restriction of accuracy. A summary of these results is presented in Table E.4. Here it is assumed, strongly simplifying actual measurement situations, that the absorption coefficient of water vapor amounts to $1 \cdot 10^{-3}$ m^{-1} for PBL measurements and $1 \cdot 10^{-4}$ m^{-1} for measurements performed in the free troposphere. The sensitivity factors were chosen as [E1] = 0.1 in the PBL and [E1] = 0.05 in the FT. This simplification was necessary to show some consistent estimates for the achievable accuracy. For the analysis of individual cases, however, detailed calculations have to be performed according to the theory presented in section B.

From the examples shown above and in particular from the statistical investigation it becomes apparent that the spectral broadening for the Rayleigh-scattered part of the backscatter is important for all measurements involving narrow absorption lines. This effect can well be the major source of error. The accuracy which can be achieved is thus strongly dependent on the accuracy of the aerosol retrieval which is necessary to perform the correction. The experience gained in the evaluation of a large number of lidar backscatter measurements suggests, however, that at least for meteorologically interesting situations involving complex aerosol and/or cloud distribution the

necessary inversion of lidar data is very difficult to perform with the required level of accuracy.

Table E.4: Confidence intervals for the relative error of water vapor retrievals due to incomplete Rayleih-Doppler-correction.

Atmospheric region	68% confidence interval		95% confidence interval	
boundary layer	- 0.004	+ 0.005	- 0.016	+ 0.016
entrainment zone	- 0.007	+ 0.027	- 0.028	+ 0.068
lower free troposphere	- 0.033	+ 0.030	- 0.180	+0.057

E.4. Comparison with other methods, in particular Raman-lidar

For investigations of the atmospheric water vapor distribution with high temporal and spatial resolution not only the DIAL technique, but also the Raman-lidar has to be considered. In the latter the Raman-scattering at water vapor and nitrogen (or oxygen) is used to determine directly the water vapor mixing ratio. This technique is already well-developed (Whiteman et al. 1992; Ansmann et al., 1992a; Eichinger et al., 1994; Goldsmith et al., 1994).

For the assessment of performance of a Raman-lidar one has to distinguish night-time and daytime operation. The main source of error is the noise induced by the background light that can generally not be suppressed efficiently because of the width of the Raman-spectrum. In Table E.5 the performance of the state-of-the-art Raman-lidar (Goldsmith and Bisson, 1995) for day- and night-time operation is summarized.

Table E.5: Statistical error of Raman-lidar measurements. Night-time measurements according to Goldsmith and Bisson (1994), daytime measurements according to Goldsmith and Bisson (1995).

	R_{max}	ΔR	Δt	max (σ_ρ)/g/kg
Night	7 km	75 m	10 min	0.2 - 0.3
	5 km	75 m	10 min	0.07 - 0.17
	3 km	75 m	10 min	0.03 - 0.06
Day	1 km	75 m	10 min	0.2
	2 km	75 m	10 min	0.3
	3 km	75 m	10 min	0.6
	4 km	75 m	10 min	1.3

Both systems used in these measurements (Sandia Livermore and NASA GSFC, Goldsmith et al., 1994) were rather big and powerful, the product of transmitted power (18 W) and receiver aper-

ture (0.76 m diameter) was 8.17 Wm^2 (for comparison: this product is 0.02 Wm^2 for the MPI DIAL system). Another Raman-lidar, which is specialized for high resolution daytime measurements, reaches a power-aperture product of 10.1 Wm^2 at a wavelength of 248 nm (Eichinger et al., 1994). Because of the strong ozone absorption in this spectral region the range of this system is restricted to 450 m. A resolution of 3 m and 0.1 s is claimed, but for close ranges only (not specified in detail). The advantage of Raman-lidars with respect to high range resolution is clearly demonstrated here. For this particular system, however, detailed assessment of accuracy for the high resolution measurements was not presented, averages agree to about 5% with standard in situ measurements. This can definitely not be expected to hold generally, as will be illustrated in section H addressing ozone measurements. However, for investigations requiring very high resolution at short range this can be an interesting method, provided that the ozone interference problem can be solved, e.g. by simultaneous ozone measurements with the same system. A detailed study on this subject still has to be performed.

For the present status of Raman-lidar performance it can be summarized, that the combination of accuracy, resolution, and range for night-time measurements is exceeding the performance of DIAL systems. E.g. a height resolution of 75 m in 10 min time in the upper troposphere does not appear feasible for DIAL measurements, at least if the system is ground-based and has to penetrate some extended boundary layer typically containing much water vapor.

For daytime measurements, however, the situation is completely different. For the Raman-lidar mentioned above, where performance has been verified, measurements performed in the boundary layer showed a random error of 0.22 g m^{-3} corresponding to 5% for 10 min average and 75 m vertical resolution. The new MPI-DIAL reached 0.05 g m^{-3} at the same resolution, hence about 4 times better performance. Above about 2.5 km daytime Raman-measurements showed an error of > 1 g m^{-3} due to background noise, which makes them not very useful for atmospheric studies. For the DIAL system, however, measurements at 5 km height with an error < 0.03 g m^{-3} have been performed with a range resolution of 900 m.

These examples show very clearly that for daytime operation even a rather small DIAL system can outperform a large Raman-lidar. The capabilities of the MPI-DIAL can still be improved considerably, e.g. by installing a larger telescope (doubling of the telescope diameter results in 4 times shorter measurement time). Whether or not the laser output power can be much increased still has to be investigated. In any case at least a second laser for the generation of the second wavelength could be installed, thus doubling the effective pulse rate and, correspondingly, the temporal resolution.

Passive techniques for water vapor retrievals have been studied for a long time already. For quite some time they will probably be the only ones which are applicable for space-borne measurements and hence the only ones to provide global data sets. A detailed study of space-borne techniques has been performed by Schlüssel (1995). According to this about two layers can be resolved, e.g. total water vapor content and content of the lowest 500 m, with an accuracy of about

0.15 m^{-2} for the total content and 1 g/kg for the specific humidity of the lowest 500 m. So the advantage of global coverage comes with the disadvantage of poor height resolution.

Rather limited height resolution is also found for ground-based passive remote sensing of humidity, about 500 m resolution is reached at best (Feltz, 1994). The accuracy is specified as 3K in dewpoint temperature, corresponding to roughly 20% error in relative humidity.

It can be concluded that high resolution measurements as required for process studies can only be provided through active remote sensing techniques. The DIAL technique appears to be particularly suited for daytime measurements, both for high resolution measurements in the boundary layer and for measurements with medium resolution throughout the troposphere.

F Temperature measurements

Temperature is one of the key parameters describing the state of the atmosphere, hence remote sensing techniques for temperature profiling are very welcome. However, several techniques for this purpose are already well established, mainly passive remote sensing techniques for satellite retrievals of temperature profiles with global coverage. A real need exists for measurements with high vertical and temporal resolution for process studies as well as for measurements with high accuracy. For global measurements the design goal is about 1K uncertainty, for process studies the requirements are generally higher.

The use of the DIAL technique for temperature profiling has been suggested rather early (Mason, 1975), and subsequently studied in theory (Schwemmer and Wilkerson, 1979; Korb and Weng, 1979; Mégie, 1980; Korb and Weng, 1982). This technique is based on the temperature dependence of the absorption by an atmospheric gas of known mixing ratio. As suitable gases, water vapor (only if an additional measurement of its density is performed simultaneously, which clearly limits the achievable accuracy) and in particular oxygen have been suggested. The mixing ratio of oxygen in ambient air is assumed to be constant to a high degree of accuracy. Although the suggested absorption lines are very narrow (see figure B.1) in the above mentioned theoretical studies the influence of Doppler-broadened Rayleigh-backscatter has not been considered. This was first introduced in a detailed study by Theopold and Bösenberg (1993). They have shown that the possible errors caused by this effect may indeed set the limits to the achievable accuracy. Experimentally this could only be confirmed using two short examples. Now here the general formalism developed in chapter B shall be used in conjunction with the statistical investigation of aerosol distributions described in chapter E to estimate the expected accuracy for a broader range of applications.

F.1. Basic theory of temperature measurements based on the DIAL technique

It has already been explained that with the DIAL technique the primary result is a profile of a differential absorption coefficient, which is a function of gas density, pressure, and temperature. Since the profiles of pressure and temperature are coupled through the barometric height equation, it is possible to derive the temperature from the absorption coefficient if the gas density is known. Oxygen (O_2) is particularly suited as an absorbing gas, because its mixing ratio in dry air is assumed to be constant in the lower atmosphere (20.95%), and because it has suitable temperature dependent absorption lines in readily accessible spectral regions. According to Korb and Weng (1982) the absorption coefficient is given by:

$$\alpha_{O_2}(\nu) = q_{O_2}(1 - q_{H_2O}) \cdot C \frac{p}{k_B T^2} \exp\left(-\frac{\varepsilon}{k_B T}\right) \cdot \Lambda(\nu, p, T)$$

$$C = \frac{S_0 \cdot T_0}{k_B} \cdot \exp\left(\frac{\varepsilon}{k_B T_0}\right) \tag{F.1}$$

when q_{O_2} and q_{H_2O} are the volume mixing ratios of oxygen and water vapor, respectively, k_B is the Boltzmann constant, S_0 the line strength and ε the ground state energy of the transition, ν the wave number of the absorbed radiation, Λ (ν, p, T) the absorption lines function (e.g. a Voigt profile), and T_0 the temperature at standard conditions.

The nonlinear relation (F.1) between the measured absorption coefficient and the temperature is best resolved using an iteration technique, since the exponential term is predominant under the prevailing conditions (Korb and Weng, 1982).

$$T_{i+1} = \frac{\varepsilon / k_B}{\ln C q_{O_2} \Lambda(T_i) - \ln k_B T_i^2 / p} \tag{F.2}$$

For typical experimental conditions the iteration converges within very few steps. In addition it has to be considered that a priori the pressure p is not precisely known as a function of height. For ground based applications an additional pressure measurement at ground level is easily performed, for satellite- or airborne applications climatological values or the analysis from the weather service has to be used. However, the sensitivity of the temperature retrieval with respect to the atmospheric pressure is relatively small, and the retrieved temperature profile can be used in an iteration procedure to improve the assumed pressure profile using the hydrostatic equation. The analysis of this procedure performed by Korb and Weng (1982) showed that the remaining errors are < 0.1 K in the lower and < 0.3 K in the upper troposphere. For most applications this level of uncertainty appears to be tolerable.

The temperature dependence of the absorption cross section at the line center is given by

$$\frac{d\alpha_{O_2}(\nu)}{\alpha_{O_2}(\nu)} = \frac{dT}{T}\left[\frac{\varepsilon}{K_B T} - \frac{5}{2} + \Xi(\Lambda)\right] \tag{F.3}$$

where $\Xi(\Lambda)$ is dependent on the actual absorption line function (see Theopold, 1990). We have $\Xi(\Lambda) = 0$ for pure Doppler-broadening and $\Xi(\Lambda) = 1$ for pure pressure broadening. The temperature sensitivity is proportional to the ground state energy of the transition. But the line strength is also dependent on the ground state energy, resulting in a decrease of line strength with increasing ground state energy, since the corresponding states are less occupied. When choosing an absorption line a compromise between line strength and temperature sensitivity has to be found. Table

F.1 shows as an example three suitable lines for different maximum range. Here R_{max} is the altitude where the optical depth for a ground based measurement is $\tau\ (R_{max}) = 1$. For these lines the temperature sensitivity is between 1.4 and 2.4% K^{-1}. This clearly shows that in order to achieve a useful accuracy for the temperature retrieval (say < 1 K) a very high precision of the determination of the absorption coefficient is required. Hence all effects have to be considered in detail which can affect the transmission of light through the atmosphere.

Table F.1: Line parameters for selected oxygen absorption lines. Values are taken from the HITRAN-data base (Rothman, 1987), except for the values for the line strength S_0 and the collision broadening halfwidth b_c^0, which were taken from Ritter (1987).

Line	ν_{on} (cm^{-1})	$S_0 \cdot 10^{25}$ $cm^2\ mol^{-1}\ cm^{-1}$	b^0_c (cm^{-1})	ε (cm^{-1})	R_{max} (km)	γ (% K^{-1})
$^P P_{27,27}$	13010.812	2.21	0.0371	1085.206	1.3	1.4
$^P P_{29,29}$	12999.959	1.08	0.0362	1248.204	2.9	1.7
$^P P_{31,31}$	12988.728	0.429	0.035	1422.502	10.9	2.4

Up to now the laser properties were very important in the error analysis of actual measurements. In particular the very demanding requirements with respect to wavelength stability, narrow bandwidth, and high spectral parity could not be met. With the development of the new laser described in chapter E this source of error can now be excluded, so the main source of systematic errors now is the incomplete Rayleigh-Doppler-correction. This will be studied in detail in the following.

F.2. Sensitivity of temperature retrievals to the Rayleigh-Doppler-correction

Detailed inspection of this correction in section B.5 had revealed that the correction term [G] which accounts for the Doppler-broadening of the Rayleigh-backscatter in regions of spatially inhomogeneous aerosol distribution can be written as:

$$[G] \equiv [G1] + [G2] \equiv [E1] \cdot \frac{dS_K}{dR} + [E2] \cdot S_K \quad .$$

The sensitivities [E1] and [E2] have been studied in section B.5.1 for two oxygen lines $^P P_{27,\,27}$ and $^P P_{31,\,31}$ under conditions of the US standard atmosphere.

In section E.3 a statistical distribution of the quantity dS_K/dR was introduced, which is based on measurements at a wavelength of $\lambda \approx 725$ nm. This statistical distribution can also be used to estimate the errors in a temperature retrieval, since dS_K/dR is only weakly wavelength dependent. For convenience Table F.2 repeats the confidence limits for the distribution of dS_K/dR for several atmospheric regions.

Table F.2: Confidence limits for dS_K/dR in m^{-1}.

Layer	68% confidence interval		95% confidence interval	
boundary layer	$- 1.3 \cdot 10^{-4}$	$+ 1.7 \cdot 10^{-4}$	$- 5.4 \cdot 10^{-4}$	$+ 5.4 \cdot 10^{-4}$
entrainment zone	$- 2.2 \cdot 10^{-4}$	$+ 8.9 \cdot 10^{-4}$	$- 9.3 \cdot 10^{-4}$	$22.8 \cdot 10^{-4}$
lower free troposphere	$- 2.2 \cdot 10^{-4}$	$+ 2.0 \cdot 10^{-4}$	$- 12.0 \cdot 10^{-4}$	$+ 3.8 \cdot 10^{-4}$

For the estimation of errors in temperature retrievals in different atmospheric regions it was assumed that boundary layer measurements are typically made at 600 m altitude using the $^{P}P_{27,\,27}$-line, and measurements in the lower free troposphere at 3000 m altitude using $^{P}P_{31,\,31}$. These are very reasonable parameters for typical measurement situations in these regions.

The results obtained with these assumptions for the correction term [G1] and the resulting error in the temperature retrieval assuming a 30% error in the retrieval of dS_K/dR are summarized in Table F.3. Possible errors caused by the term [G2] have been neglected.

The table demonstrates very clearly, that only in the well mixed boundary layer acceptable accuracies can be achieved, but even then only if the 68% confidence limits for an uncertainty of < 1 K are deemed appropriate. For process studies rather the 95% confidence limits should be used. If this is required, the accuracy is not sufficient in any atmospheric region. The conclusion from this statistical investigation is that the DIAL technique in its present form is of limited usefulness only for atmospheric temperature profiling.

Table F.3: Confidence limits for the correction term [G1] in m^{-1} and the error in temperature retrievals in K. For the conditions see text.

Layer	68% confidence interval		95% confidence interval	
correction term [G1] / m^{-1}				
boundary layer	$- 3.3 \cdot 10^{-5}$	$+ 4.3 \cdot 10^{-5}$	$- 13.5 \cdot 10^{-5}$	$+ 13.5 \cdot 10^{5}$
entrainment zone	$- 1 \cdot 10^{-4}$	$+ 4 \cdot 10^{-4}$	$- 5 \cdot 10^{-4}$	$11 \cdot 10^{-4}$
lower free troposphere	$- 4 \cdot 10^{-4}$	$+ 4 \cdot 10^{-5}$	$- 2.0 \cdot 10^{-4}$	$+ 8 \cdot 10^{-5}$
temperature retrieval/K				
boundary layer	- 0.8	1.1	- 3.4	3.4
entrainment zone	- 2.5	10.1	- 12.7	27.9
lower free troposphere	- 5.0	5.0	- 24.8	9.9

G. DIAL modification to avoid the Rayleigh-Doppler-correction

The previous studies of water vapor and particularly temperature retrievals have demonstrated very clearly that the Rayleigh-Doppler-correction is a major cause of limited accuracy for measurements involving narrow absorption lines in the near IR. It can not be expected that dS_K/dR can be measured with significantly improved accuracy as long as it is determined in a simple backscatter experiment the solution of which is under-determined.

The problem of the Rayleigh-Doppler-correction is caused by the fact, that the two contributions to backscatter, molecular and particulate scattering, have significantly different spectra. Hence it can be avoided if not only the transmitter but also the receiver has sufficiently narrow bandwidth such that the details of the spectral distribution need not be considered. For the laser and hence the propagation from the lidar to the scattering volume this problem has already been treated. In section B.5 it has been shown, e.g., that an error of < 2% in the absorption cross section can be achieved if the laser line width is smaller than 15% of the absorption line width. Of course the same applies for the propagation from the scattering volume to the receiver, where in this case the receiver bandwidth has to be as narrow as necessary to determine the effective absorption cross section. In order to make water vapor measurements sufficiently independent of the Rayleigh-Doppler-correction a filter width (FWHM) of about $b_F < 0.01$ cm^{-1} $\triangleq$ 300 MHz is required, for temperature measurements this would be $b_F < 0.003$ cm^{-1} $\triangleq$ 90 MHz. Such small filter widths can be achieved using different interferometric methods. On the one hand either a Fabry-Perot or a Michelson-interferometer with correspondingly small bandwidths can be used with subsequent direction detection of the transmitted photons. A second possibility is the use of coherent or heterodyne detection, where the backscattered radiation is mixed with the wave field from a local oscillator, resulting in a signal having the difference frequency of the two waves. This detection technique has long been used in Doppler-lidars for wind measurements, where just the Doppler-shift of the backscattered light is used to determine the velocity of the aerosol particles which are carried along with the wind.

In principle both techniques require the same performance of the optics and adjustments, the wave fronts have to be maintained to a sufficient degree of accuracy to provide for homogeneous interference patterns. The main difference is the use of a local oscillator in the heterodyne technique instead of different parts of the backscattered light for the direct techniques. An important consequence of this use of a local field instead of the received field is that the detector signal is proportional to the amplitude of the backscattered wave rather than its intensity as for the direct detection. This results in a major reduction of signal dynamics, e.g. because the amplitude is proportional to R^{-1} while the intensity goes with R^{-2}. This is an important advantage, since the dynamic range of the signal causes serious problems in all DIAL applications.

Another important difference between the two detection schemes is that for the heterodyne detection the interference pattern of the backscattered waves in the detection plane has to be consid-

ered. Formally that can be done to good approximation by introducing the "effective" receiver area A_{het}, where

$$\frac{1}{A_{het}} = \frac{1}{\eta_{ant}}\left(\frac{1}{A_T} + \frac{1}{A_R} + \frac{1}{A_\rho}\right). \tag{G.1}$$

Here η_{ant} is an antenna loss factor, and

$$A_T = \frac{2\pi b_T^2}{1+N_T^2} \qquad A_R = \frac{2\pi b_R^2}{1+N_R^2} \tag{G.2}$$

describe the areas where the phases of the transmitted respectively local oscillator beams are sufficiently constant to produce homogeneous interference patterns. N_T and N_R are the Fresnel-numbers for focusing at u_T and u_R, respectively, and b_T and b_R are the Gaussian beam radii of the transmitted and the reference beams, where we have

$$N_T = \frac{\pi b_T^2}{\lambda}\left(\frac{1}{u_T} - \frac{1}{R}\right) \qquad N_R = \frac{\pi b_R^2}{\lambda}\left(\frac{1}{u_R} - \frac{1}{R}\right). \tag{G.3}$$

The effect of turbulent refractive index modulations within the propagated beam is approximately accounted for by the term $1/A_\rho$, with

$$A_\rho = \pi \cdot (0.545\, k^2 R C_n^2)^{-6/5}, \tag{G.4}$$

where C_n^2 is the structure constant of the turbulent refractive index fluctuations and k is the wave vector (Yura, 1979).

The requirement of homogeneous wave fronts for the backscattered waves from all distances leads to a strong suppression of all signals except for those from the focal regions u_T and u_R. On the one hand this can be used to further suppress the signal dynamic range, which is a clear advantage, on the other hand the signals from the suppressed regions are weaker, hence the statistical error increases. The optimization therefore depends strongly on the details of the system and can only be performed when all the details are known.

The two detection techniques also show significant differences in the signal statistics. While for the direct detection the statistic is determined by the Poisson-distribution of both the signal and the background light, for the heterodyne detection the rapidly varying "speckle" patterns govern the statistics. Most heterodyne detectors are operated in a way that the noise is solely determined by the local oscillator. The textbook result for the signal-to-noise, here called carrier-to-noise ratio CNR, is (Yarif, 1985)

$$CNR = \frac{\eta_{opt}\eta_{det}P(R)}{h\nu B_{het}}, \tag{G.5}$$

where η_{opt} and η_{det} are the efficiencies for the optics and the detector, and B_{het} is the bandwidth of the heterodyne detection. Hence, the number of signal photons in the observation interval $1/B_{het}$ can be determined with the precision of one photon. But this is not the uncertainty of the measurement of an average backscatter signal, since the signal intensity at the receiver area is itself a stochastic variable having an exponential probability distribution (Goodman, 1965; Hardesty et al., 1981). For a given mean value $\overline{P}$ for this distribution the variance is given by $\overline{P}^2$, hence the standard deviation is equal to the mean. For the total signal-to-noise ratio we then have

$$SNR_{het} = \frac{CNR}{\sqrt{CNR^2 + 2CNR + 1}} \tag{G.6}$$

or, using $\eta_{tot} = \eta_{opt} \cdot \eta_{det}$

$$SNR_{het} = \frac{\eta_{tot}P}{\eta_{tot}P + h\nu B_{het}}. \tag{G.7}$$

This result of a simplified classical treatment is very close to the result of a full quantum-electrodynamic treatment of a similar case (Jakeman et al., 1975),

$$SNR_{het} = \frac{CNR}{\sqrt{2CNR^2 + 2CNR + 1}}. \tag{G.8}$$

It is beyond the scope of this paper to clarify which result would be the correct one for the case under study. The main result, namely that for a single measurement we always have SNR < 1, is contained in both solutions. The necessary improvement of the signal-to-noise ratio (at least by a factor of 100 for typical DIAL measurements) has to be achieved by averaging over n independent measurements, according to

$$SNR_n = SNR \cdot \sqrt{n}. \tag{G.9}$$

One independent estimate is made in the time $1/B_{het}$, which is determined by the maximum Doppler-shift of the backscatter signal. For the wavelength region around 750 nm this time is about 40 ns for vertical measurements, corresponding to about 5 m height resolution. For measurements with "high" vertical resolution of about 50 m we than have about 10 independent estimates for one laser shot. If high temporal resolution of < 10 s shall be achieved repetition rates > 100 Hz are

necessary. If further noise sources are considered, too, repetition rates on the order of 1 kHz are more likely to be necessary.

The estimates presented here clearly show that significant differences are existent for the direct detection using extremely narrow band interferometers on the one hand, and heterodyne detection on the other hand. The full characterization of both methods is clearly beyond the scope of this paper, it would require an extensive parametric simulation study. But at this point it can already be stated that:

- The heterodyne detection technique is capable of providing receiver bandwidths clearly meeting the requirements for suppressing the Doppler-broadening effects of Rayleigh-scattering.
- If this technique is used the signal-to-noise ratio is mainly determined by the "speckle" statistics. This implies, that the accuracy needed for DIAL measurements can only be achieved by averaging over many shots. Consequently lasers with high repetition rates are required to achieve high resolution measurements. Use of a corresponding high speed data acquisition system is necessary, too.

Belinda: Previously a different measurement scheme to reduce the influence of Rayleigh-Doppler-broadening had been suggested (Theopold et al., 1992), which was called BELINDA (Broadband Emission Lidar with Narrowband Determination of Absorption). In this technique a broadband laser should be used in conjunction with narrowband detectors at both on- and off-line wavelengths. It has been shown theoretically that for proper selection of both wavelength off the absorption line center the errors due to Doppler-broadening can be partially compensated, a reduction by at least a factor of 4 can be achieved. The filters used for this technique have to be as narrow as for the technique using narrowband emission.

In this technique it is not necessary to use a narrowband laser source, but the broadband emission has to be homogeneous or at least repeatable over a larger wavelength interval. Whether or not this is easier to achieve the narrowband emission shall not be discussed here. The detection system for this technique requires a larger effort than that proposed in the present paper, since two narrowband filters at two predetermined wavelength off the absorption line center are necessary. In addition the error due to Doppler-broadening is not completely eliminated but only reduced, a correction including a determination of the aerosol backscatter is still necessary. The transmitted laser energy is used only to the extent which falls into the receiver windows, most of the energy remains undetected. Since now a suitable narrowband laser is available, the technique using narrow bandwidth in both transmission and detection appears to have clear advantages over the Belinda concept.

Avoiding the Rayleigh-Doppler-correction by narrowband detection of the backscattered radiation, using either direct or heterodyne detection is a very promising development goal, since only in this way the full accuracy for DIAL measurements involving narrow absorption lines in the

near IR can be achieved. This holds for both water vapor retrievals in regions of spatially inhomogeneous aerosol distribution and for temperature retrievals, for which the modifications suggested here are mandatory.

A distinct advantage of using heterodyne detection as a narrowband receiver is that it has the potential of measuring the radial wind velocity simultaneously by measuring the Doppler-shift. Measuring the wind is an important task of its own, measuring it simultaneously with e.g. humidity using the same system would be a major breakthrough for flux measurements using the eddy correlation technique.

Last not least by avoiding the Rayleigh-Doppler-correction the most difficult part of the DIAL evaluation would be abandoned. The main difficulty actually is the insertion of aerosol parameters needed for the calculation of the aerosol distribution. Since this estimation requires the interaction of a skilled scientist (and is guesswork to a certain degree anyhow!), only dropping of this step makes an automatization possible. This would greatly simplify the evaluation of long sequences of measurements.

H. Measurements of the ozone distribution

The DIAL technique has been used for the determination of the vertical distribution of ozone in the atmosphere already for more than 10 years. First measurements were restricted to the stratosphere, on the one hand because of the importance to study stratospheric ozone depletion at high latitudes, but on the other hand because accurate measurements are mostly easier to perform in the stratosphere as compared to the troposphere. This is due to the fact that regions with strongly inhomogeneous aerosol distribution occur much more frequently in the troposphere, and this has a major impact on the achievable accuracy. But in the past years the measurements have been extended to the troposphere, because the importance of the negative effects of tropospheric ozone on the health of humans and organisms in general has been increasingly recognized. For studies of the processes which control formation and destruction of ozone in this atmospheric region the DIAL technique is particularly suited because of its capability to make continuous high resolution measurements.

H.1. Analysis of the achievable accuracy

For measurements of ozone utilizing the DIAL technique mostly the Hartley-Huggins absorption band in the UV is used, which shows only little structure. Figure H.1 shows the measured absorption cross section as a function of wavelength (after Molina and Molina, 1986). The figure shows that it is possible to choose the absorption cross section within wide margins by choosing the proper wavelength. Hence it is possible to adapt the system to very different measurement situations just by tuning the wavelength. This feature is important since ozone in the troposphere is highly variable. It should be noted that by choice of the wavelength both the sensitivity and the maximum range are controlled.

The choice of the reference wavelength is also determined by the prevailing measurement conditions. Assuming that with a DIAL system a difference in optical depth of about $1 \cdot 10^{-3}$ can be detected, then in order to perform measurements with 5% accuracy and 100 m range resolution at an ozone density of 100 $\mu g\ m^{-3}$ the differential absorption cross section has to be larger than $\Delta\sigma \geq 160 \cdot 10^{-20}\ cm^2$. Except for some small structures the maximum slope according to Fig. H.1 is about 40 cm^2/nm. Therefore, at least a wavelength separation of 4 nm is required to achieve the specific accuracy. With this rather large wavelength separation differences in both backscatter and extinction for λ_1 and λ_2 have to be considered explicitly, as already explained in general in section B.4. This shall now be studied in greater detail.

The appropriate DIAL equation for this case is eq. (B.54). In the form suitable for a retrieval of the ozone density ρ_{O_3} from the measured backscatter signals this equation reads

$$\rho_{O_3} = -\frac{M_{O_3}}{2\Delta\sigma}\frac{d}{dR}\ln\frac{P_1(R)}{P_2(R)} \quad [1]$$

$$-\frac{2M_{O_3}}{2\Delta\sigma}\Delta\alpha_m \quad [2]$$

$$-\frac{2M_{O_3}}{2\Delta\sigma}\Delta\alpha_p \quad [3] \qquad \text{(H.1)}$$

$$+\frac{2M_{O_3}}{2\Delta\sigma}\frac{d}{dR}\ln\frac{\beta_1}{\beta_2} \quad [4]$$

$$-\frac{2M_{O_3}}{2\Delta\sigma}\Delta\alpha_q \quad [5]$$

This implies that for the error analysis we have to inspect the quantities

$$\Delta\sigma,\ \frac{d}{dR}\ln\frac{P_1(R)}{P_2(R)},\ \Delta\alpha_m,\ \Delta\alpha_p,\ \frac{d}{dR}\ln\frac{\beta_2}{\beta_1},$$

and the differential absorption by other gases $\Delta\alpha_q$. In the worst case the error is given as the sum, in the optimal case by the root of the sum of squares of the individual error terms.

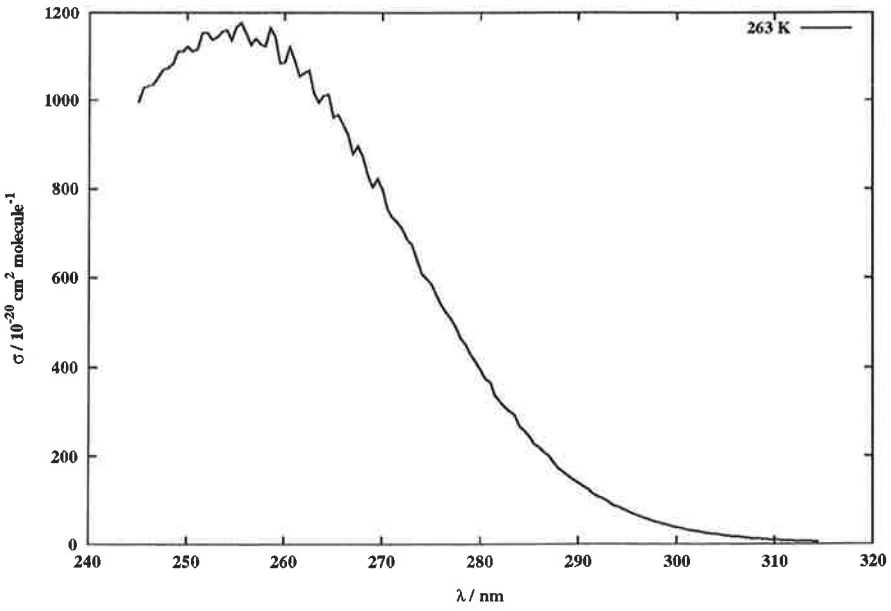

Figure H.1: Ozone absorption cross section in the Hartley-Huggins band (after Molina and Molina, 1986).

H.1.1. Accuracy of the differential absorption cross section

The accuracy claimed by the authors is 1% for each single value, hence the accuracy of the differences is about 1.5%. The temperature dependence of the ozone absorption cross section is very small in the region close to the absorption maximum, at the detection limit for $\lambda < 270$ nm, and increases to values of about $1 \cdot 10^{-3}$ K^{-1} in the region up to 300 nm. So if on-line wavelengths $\lambda_{on} > 285$ nm are used the temperature dependence should be considered, but a coarse correction with a temperature estimation to some K is sufficient. In the wavelength region under consideration the measurements published by Molina and Molina (1986) and by Malicet et al. (1995) are deemed most reliable.

H.1.2. Cross sensitivity with respect to other gases

In the wavelength region from 248 to 320 nm which is used for ozone measurements many gases do absorb. The most important gases to consider are O_2, SO_2, and NO_2. Many hydrocarbons have absorption bands in this region, too, but their density is mostly rather small, so that they have to be considered in extremely polluted areas only. Table H.1 shows the cross sensitivities for SO_2 and NO_2 for those wavelength combinations which are in use for the MPI ozone system. For the wavelength pairs used for lower tropospheric measurements the cross sensitivities are small, only if the other gases are present at very elevated concentrations they will have a marked influence on the accuracy of ozone retrievals. In such cases these gases should be measured as well and the ozone values corrected correspondingly. Only for the combination 292/319.9 nm the cross sensitivity for SO_2 is relatively large, but this pair is used for mid- and upper tropospheric measurements only, where the SO_2 concentration is rather small.

Table H.1: Cross sensitivities for ozone retrievals with respect to the most important trace gases for selected wavelength pairs. The entries are the ratio of trace gas to ozone concentration calculated from differential absorption.

λ_{on} / λ_{off}	268.5/292	277.2/292	277.2/313.3	292/319.9	Reference
SO_2	- 0.03	- 0.01	0.12	0.6 5	Thomson, 1990 Brassington, 1981
NO_2	- 0.01	- 0.2	- 0.04	0.10	Bass et al., 1976

Absorption by molecular oxygen has to be considered for wavelengths < 270 nm, too. In principle this correction is easy to perform since the atmospheric density of oxygen is rather well known. A potential source of error, however, is the rather large uncertainty in the values of the absorption cross section. Values calculated by Cann et al. (1984) are currently deemed as the most reliable source. Measurements at high spectral resolution have not been reported. For the wavelength combination 268/292 nm the differential absorption caused by oxygen corresponds to 9 $\mu g\ m^{-3}$

ozone under standard conditions, for the other wavelength pairs it is negligibly small.

H.1.3. Accuracy of the measured signals

The measured signals always contain noise, often at a rather high level, which is caused by the statistical distribution of the incident photons, originating from both the backscatter and sometimes from background light. According to section B.6.1 the random error of the density retrieval is given by

$$\delta(\rho_{O_3}) = \frac{M_{O_3}}{\sqrt{2}\Delta\sigma \cdot \Delta R} \cdot \sqrt{\frac{\delta^2(P_1)}{P_1^2} + \frac{\delta^2(P_2)}{P_2^2}} \qquad \text{(H.2)}$$

assuming that the noise in the signals is the main source of random errors. In the latest version of the data acquisition of the MPI-lidars not only the mean values of the signals are recorded, but also their sum of squares, so that their variances can be calculated. The calculated standard deviations contain the noise as well as the signal variability due to backscatter variations, atmospheric transmittance variations, and variations of transmitted laser pulse energy. Since the latter terms are at least partially correlated for on- and off-line signals the measured variances yield an upper limit for the random error of the ozone retrieval. Figure H.2 shows an example of a time-height-distribution of the variances estimated with this method, actually the relative error of the mean value is plotted. The temporal resolution was 10s (100 shot averages), the vertical resolution was 15 m. Up to 1500 m altitude this error is less than 5%, further averaging to typically 75 m and 30 s resolution reduces this error in the off-line signal to about 1%.

H.1.4. Extinction by molecular scattering

Term [2] from eq. (H.1), the differential extinction caused by molecular scattering $\Delta\alpha_m = \alpha_{m,1} - \alpha_{m,2}$ depends solely on the on- and off-line wavelength and the density of the air.

To estimate an upper limit for this error we assume a rather short wavelength of 268 nm. For this wavelength under standard conditions we have $\alpha_m = 2.31 \cdot 10^{-4}$ m^{-1}. The air density is generally known with an uncertainty of less than 3% (Russell et al., 1982). The error in the absorption coefficient then is less than $\delta\alpha_m = 7 \cdot 10^{-6}$ m^{-1} corresponding to $\delta\rho_{O_3} \leq 0.8$ µg m^{-3} for a measurement using the wavelength pair 268/292 nm. In most cases this error will be negligible compared to other possible errors. If this appears critical, however, it requires relatively little effort to determine the air density to better than 1%. Additionally a relatively small wavelength separation should be used, where the error decreases proportional to $4\Delta\lambda/\lambda_2$. Hence we can practically exclude significant errors caused by term [2].

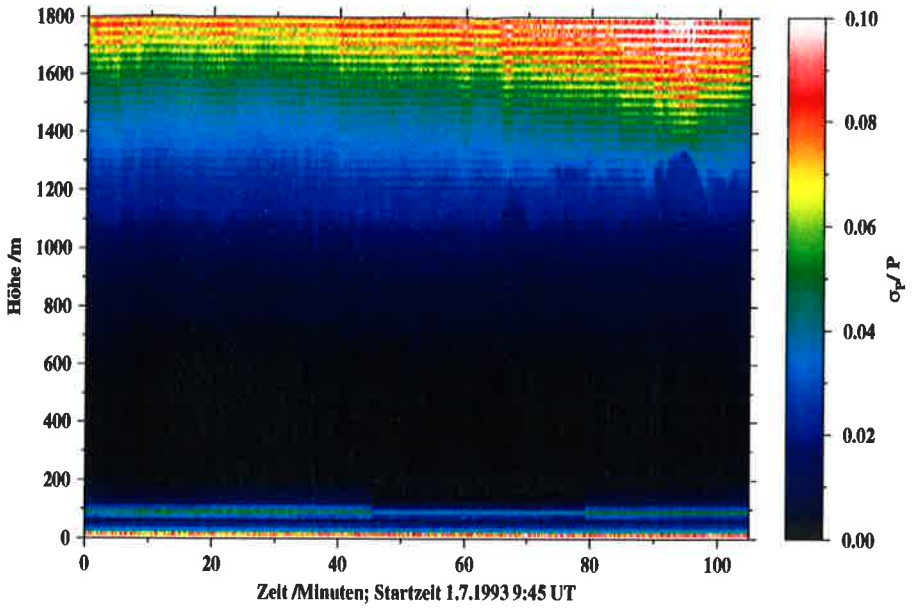

Figure H.2: Relative standard deviation of lidar signals, δp/P, for 100 shot averages corresponding to 10 s averaging time. Height resolution is ΔR = 15 m.

H.1.5. Extinction by particle scattering

Term [3] of eq. (H.1), the differential extinction due to particle scattering, can be estimated as follows:

For DIAL applications we generally have $\Delta\lambda = \lambda_1 - \lambda_2 \ll \lambda_2$. Then the wavelength dependence of α_p my be approximated by a power law with the Ångström-coefficient k_α

$$\alpha_{p,1} = \alpha_{p,2}\left(\frac{\lambda_1}{\lambda_2}\right)^{k_\alpha}$$

From that it follows that

$$\left(\frac{\lambda_1}{\lambda_2}\right)^{k_\alpha} = \left(1 + \frac{\Delta\lambda}{\lambda_2}\right)^{k_\alpha} \approx 1 + k_\alpha \frac{\Delta\lambda}{\lambda_2}$$

$$\Delta\rho_{O_3} = \frac{M_{O_3} \cdot \Delta\alpha_p}{\Delta\sigma} = \frac{M_{O_3}}{\Delta\sigma}(\alpha_{p,1} - \alpha_{p,2}) \approx \alpha_{p,2} \cdot k_\alpha - \frac{M_{O_3} \cdot \Delta\lambda}{\Delta\sigma \cdot \lambda_2} \quad . \tag{H.3}$$

Hence the accuracy of the $\Delta\alpha_p$ retrieval is dependent on how accurate the aerosol extinction $\alpha_{p,2}$ at the reference wavelength can be determined, and how well the aerosol properties are known

which determine the Ångström-coefficient k_α. For a first estimate we can insert some typical numbers: the factor $M_{O_3} \cdot \Delta\lambda/2 \cdot \Delta\sigma \cdot \lambda_2$ is given in table H.2 for some commonly used wavelength pairs. For measurements in the boundary layer a likely maximum value is $\alpha_p < 2 \cdot 10^{-3}$ m^{-1}. A typical wavelength combination for measurements in this atmospheric region is 268/292 nm, we then have

$$\Delta\rho_{O_3} \leq 2 \cdot 10^{-3} \cdot 0.6 \cdot 8970 \mu g m^{-3}$$

$$\Delta\rho_{O_3} \leq 11 \mu g m^{-3}.$$

For measurements in the free troposphere using 277/313 nm the sensitivity is larger by a factor of 2, but generally the aerosol extinction is much smaller in that region, hence the correction most likely will not exceed 5 $\mu g\ m^{-3}$.

Assuming that the extinction coefficient can be estimated with an uncertainty of about 30%, and k_α to about 20%, the uncertainty of the correction is about 35%. This corresponds to an uncertainty in the ozone retrieval of 4 $\mu g\ m^{-3}$ at the maximum, and $\leq 2\ \mu g\ m^{-3}$ in the majority of cases.

H.1.6. Differential backscatter

The correction term for differential backscatter reads

$$[4] = \frac{M_{O_3}}{2\Delta\sigma}\frac{d}{dR}\ln\left(\frac{\beta_1}{\beta_2}\right) = \frac{M_{O_3}}{2\Delta\sigma}\frac{d}{dR}\ln\left(\frac{\beta_{m,1}\cdot S_{K,2}}{\beta_{m,2}\cdot S_{K,1}}\right) \tag{H.4}$$

where the inverse scattering ratio $S_K = \beta_m/\beta$ has been used. Assuming again an Ångström-law for the wavelength dependence of the aerosol backscatter coefficient with an Ångström-coefficient k_β:

$$\beta_{p,1} = \beta_{p,2} \cdot \left(\frac{\lambda_1}{\lambda_2}\right)^{k_\beta}$$

it follows that

$$[4] = \frac{M_{O_3}}{2\Delta\sigma}\frac{d}{dR}\ln\left(S_K + (1-S_K)\cdot\left(\frac{\lambda_1}{\lambda_2}\right)^{4+k_\beta}\right) \tag{H.5}$$

In order to make clear which factors actually determine the correction term some simplifications will be introduced. For typical measurement wavelengths we have $\Delta\lambda \leq \lambda_2$ and hence

$$\left(\frac{\lambda_1}{\lambda_2}\right)^{4-k_\beta} \approx 1(4+k)\cdot\frac{\Delta\lambda}{\lambda_2} \ .$$

After some transformations eq. (H.5) comes down to

$$[4] \approx \frac{M_{O_3}\cdot\Delta\lambda}{2\cdot\Delta\sigma\cdot\lambda_2}\cdot(4+k_\beta)\cdot\frac{dS_K}{dR} \ . \qquad \text{(H.6)}$$

Hence the correction for differential aerosol backscatter is determined by

$\frac{M_{O_3}\cdot\Delta\lambda}{2\cdot\lambda\sigma\cdot\lambda_2}$, which is completely determined by the choice of wavelengths

$4+k_\beta$, which is determined by the wavelength dependence of aerosol backscatter

$\frac{dS_K}{dR}$, which is determined by the spatial gradients in the aerosol distribution.

Figure H.3 shows the factor $M_{O_3} \cdot \Delta\lambda/2 \cdot \Delta\sigma \cdot \lambda_2$ as a function of the on-line wavelength and the wavelength separation $\Delta\lambda$. Some dots mark the wavelength pairs which are used in some typical DIAL configurations. Table H.2 gives a quantitative presentation of these sensitivities.

The sensitivity of the correction for differential aerosol backscatter (and for differential aerosol extinction, too!) shows a minimum around λ_1 = 270 nm, the region where the ozone absorption cross section shows the strongest wavelength dependence. The wavelength pairs 268/292 nm and 266/289 nm, which are produced from KrF and NdYAG-lasers, respectively, with subsequent Raman-conversion in deuterium are very well suited for measurements under high aerosol load conditions. If measurements at longer ranges are attempted the on-line wavelength has to be chosen larger. For this the pairs 277/292 and 289/299 (KrF respectively NdYAG with Raman-conversion in deuterium and hydrogen) are well suited. The combinations of 277/313 and 292/319 which can be realized using one Raman-cell only are clearly more sensitive to differential aerosol backscatter, about a factor of 2 compared to the optimum at the corresponding on-line wavelengths. If these pairs are used for measurements in the free troposphere only, where aerosol gradients are generally rather weak, the errors can still be kept small. The combination 286/298.3, which has been used in many campaigns of the NASA airborne system, is well suited for measurements at longer ranges, but is more than two times as sensitive to differential backscatter than the combination 268/292 which has been used for most lower tropospheric measurements in the MPI system.

It is worth noting that nowhere in this region a substantial decrease in sensitivity to differential backscatter can be achieved by making the wavelength separation very small.

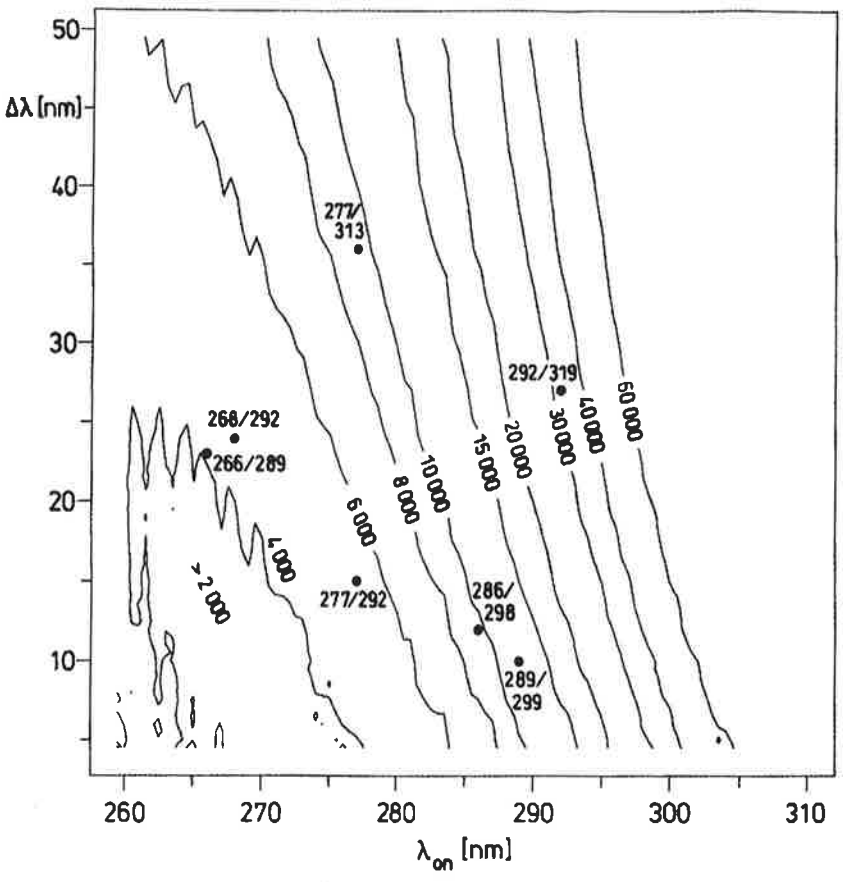

Figure H.3: Sensitivity to differential aerosol backscatter, in $\mu g\ m^{-2}$.

Table H.2: Sensitivity to differential aerosol backscatter.

λ_1/λ_2, nm	$\frac{M_{O_3} \cdot \Delta\lambda}{2 \cdot \Delta\sigma \cdot \Delta\lambda_2}$, $\mu g \bullet m^{-2}$
266 / 289	4038
268 / 292	4485
277 / 292	5118
286 / 298.3	9452
277 / 313	9531
289 / 299	11965
292 / 319	31640

It also has to be considered that a larger $\Delta\sigma$ reduces the sensitivity to other measurement errors. Hence $\Delta\lambda$ should rather be chosen relatively large, in particular for measurements at long range. Figures H1. and H.3 can be used to find a optimal choice for each application.

The wavelength dependence of the aerosol backscatter coefficient is not very well known in the spectral region below about 300 nm. Calculations for standard aerosol types based on the Mie theory, where typical size distributions and the complex refractive index were prescribed, have resulted in values $-1 \leq k_\beta \leq 1$ (Völger, 1993; Völger et al., 1996). In particular it has to be considered that hygroscopic aerosols change both their size distributions and refractive index due to uptake (or loss) of water when the relative humidity of the surrounding air changes. This results in considerable changes in k_β. Assuming $k_\beta = 0$ for all cases where there is no information available about the aerosol, the error caused by the wavelength dependence is most likely smaller than 25%.

The inverse scattering ratio S_K can only assume values between 0 and 1, corresponding to pure particle and molecular scattering, respectively. At typical wavelengths below 300 nm as typically used for ozone measurements it is more likely that $1 > S_K > 0.5$. Hence the gradient dS_K/dR cannot be larger than $1/\Delta R$ for measurement with a height resolution of ΔR, mostly we have $dS_K/dR < 1/2\Delta R$.

Then the following estimate holds:

- The factor $M_{O_3} \cdot \Delta\lambda/2 \cdot \Delta\sigma \cdot \lambda_2$ is at best about 4000 $\mu g\ m^{-2}$. The factor $(4 + k_\beta)$ is about 4. For high resolution measurements, e.g. $\Delta R = 100$ m, we can assume $dS_K/dR \leq 3 \cdot 10^{-3}\ m^{-1}$. So even for the best choice of wavelengths the correction can be as high as 80 $\mu g\ m^{-3}$. This value is comparable with the ozone density typically found in the lower troposphere, hence the correction is of utmost importance. It should, however, be noted that such high values for the correction can only be reached in very small regions at layer boundaries, e.g. at the top of the boundary layer.

- Increasing the height resolution interval causes a reduction of the correction inversely proportional to ΔR. If only low resolution is required, e.g. $\Delta R = 500$ m, the corrections are rather small, even for wavelengths used for long range measurements as e.g. 277/313 nm the correction will stay below 35 $\mu g\ m^{-3}$. Practically such a large gradient is only observed at the top of the boundary layer or at some rare events of similarly pronounced aerosol layers. Mostly it is much smaller, and hence the correction for differential aerosol backscatter typically is much smaller, too.

H.1.7. Correction methods

Equation (H.5) or (H.6) can be used to estimate the correction term [4]. This was first introduced by Browell et al. (1985). In this method first one of the standard backscatter lidar inversion algorithms (e.g. Fernald, 1984; Klett, 1981; Sasano et al., 1985) is used to retrieve the aerosol backscatter and estimation coefficients from the off-line signal. However, some parameters have to be specified, which in principle require some detailed knowledge about the aerosol properties:

- $\beta_{p,2}\ (R_c)$, in a suitably selected calibration height R_c
- $S_L = \alpha_p/\beta_p$, the so-called lidar ratio, if possible as a function of height R

- k_β, the Ångström-coefficient of the wavelength dependence of β_p.

If the gaseous absorption $\alpha_{g,2}$ at the reference wavelength is not negligible, an iteration procedure has to be used. First α_g is calculated using the DIAL equation without aerosol correction, then this value is used in the aerosol retrieval, and then the correction term is calculated and applied. These steps are iterated, usually very fast convergence is observed where often one iteration is sufficient.

A serious disadvantage of this correction method is that it requires a rather large effort and can hardly be automatized, because several aerosol parameters have to be specified. The estimation of these parameters requires a lot of experience and a careful analysis of the prevailing atmospheric conditions. In addition the complexity of aerosol distribution often found in the lower troposphere can make it very difficult to find a suitable calibration height. For single profiles this is generally not too big a problem, but for extended time series this mostly is impossibly. In this case the time series have to be split into short intervals, which requires some effort and, what is worse, leads to differences in the treatment of continuous scenes.

H.1.7.1. Simplified correction scheme

For these cases as well as for a general estimation of the achievable accuracy a simplified correction scheme is proposed.

The factor dS_K/dR of equation (H.6) can easily be approximated by forming the logarithmic derivative of the range corrected signal.

$$\begin{aligned}
\frac{d}{dR}\ln(P\cdot R^2) &= \frac{d}{dR}\ln\left[\beta\cdot\exp\left(-2\int_0^R \alpha dR\right)\right] \\
&= \frac{d}{dR}\ln\beta - 2\alpha_{tot} \\
&= \frac{d}{dR}\ln\beta_m - \frac{d}{dR}\ln S_K - 2\alpha_{tot} \\
&= \frac{d}{dR}\ln\beta_m - \frac{1}{S_K}\frac{dS_K}{dR} - 2\alpha_{tot}.
\end{aligned} \tag{H.7}$$

The gradient of the Rayleigh backscatter coefficient β_m can be calculated to good precision, since it is only dependent on the air density. The total extinction coefficient, α_{tot}, includes the extinction due to molecular scattering, particle scattering, and gaseous absorption. The molecular extinction again can be calculated, and is rather small, the aerosol extinction generally is not too important

either, and the gaseous absorption at the reference wavelength either is small or can be calculated by iteration (see above).

The factor $1/S_K$ in principle requires full calculation of $\beta_{p,2}$. But the term dS_K/dR and hence the total correction can only assume large values if $\beta_{p,2}$ is sufficiently large and hence S_K rather small, at least as long as the height interval is not chosen particularly small. Further, if lidar measurements are possible at all, we mostly have $S_K \geq 0.3$. Without any specific information about the aerosol distribution we thus have $0.3 \leq S_K \leq 0.7$. Assuming $S_K = 0.45$ in the standard case leads to an error of probably less than 30% in the estimation of the correction term.

But even when the extended correction procedure is applied some errors exist, certainly not less than 20%, caused by insufficiently known parameters and by numerical instabilities. Hence it is well justified to use the simplified method.

In the simplified correction scheme the formula

$$\Delta\rho_{O_3} \approx \frac{M_{O_3} \cdot \Delta\lambda}{2 \cdot \Delta\sigma \cdot \lambda_2} \cdot 4 \cdot \left(0.45 \frac{d}{dR} \ln P \cdot R^2 + \frac{d}{dR} \ln \beta_m - 2\alpha_{tot}\right) \tag{H.8}$$

is used. The uncertainty in k_β is about 20%, according to Völger et al. (1996). Considering both uncertainties (uncorrelated) in the estimation of the aerosol correction results in a total uncertainty of about 35% for term [4] of equation (H.1). The estimated uncertainty for the extended correction scheme is 28%, hence only marginally better.

This simplified correction, in conjunction with a calculation of the random error due to noise using the measured variance of the backscatter signals, as explained in section H.1.3, is now used routinely to estimate the uncertainty of ozone lidar measurements.

H.1.8. Statistical investigation of the aerosol correction

At the Max-Planck-Institut für Meteorologie in Hamburg lidar measurements of the ozone vertical distribution have been performed since 1991, about once per week weather permitting. A small portion of this data set, those performed in March, June, and July, 1993, have been used to study the statistical distribution of the vertical gradient of the aerosol backscatter coefficient in several atmospheric regions. This partial data set contains 100 hours of measurements on 19 days, corresponding to about 20000 individual profiles. The quantity $D_S = \frac{d}{dR} \ln P \cdot R^2$ has been determined from the off-line signal, which can serve as a reasonable approximation for $\frac{1}{S_K} \frac{dS_K}{dR}$. Neither a correction for Rayleigh extinction was applied nor a correction for ozone absorption in cases the off-line wavelength 292 nm was used. The neglection of Rayleigh extinction results in a pure shift of the corresponding distribution, the neglection of ozone absorption results mainly in a shift, too, the broadening of the distribution is rather small. The height resolution was chosen as

90 m, temporal resolution was 30 s.

For the purpose of this statistical investigation the following atmospheric regions were distinguished: planetary boundary layer (PBL), entrainment zone (EZ), lower (LFT) and upper (UFT) free troposphere. These layers were also determined from the time height distribution of D_S. Figure H.4 shows an example of this distribution for July 1, 1993, 09:45 to 11:30 UT measured in the lower troposphere.

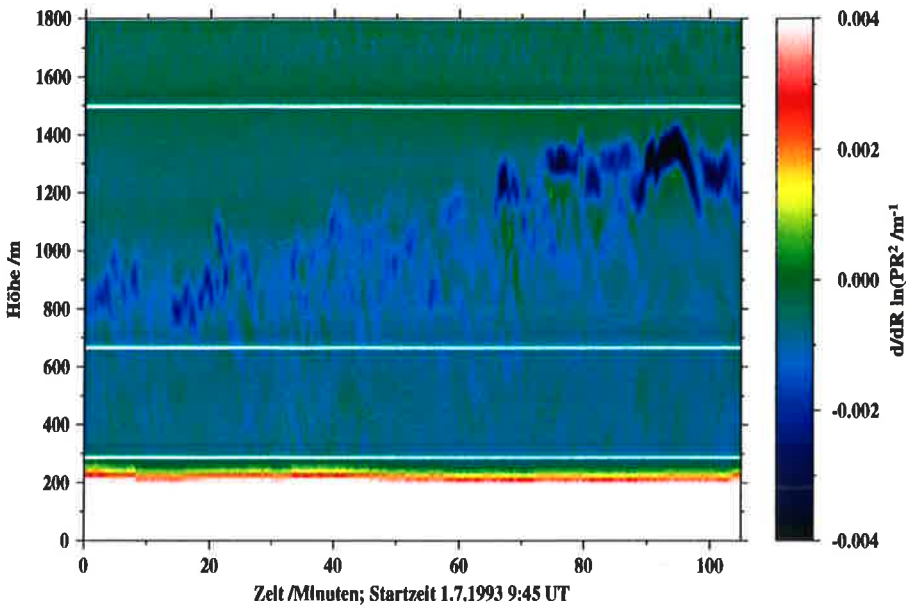

Figure H.4: $\frac{d}{dR}\ln(P \cdot R^2)$ for $\lambda = 292$ nm. July 1, 1993 09:45 to 11:30 UT.

The off-line signals (292 nm) were suitable for evaluation in the region from about 285 m to 1800 m altitude. The lowest layer up to 660 m, where no direct mixing with free tropospheric air was observed, was designated as PBL.

The region from 660 m to 1500 m, where rather strong negative aerosol gradients occurred, was called entrainment zone (EZ), and the region up to 1800 m was considered to be the lower free troposphere (LFT). Certainly these assignments are somewhat arbitrary, in particular because of the clearly visible temporal development of the PBL-height, which rose by about 500 m within 1:45 hours of measurement. But for the purpose of this investigation the assignments are considered sufficiently accurate.

In figures H.5 and H.6 the cumulative distribution functions for D_S are shown for the different regions. Also indicated are the intervals for 68% and 95% probability to find values between these limits. D_S does not exhibit a normal distribution, which is clearly visible e.g. from abrupt changes of the slope. A normal distribution is not expected, since gradients in the aerosol distributions can originate from different processes, which will affect the distribution function in different portions.

An important feature of the measured distribution is that large values of the gradients occur more frequently than expected for a normal distribution. The observed shift to negative gradients is not important here, since it is a result of the neglection of Rayleigh extinction and ozone absorption at $\lambda = 292$ nm. Hence only the width of the distributions should be examined here.

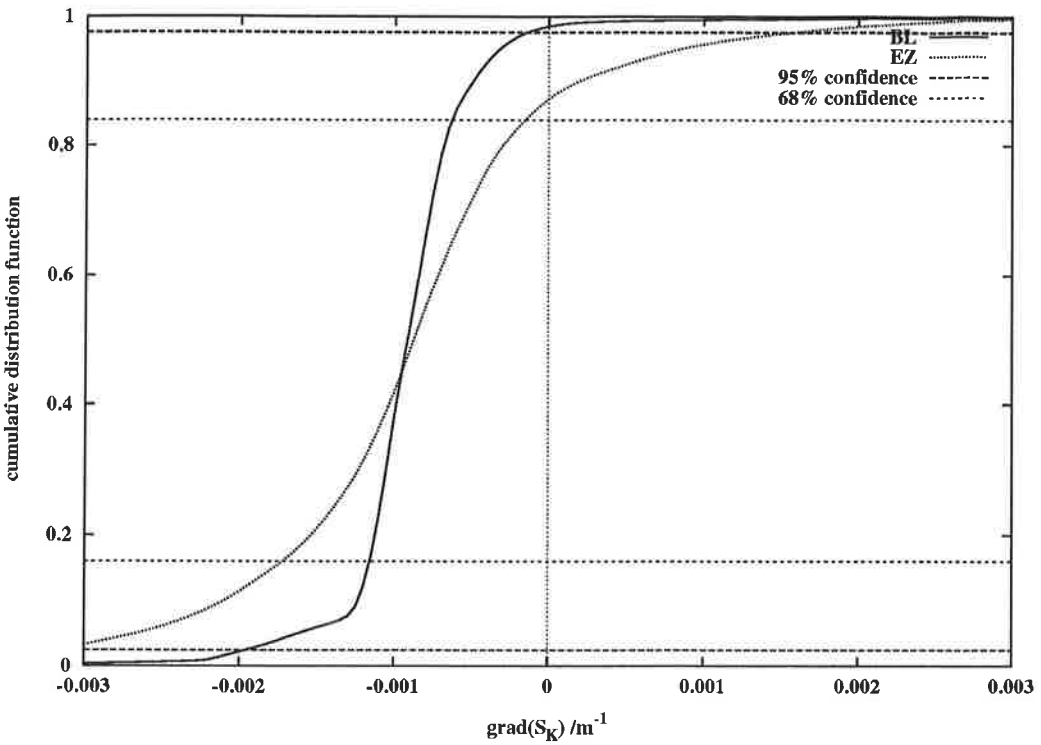

Figure H.5: Cumulative distribution function for $D_S = \frac{d}{dR}\ln(P \cdot R^2)$, $\lambda = 292$ nm, for the boundary layer (BL) and entrainment zone (EZ).

Table H.3 summarizes the observed widths ΔD_S for the different atmospheric regions, for both 68% and 95% confidence. The table also contains the estimated error in the ozone retrieval, assuming that the error is 35% of the correction according to equation (H.8)

$$\delta\rho_{O_3} \approx 0.63 \cdot \frac{M_{O_3} \cdot \Delta\lambda}{2 \cdot \Delta\sigma \cdot \lambda} \frac{\Delta D_S}{2} \tag{H.9}$$

This yields

$$\delta\rho_{O_3} \approx 1.4 \cdot 10^3 \mu g \cdot m^{-2} \cdot \Delta D_S$$

for the wavelength pair 268/292 nm, and

$$\delta\rho_{O_3} \approx 3.0 \cdot 10^3 \mu g \cdot m^{-2} \cdot \Delta D_S$$

for 277/313 nm.

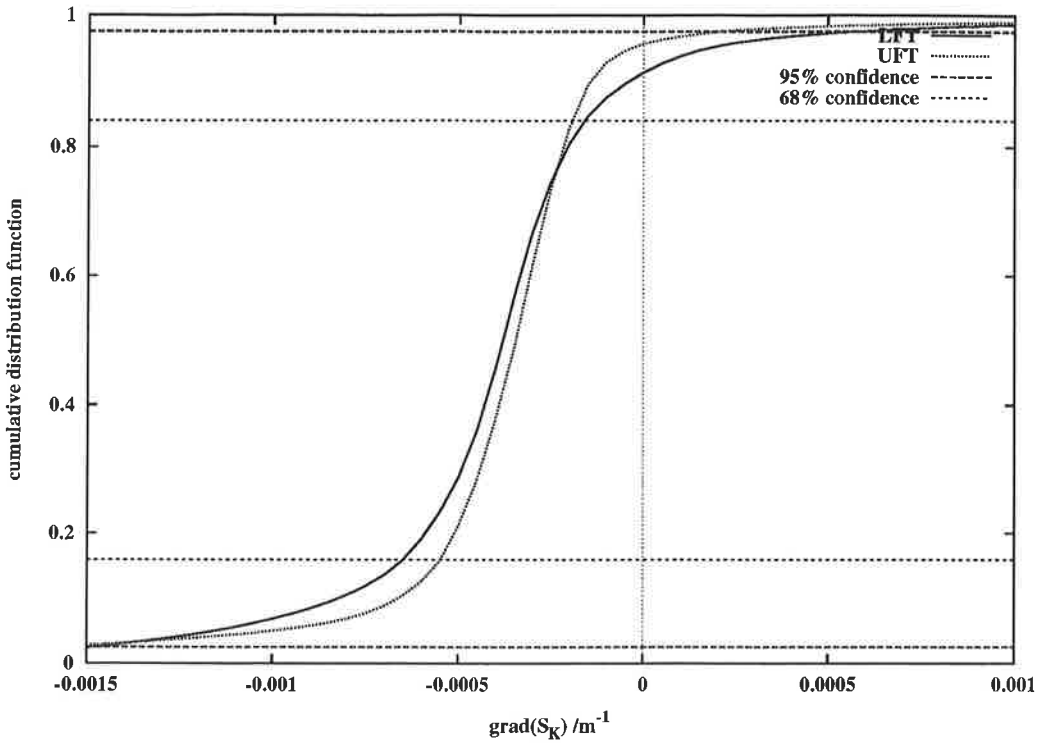

Figure H.6: Cumulative distribution function for $D_S = \frac{d}{dR}\ln(P \cdot R^2)$, λ = 313 nm, for the lower and upper troposphere.

Table H.3: Confidence intervals (68% and 95%) for $D_S = \frac{d}{dR}\ln(P \cdot R^2)$, and for the corresponding error in the ozone retrieval, $\delta\rho_{O_3}$, for the boundary layer (BL), entrainment zone (EZ), and lower (LFT) and upper (UFT) troposphere

atmospheric region	ΔD_S, 68%	ΔD_S, 95%	$\delta\rho_{O_3}$, 68%	$\delta\rho_{O_3}$, 95%
BL	$5.3 \cdot 10^{-4}$ m^{-1}	$1.9 \cdot 10^{-3}$ m^{-1}	0.8 µg • m^{-3}	2.7 µg • m^{-3}
EZ	$1.6 \cdot 10^{-3}$ m^{-1}	$6.0 \cdot 10^{-3}$ m^{-1}	2.3 µg • m^{-3}	8.6 µg • m^{-3}
LFT	$4.8 \cdot 10^{-4}$ m^{-1}	$2.4 \cdot 10^{-3}$ m^{-1}	1.4 µg • m^{-3}	7.2 µg • m^{-3}
UFT	$3.6 \cdot 10^{-4}$ m^{-1}	$1.8 \cdot 10^{-3}$ m^{-1}	1.1 µg • m^{-3}	5.4 µg • m^{-3}

The 68% confidence intervals are rather small in all atmospheric regions, the resulting error is likely to be about 1 µg • m^{-3}, except for the entrainment zone, where the large gradients may cause errors twice as large. The 95% confidence intervals are 3 to 5 times larger, again showing that the distribution is not normal. The largest errors again occur in the entrainment zone, almost 9

$\mu g \cdot m^{-3}$, but the errors expected in the free troposphere are not much smaller either. In part this is due to the fact that here the wavelength pair 277/313 nm had been used, for which the sensitivity to aerosol gradients is more than doubled compared to 268/292 nm. On the other hand this reflects the fact that in the free troposphere aerosol layer with sharp boundaries and hence strong gradients do occur.

The extreme values of the distribution functions shall not be examined in further, since it cannot be excluded that some outliers entered the data set. In particular some data points from cloud boundaries may be included, where extremely large aerosol gradients are observed.

For the presentation of averaged profiles the 68% confidence limits are considered appropriate. The results obtained here clearly show that mean profiles can be determined with excellent confidence. For process studies, however, errors may be important which occur much less frequently, hence the 95% confidence limits are certainly more appropriate. For the boundary layer even the errors for 95% confidence are rather small, 2.7 $\mu g\ m^{-3}$, but in the entrainment zone and at the boundaries of aerosol layers in the free troposphere one should be careful with the interpretation of high resolution ozone lidar data.

H.1.9. Possibilities for further error reduction

The accuracy which can be achieved using the above mentioned correction schemes is certainly sufficient for a broad range of applications, e.g. for trend analysis, classification of vertical profiles, or studies of regional differences. For other applications, however, the remaining errors may be too large for permitting a detailed process study. Examples are studies of exchange processes at the top of the boundary layer (entrainment), and the impact of convective clouds on the ozone distribution. In particular for the latter case one is concerned with the detection of small differences in the ozone density in regions with large differences in the aerosol content and in aerosol scattering properties. Because the lidar technique is particularly well suited for such investigations with respect to high temporal and spatial resolution and because of it's ability to yield continuous measurements, techniques have been explored which allow further reduction of aerosol-induced errors. These techniques require additional measurements to be performed.

The main problem of the standard DIAL technique is that one has two sets of measured quantities (as a function of height), but at least five sets of unknowns: the ozone density, the aerosol extinction and backscatter coefficients, and at least one parameter each for the wavelength dependencies of the latter two parameters, e.g. the Ångström-coefficients k_α and k_β. To solve this problem it is usually assumed that the lidar ratio $S_L = \alpha_p/\beta_p$ is known (in principle for each height individually, but mostly a constant value is assumed because better information is lacking), and that the wavelength dependencies of α_p and β_p are given by Ångström laws with the know parameters k_α and k_β, which again are usually assumed to be independent of height.

An a additional information about the unknown aerosol parameters may be obtained by measuring the Raman-scattering of a gas of known density. Raman-scattering of either nitrogen or oxygen may be used for this purpose, the larger Raman-scattering cross section of oxygen by and large makes up for the lower density. Raman measurements have the distinct advantage that hey allow a retrieval of the aerosol extinction coefficient independently from the backscatter (Ansmann et al., 1992b).

The use of Raman measurements for improved correction of ozone measurements was first studied by Papayannis et al. (1990). He described an iterative solution, where first the extinction coefficient was calculated from the Raman measurement, then the Klett-inversion technique was used to calculate the aerosol backscatter, and finally the correction for the ozone retrieval was applied.

Matthias et al. (1994) described an analytical solution for the system of equations formed by three lidar equations, two for elastic scattering and one for Raman-scattering. The analytical method revealed that in general two solutions exist, but mostly only one yields realistic values. The advantage of the analytical inversion is that both solutions are obtained, from which the most appropriate may be chosen. When the iteration scheme is used there is little chance to determine which of the two solutions are approached.

An analytical solution also exists for the case that three elastically scattered signals at three different wavelengths are measured. Then at least in principle one parameter of the wavelength dependencies of aerosol scattering properties can be derived from the measurements. Simulations show that all these three-wavelengths-techniques yield better accuracies compared to the standard DIAL. In particular the error is confined to the region of aerosol inhomogeneity rather than propagating into other parts of the profile as observed for the standard DIAL (Bösenberg et al., 1996). But even with these techniques the remaining error may be rather large.

For some applications at least this error may be further reduced by applying the so-called Raman.-DIAL-technique, which has been used successfully for stratospheric measurements (McGhee et al., 1993). In this technique Raman measurements at two wavelengths are used, hence it is completely independent from aerosol backscatter. In addition to the ozone differential absorption only a small differential aerosol extinction enters the analysis. As explained before this error is much smaller than that caused by differential aerosol backscatter, and it can be very much reduced by proper choice of wavelengths.

The major disadvantage of Raman measurements is the long integration time necessary because of the small Raman-scattering cross section. This is true already for the "Raman-assisted-DIAL", where one Raman measurement only is used for an independent retrieval of the aerosol extinction. For the Raman-DIAL-technique the necessary integration times are even longer, since much better accuracy is required due to the necessary differentiation.

Up to now there is no clear evidence which of the different techniques will provide the optimum

reduction of errors in regions of inhomogeneous aerosol distribution. This is made particularly difficult by the fact, that in regions of inhomogeneous aerosol distribution also an inhomogeneous ozone distribution is expected, such that high resolution measurements are required in order to avoid errors caused by averaging (see section B.6.2.1). Probably the best solution will be a combination of the standard DIAL with high resolution and a determination of aerosol properties from Raman measurements with low resolution.

H.1.10. Intercomparison measurements

From the full analysis of the DIAL technique it is evident that there is a number of sources of errors. There are both unavoidable errors due to unknown aerosol properties and instrumental errors due to the very demanding requirements with respect to signal acquisition. It is therefore very important to check the overall performance of the system in actual atmospheric measurements under realistic conditions by comparison to other instruments. However, as for any measurement of the vertical distribution of some atmospheric parameter an accurate intercomparison is rather difficult to perform, since it is not possible to just operate a calibration standard at the desired altitude with the desired spatial and temporal sampling properties. Hence even intercomparison experiments will yield only approximate estimates for the achievable accuracy.

The DIAL system of the MPI has been involved in two major intercomparison experiments. From the first exercise, TROLIX '91, performed at the RIVM in The Netherlands, only the intercomparison between the horizontally pointing lidar and in-situ measurements with a UV-photometer at 20 m height shall be presented here. This type of intercomparison is important because the result shows which accuracy can be achieved in regions of homogeneous aerosol distribution. The UV-photometer is regarded as a very precise and stable instrument, repeated calibrations have shown errors less than 3 $\mu g\ m^{-3}$. The differential aerosol backscatter does not play a role in these measurements, since the aerosol may safely be regarded as horizontally homogeneous when sufficiently long time averages are taken. Figure H.7 shows such an intercomparison for a period of eight hours, the measurements were amended by lidar measurements of the Lund Institute of Technology and by DOAS-measurements (Differential Optical Absorption Spectroscopy) performed by the IVL Göteborg. The range resolution was 150 m for the lidar, the temporal resolution 15 min for all instruments. The agreement between lidar and UV-photometer is excellent, the mean difference is 2.2 $\mu g\ m^{-3}$ only. The agreement with the other instruments is very good, too. Further details of this experiment are described in detail in Bösenberg et al. (1993).

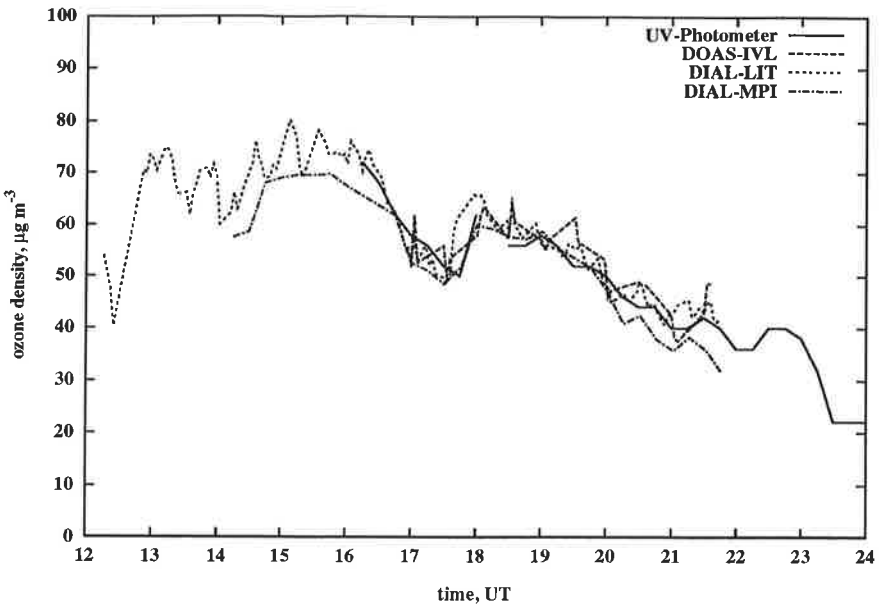

Figure H.7: Intercomparison between MPI-lidar, UV-photometer, Lund-lidar, and IVL-DOAS during TROLIX '91.

The second series of intercomparisons has been performed at the Observatory of the German Weather Service in Lindenberg. The main objective of this experiment was to assess the accuracy of high resolution measurements in the boundary layer, which are particularly difficult because of the highly variable aerosol content. Because of the rather large variability of the ozone density in the lower troposphere, e.g. changes of up to 15 $\mu g\ m^{-3}$ within 1 minute have been observed, carefully prepared ECC-sondes (Vaisala ECC5A) attached to a tethered balloon have been operated for extended periods of time for the intercomparison. For the measurements it was attempted to keep the altitude of the sondes as constant as possible. For a longer time series the moments of the distribution, in particular mean and variance, should not depend on the exact location of the instruments. Hence by comparing mean values the uncertainty can be removed which is always contained in comparison of instantaneous values measured at different locations. The intercomparison of variances also allows an assessment of accuracy for the high resolution measurements.

Table H.4 shows the differences between mean values from sonde and lidar measurements for six time series.

Table H.4: Intercomparison between lidar and tethersonde. The mean difference of measured ozone densities, the standard deviation of differences for 1-minute measurements, and the standard deviations of the individual time series, also based on 1-minute values, are presented.

Date	time interval UT	altitude range m	wave-length pairs nm	mean differ-ence lidar-sonde $\mu g/m^3$	standard deviation of differ-ence $\mu g/m^3$	δ_{O_3} lidar $\mu g/m^3$	δ_{O_3} ECC-sonde $\mu g/m^3$
08.06.94	3:32 - 4:21	270-330	268/292	- 0.1	5.6	4.63	1.86
08.06.94	8:34 - 10:10	720-330	268/292	2.3	2.6	2.72	1.50
08.06.94	14:04 - 15:01	400-490	268/292	1.9	2.7	1.17	1.51
14.06.94	14:44 - 15:19	310-400	277/313	5.8	2.1	1.26	0.82
14.06.94	19:22 - 19:45	200-260	277/313	- 6.7	-----	-----	-----
20.06.94	15:47 - 15:52	210-300	268/292	- 4.4	-----	-----	-----

Differences of mean values between -6.7 and +5.8 $\mu g\ m^{-3}$ have been observed, corresponding to relative deviations of -5.6% and +6.0%. Individual differences may be larger. For the extended time series also the standard deviations of the differences based on 1-minute values are indicated. This standard deviation mostly is not significantly larger than the differences of the mean, with one exception. This result is very satisfying, considering the fact that the 1-minute values still contain differences due to the slightly different position of the probed volumes. The measurements demonstrate very clearly that there is no systematic bias of either lidar or sonde measurements.

For the four measurements extending sufficiently long in time also variances and variance spectra were calculated, using averages of 1-minute resolution for both time series. This averaging was necessary because the original sonde readings were not equidistant. Table H.4 shows that in three out of four cases the variances of the lidar measurements were considerably larger than those of the sonde measurements, only for one case it was the other way round. The variance spectra, not shown here, revealed that this was neither due to a too long time constant of the sonde nor to an increased noise level of the lidar (Grabbe et al., 1996). A detailed examination of the atmospheric conditions showed that the increased variance of the lidar results is most probably due to the incomplete aerosol correction. The more inhomogeneous the aerosol distribution was, the larger was the observed additional variance in the lidar results. This demonstrates the limits of achievable accuracy in DIAL measurements in regions of spatially and temporally inhomogeneous aerosol distribution.

H.2. Ozone lidar applications

Measurements of the ozone vertical distribution in the troposphere with a lidar instrument are useful for a broad range of applications. Possible applications range from regular measurements of mean profiles to establish a long term statistical data set, via studies of the diurnal variations under different conditions, to investigations of the turbulent vertical transport. Some results of such studies shall be presented in the following section.

H.2.1. Long term statistics

The ozone lidar of the Max-Planck-Institut für Meteorologie has been used for numerous measurements since 1991, most of them were performed in the frame of the TOR subproject of the European cooperative project EUROTRAC. These measurements, which have been performed under a variety of meteorological conditions in all seasons, can be used to determine some statistical properties of the ozone distribution in the lower troposphere.

To establish a suitable data set a large number of profiles have been evaluated, mostly as an average over 10 min. The atmospheric stratification for each case has been determined from the off-line backscatter signals and sometimes also from radio soundings. A coarse distinction between boundary layer (PBL) and lower free troposphere (LFT) has been made. For the purpose of this study the so called residual layer, which is the atmospheric layer remaining from the daytime convective PBL during the following night has been labelled as PBL, too. In this layer the ozone distribution of the previous day can be preserved without detectable change for the whole night if mixing is largely suppressed.

Figures H.8 and H.9 show the statistical distribution for the PBL and LFT. Both individual data and monthly averages are indicated. The dashed lines represent weighted averages, which result from making daily averages first before forming the monthly means. This has been made to avoid that the relatively large number of measurements performed purposely on specific days during ozone episodes introduce a bias in the averages. Apparently this bias is only small.

It should be noted, however, that the weather conditions under which the measurements have been performed were selected in so far that lidar observations are not possible in the presence of low clouds or precipitation. deBacker et al. (1994) have shown that the results are unbiased only if the measurements are performed up to a cloud coverage of 6 octas. This was not attempted in our study, but the data do include measurements for such large cloud coverage.

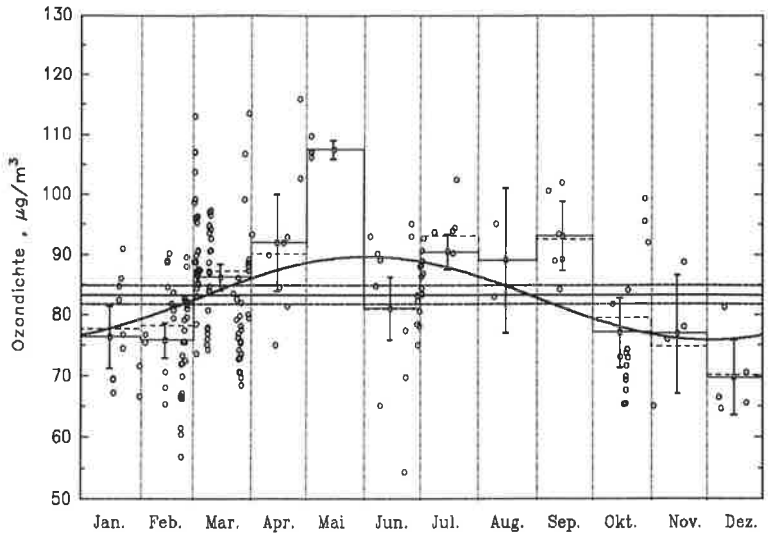

Figure H.8: Annual cycle of the ozone density in the lower free troposphere. All individual measurements (o) are displayed as well as monthly arithmetic means (—), weighted means (---), and a fitted cosine function. For the arithmetic monthly mean values and the overall mean the 95% confidence limits are also indicated.

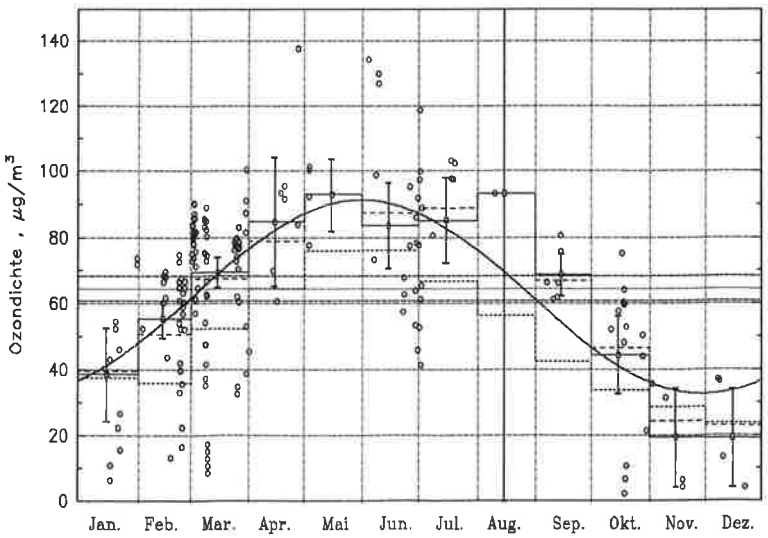

Figure H.9: Annual cycle of the ozone density at the ground. All individual measurements (o) are displayed as well as monthly arithmetic means (—), weighted means (---), and a fitted cosine function. For the arithmetic monthly mean values and the overall mean the 95% confidence limits are also indicated.

The most striking feature of the results is the relatively high value of the ozone density in the free troposphere of about 80 μg m^{-3} during the whole year, even in winter. The annual cycle in the free troposphere is much less pronounced than at the ground, with a maximum of about 90 μg m^{-3} in late spring and a minimum of about 75 μg m^{-3} in late fall. Large deviations from the average mainly occur during spring and summer, both towards higher and lower values. Such high values in the free troposphere all over the year have also been observed at other stations (deMuer, 1995; Ancellet, 1995). The relatively small temporal and spatial variability make evident that the observed high ozone concentration is not caused by local effects. In the free troposphere ozone production is attributed mainly to oxidation of CH_4 and CO with NO serving as catalytic converter (Crutzen, 1979; Seiler and Fishman, 1981). The permanently high values clearly evidence that the pollution of the atmosphere with precursor gases is permanently high at least for the Northern Hemisphere.

Table H.5: Regression analysis for ozone in the lower free troposphere and at ground level. Linear regressions of the form $y = c_1 + c_2 \cdot x$ have been calculated for x = temperature T, relative humidity r, and wind speed ff. A periodic function of the form $y = c_1 + c_2 \cos(2\pi \cdot x + c_3)$ has been fitted for y = number of day/365 and for the wind direction dd/360. $\mathcal{P}$ is the correlation coefficient, $\mathcal{F}$ the fraction of variance explained by the regression, δ_r the standard deviation of the residuals, and δ_d the standard deviation of the original data set.

Lower free troposphere							
Parameter	c_1 μg/m^3	c_2 μg/m^3	c_3	$\mathcal{P}$	$\mathcal{F}$	δ_r μg/m^3	δ_d μg/m^3
number of day/365	82.8	- 6.92	0.5	- 0.32	0.05	10.86	11.45
T	85.6	0.68/K^{-1}		0.40	0.08	10.50	
r	87.6	- 0.10		- 0.20	0.02	11.22	
ff	84.5	-0.13/m^{-1}•s		- 0.06	0.00	11.43	
dd/360	83.1	- 7.26	0.42	- 0.47	0.12	10.09	
Ground level							
number of day/365	62.1	- 29.50	0.51	0.23	0.20	21.15	26.34
T	54.4	1.95/K^{-1}		0.58	0.19	21.43	
r	123.6	- 0.87		- 0.59	0.19	21.25	
ff	49.51	3.45/m^{-1}•s		0.35	0.06	24.69	
dd/360	62.9	7.23	0.38	0.02	0.01	25.99	

In addition to the correlation of the ozone density with the time of the year the correlation with simple meteorological parameters has been investigated. Table H.2.1 provides an overview over these results.

The table clearly shows that only a small fraction of the observed variance can be explained by the correlations studied here. The dependencies as established by the given correlations are statistically not significant. Actually for the ground level observation the correlations with season, temperature, and humidity are statistically significant, but hey are mere manifestations of the well known fact that elevated ozone concentrations are often observed in summer on warm and dry days. Hence the analysis of correlations does not bring about any new explanations for the variability of the ozone concentration. Since it is already well known that the formation and destruction of tropospheric ozone is the result of a complex reaction scheme involving many trace gases and different time scales, this result is not at all surprising. The ozone concentration at a given location is the result of a long and complex development at different locations and times. It cannot be expected that this can be described simply by correlation with one of the basic meteorological parameters.

H.2.2. Development of the ozone distribution during an ozone episode

High ozone concentration in the lower troposphere is mainly observed during so called ozone episodes, which are characterized by high atmospheric pressure in conjunction with larger scale subsidence, high insolation, high temperature, low humidity, and little exchange of air masses. The processes which control the ozone concentration under these conditions are of particular interest because of the adverse effects of extreme ozone concentrations.

The ozone concentration in the lower troposphere is dependent on photochemical processes as well as on horizontal and vertical exchange. Observations at ground level only, as provided by the standard networks measuring air quality, do not provide the information which is necessary to separate the effects of the above mentioned processes. But this becomes possible when the temporal development of the vertical distribution of ozone is measured, either with tethersondes (deMuer et al., 1990) or using DIAL.

The principal features of the diurnal development of the boundary layer under the conditions of an ozone episode has been described in a simple model by Stull (1988). Here three regions are distinguished within the boundary layer: during daytime a strongly turbulent, convectively mixed layer, during night-time a near neutral residual layer comprising the upper part of the previous days boundary layer, and a stable nocturnal boundary layer close to the ground in which mixing is almost completely suppressed. With the onset of convective mixing in the morning, starting from the ground, the residual layer with enhanced ozone concentration will get mixed with the bottom layer, where most of the ozone has been destroyed during the night by deposition at the surface. Therefore the ozone concentration at the ground strongly increases when the convection starts,

while it decreases in that part of the residual layer which is involved in the mixing process. This continues until the residual layer is completely "eaten up" by the newly developed convective boundary layer.

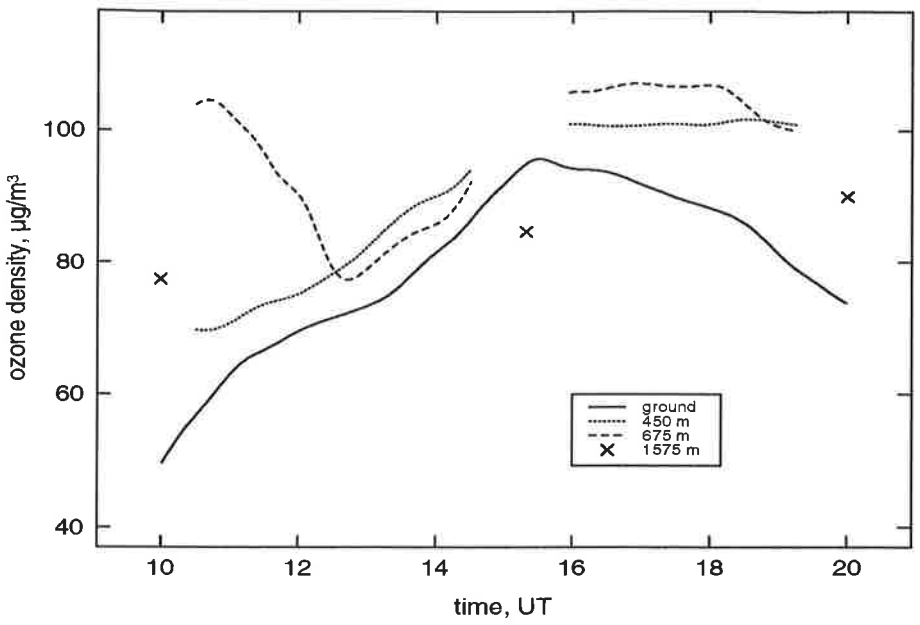

Figure H.10: Diurnal cycle of the ozone density in selected height levels on June 30, 1993.

Figure H.10 shows an example which is typical for such a development. The altitude of 675 m is still within the residual layer until about 10:30 UT, at about 12:30 UT the mixing with the new boundary layer is about complete at this height. The mixing of air from the residual layer into the new boundary layer still continues after that until about 13:30 UT, so that the observed strong increase of the ozone concentration at the ground is caused mainly by mixing in the beginning, but later also by ozone production in the boundary layer. In this particular case the residual layer had vanished completely at about 13:30 UT. The most important aspects of this development are:

- The residual layer is largely decoupled from the ground during night, there is virtually no ozone destruction within the residual layer.
- During the night the ozone destruction at the ground affects the shallow stable boundary layer only.
- Because of the largely suppressed mixing the ozone concentration at the ground can be very low.
- The increase of ozone density before noon in the lower layers is largely caused by mixing with the residual layer, from the rate of increase alone it is not possible to deduce a production rate.
- The free troposphere remains almost unaffected, the strong inversion apparently suppresses the exchange between boundary layer and free troposphere very effectively.

H.2.2.1. Measurement of the ozone budget

It has been explained above that the measurement of time series at a single height is not sufficient to determine a production rate for ozone, at least the vertical transport has to be considered, too. The mass budget in a turbulent boundary layer is described by the following form of the continuity equation, assuming that molecular diffusion, compressibility of the air, and horizontal components of the flux divergence can be neglected:

$$\frac{\partial \bar{\rho}_{O_3}}{\partial t} + \bar{u}\frac{\partial \bar{\rho}_{O_3}}{\partial x} + \bar{w}\frac{\partial \bar{\rho}_{O_3}}{\partial z} + \frac{\partial \overline{w'\rho_{O_3}'}}{\partial z} = \bar{S}_{O_3} \qquad \text{(H.10)}$$

where $\overline{\rho_{O_3}}$ is the ozone density, x the coordinate in the wind direction, z the vertical coordinate, $\overline{w'\rho'_{O_3}}$ the turbulent vertical ozone flux, and S_{O_3} the source term for ozone. The neglection of the horizontal components of the flux divergence is the most critical assumption, which is not always justified. In particular when the sources for precursors are inhomogeneously distributed, or in the presence of clouds, these terms may not be negligible. Such flow fields cannot be characterized by measurements at just one location, four-dimensional temporally and spatially extended measurements have to be performed for a full characterization. In the case of horizontal homogeneity, however, equation (H.10) is valid, in this case the source term is determined by the sum of temporal change, horizontal and vertical advection, and vertical flux divergence. The temporal change of the ozone density can be measured using the DIAL technique. Under a certain range of meteorological conditions the turbulent flux of ozone can be measured directly by combination of high resolution measurements of the vertical ozone distribution and of the vertical wind profile. These measurements can be performed at several heights simultaneously in a major part of the boundary layer (Schaberl, 1995; Senff et al., 1996), such that the vertical flux divergence can be calculated. The vertical advection cannot be measured directly, but a value for the mean vertical wind $\overline{w}$ may be obtained from the analysis of the weather services, the gradient of the ozone density is measured by the lidar. In the case of horizontal homogeneity we then have available from measurements all terms which are necessary to calculate the source term for ozone. For measurements of the horizontal advection at least one additional lidar located upstream is necessary.

Hence the high temporal and spatial resolution of the lidar measurements, in conjunction with continuous operation, and in combination with another remote sensing instrument to measure the vertical wind, make it possible to determine vertical profiles of ozone production or destruction in the convective boundary layer.

This method has been developed at the Max-Planck-Institut für Meteorologie and has been tested during a period of high ozone concentration in the summer of 1993 (Senff et al., 1996, Schaberl, 1995). The measurements were performed in the joint test area of the Max-Planck-Institut für Meteorologie and of the Meteorologisches Institut of the University of Hamburg, which is located at the air field "Hungriger Wolf" in the vicinity of the city of Itzehoe. For a description of that site

the reader is referred to Bösenberg (1994).

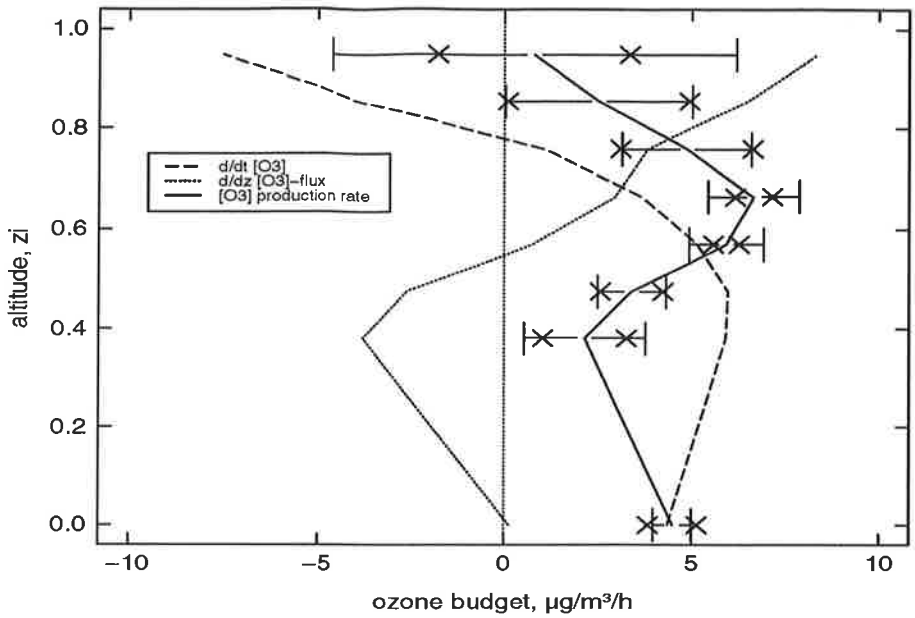

Figure H.11: Ozone budget in the boundary layer on June 30, 1993, 11:34 – 13:14 UT. The temporal rate of change, the vertical flux divergence of the ozone concentration, and the calculated ozone production rate are shown. For the latter error estimates are included, both for the instrumental errors (x) and for the sampling errors (⊣).

Figure H.11 shows vertical profiles of the individual terms of the budget for June 30, 1993, 11:34 – 13:14 UT, which have been derived from combined DIAL and Radar/Rass measurements. At this time the ozone concentration in the upper part of the boundary layer is still strongly decreasing, up to 8 µg m^{-3} h^{-1}, obviously due to redistribution from top to bottom, as may be seen from the flux divergence profile. The vertical advection did not play a major role in this case. The profile of the ozone production is about constant at 5 µg m^{-3} h^{-1}, perhaps with a maximum at about 0.6 of the boundary layer height z_i, and a decrease at the top of the boundary layer which is rather uncertain due to the relatively large measurement errors. The observed pattern is very plausible; the precursor gases can be assumed to be rather well mixed at this location, the radiation needed for photochemical production is almost constant with altitude, too. At the ground the source term should be somewhat smaller due to ozone destruction of the surface.

Figure H.12 shows the diurnal cycle of ozone production on June 30, 1993. The three profiles measured at about 11, 12, and 14 UT show ozone production all over the boundary layer between about 3 and 10 µg m^{-3} h^{-1}. In the late afternoon the ozone destruction dominates at ground level, while at greater heights still ozone is produced. In the evening ozone destruction is observed everywhere in the BL, but much more pronounced at ground level, -10 µg m^{-3} h^{-1}, as compared to

greater heights where values of about -2 $\mu g\ m^{-3}\ h^{-1}$ were observed. Again the observed pattern is very plausible and is supported by the existing theories of the processes involved. But in this experiment for the first time the production rates have been measured directly. The errors in the derived production rates are relatively large, but in systematic studies they may be greatly reduced by repeating these measurements under similar conditions. The errors are mainly of random nature, they are caused by the small number of convective cells which actually cause the vertical transport. Ground based remote sensing is particularly suited for such repeated measurements due to the relatively small effort needed to run the systems.

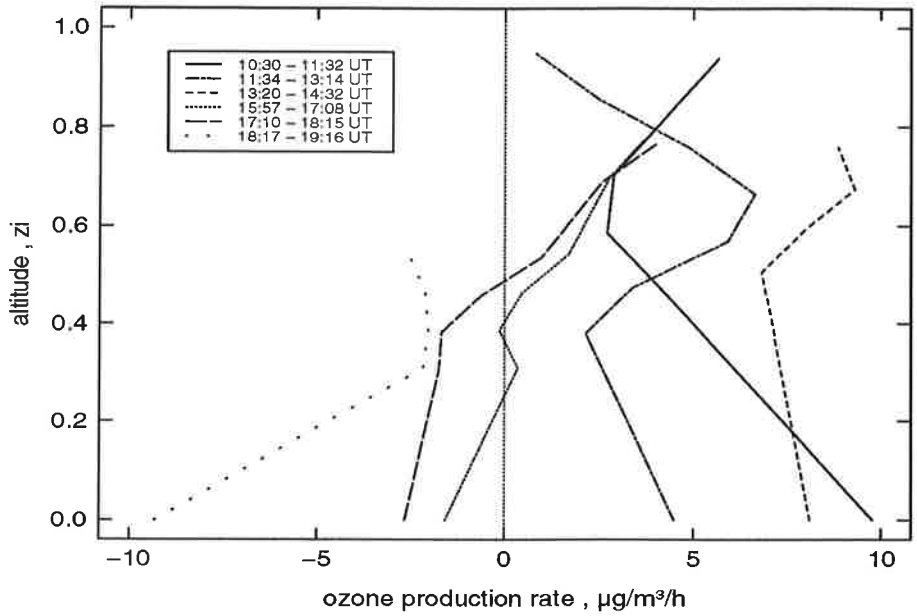

Figure H.12: Diurnal cycle of the ozone production rate in the boundary layer on June 30, 1993.

H.2.3. Impact of clouds on the ozone distribution

The chemical processes governing the production and destruction of photo-oxidants are different in clouds as compared to cloud free regions. The different radiation flux and in particular the interaction with cloud droplets or ice crystals have a marked influence on e.g. the ozone concentration. Since wet deposition goes through the stadium of cloud droplets, too, a detailed knowledge of cloud processes is very important. Because of the complex cloud structure the influence of clouds is hard to assess quantitatively through actual measurements. In situ measurements require a large effort, in particular when simultaneous measurements in different heights are required. For such cloud studies lidar measurements can be very useful, since continuous measurements below and between clouds are possible, which can reveal the modification of the ozone distribution by the cloud processes. Such measurements have not yet been performed in a systematic way, mainly because the necessary correction for differential aerosol backscatter and extinction is still too

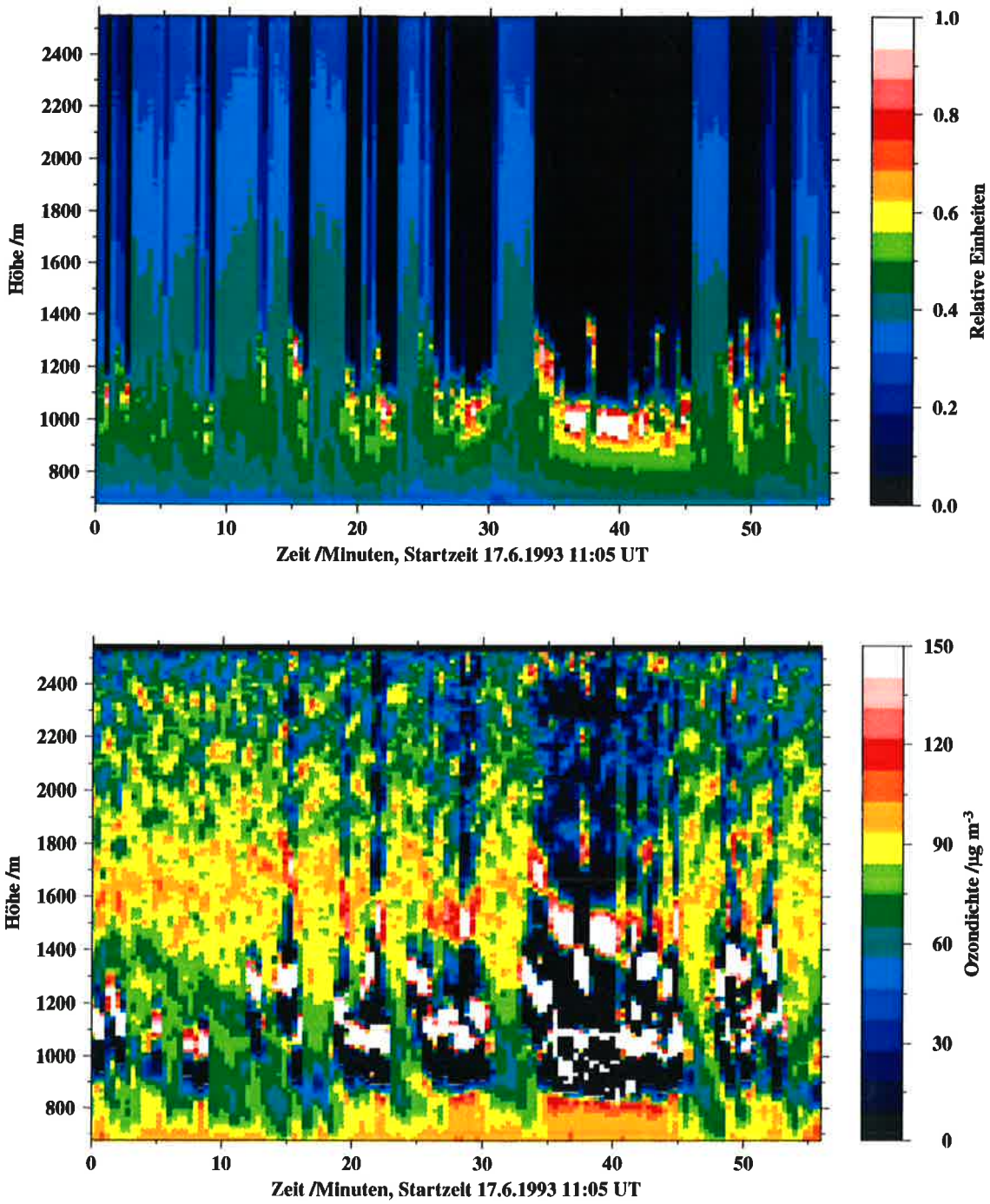

Figure H.13: Aerosol and ozone distributions in the surroundings of boundary layer clouds.

uncertain to yield reliable results in regions of strongly inhomogeneous aerosol distribution in the vicinity of clouds. Improved correction methods using elastic scattering at several wavelengths and/or Raman-scattering are currently under development, as explained in section H.1.9.

One example based on the standard DIAL technique shall be presented here to demonstrate which kind of processes can be studied by lidar provided that sufficiently accurate measurements can be performed in regions of strong aerosol gradients. For this purpose figure H.13 shows time-height distributions of ln ($P \cdot R^2$), reflecting the aerosol distribution (upper panel), and of the ozone density (lower panel), In the backscatter signal a layer of small isolated cumulus clouds above about 900 to 1100 m altitude is clearly visible. The clouds are optically dense, the lidar signal is absorbed rapidly within the clouds, so that no measurements are possible beyond the clouds.

Below and between the clouds the ozone density can be measured up to 2000 m altitude. High values of ozone below the cloud base in the updraft regions are clearly visible, while between the clouds, and in regions where downdrafts may be assumed, the ozone concentration apparently is smaller. In the region of the cloud tops again elevated ozone values are observed. If these measurements can be confirmed by measurements with improved accuracy, they can be used to deduce the ozone destruction in clouds. In conjunction with measurements of the wind field this destruction can be quantified, but for a full understanding of the processes causing this destruction measurements of more substances in the cloud region are required.

I. Summary and conclusions

In this paper the methodology of laser remote sensing of the atmosphere using the technique of differential absorption and scattering has been studied in detail. A general solution for a broad range of applications has been presented and extensively discussed, as well as approximate solutions for the most applications.

In particular it has been demonstrated that for applications involving narrow absorption lines of e.g. water vapor or oxygen in the near infrared all details of the spectral distribution of both the transmitted and the backscattered light have to be accounted for in order to reach the required accuracy. This puts stringent requirements on the spectral properties of the laser, which can be met only since very recently. The inhomogeneity of the aerosol distribution in the atmosphere has a large influence on the accuracy which can be achieved in measurements where either narrow absorption lines or broad absorption bands with little structure are involved. From measured data sets it has been deduced that ozone measurements in the troposphere are mostly possible with good accuracy, provided that the wavelengths used for the experiment have been chosen properly and that the necessary corrections have been applied during the evaluation. This result is confirmed by carefully performed intercomparison experiments. Improved methods which are currently under development are necessary only for special purposes.

A mandatory condition for achieving high accuracy in water vapor measurements is the careful application of the Rayleigh-Doppler-correction. At least for a certain range of conditions the uncertainty caused by this effect is the major source of error. This is even more pronounced for temperature measurements using oxygen absorption, where this uncertainty makes measurements performed with the standard technique almost useless. In order to avoid this problem it is suggested to use narrowband detection in addition to narrowband laser transmission. This will make the effective absorption cross section independent of the details in the spectral distribution of the backscattered light. The requirements for both heterodyne and direct detection are briefly presented and discussed. Using this modified DIAL technique will permit both high accuracy water vapor measurements under all conditions where lidar measurements can be performed at all, as well as high resolution temperature measurements with a level of precision which is sufficient for process studies.

The method has been demonstrated to be suitable for water vapor measurements throughout the troposphere, and particularly suitable for high resolution measurements in the boundary layer. For day-time measurements the DIAL technique is clearly superior compared the Raman measurements, for night-time observations it is the other way round.

Ozone measurements have been performed regularly over a period of several years, routine measurements now require relatively little effort. The data set presently comprises four years of measurements, it has been used for studies of the dependence of tropospheric ozone concentration on

meteorological parameters. An important result is the observation that the ozone concentration in the lower free troposphere is rather high around 80 $\mu g\ m^{-3}$ all over the year, showing little variability and annual cycle only. This result, which is confirmed by measurements at other stations, suggests that the ozone distribution in this layer is spatially homogeneous, too. Hence the sources for this high level of ozone have to be distributed on a rather large scale as well. Apparently the pollution of the atmosphere has reached such a high level that probably at least in a larger part of the Northern Hemisphere a critical ozone level is permanently reached.

Another result is that correlations with simple meteorological parameters are not significant to a degree which would permit a reliable forecast of the ozone concentration. Except for the well known fact that high pressure systems in summer, associated with larger scale subsidence, strong insolation, high temperature, and low humidity will cause periods with high ozone concentration, the correlations which have been investigated do not lead to any useful conclusion. However, this result was expected, since ozone is formed by a complex process involving many precursors and photochemical reactions as well as atmospheric transport processes. Lidar measurements are demonstrated to be particularly suitable to separate the influences of transport from chemical reactions, because of the continuous high resolution measurement capability.

It is also shown that lidar measurements can be used to study turbulent transport processes because of the high spatial and temporal resolution which can be achieved in conjunction with high accuracy. The vertical transports of water vapor and ozone have been measured directly in the boundary layer under convective conditions using the eddy correlation technique. For these measurements the corresponding DIAL systems were used in combination with a Radar/Rass which provides high resolution measurements of the vertical wind. A major advantage of this method is that vertical profiles of the vertical transport are obtained such that the flux divergence can be calculated, too. In the ozone case this has been used for the first time to determine the individual components of the ozone budget under conditions of negligible horizontal advection. From these measurements it was possible to deduce ozone production rates as a function of height in the boundary layer.

After proving the general capability of the DIAL technique for investigating turbulent transport processes further improvement of this method is desirable. First priority should be given to an improvement of both temporal and vertical resolution. This is required for applications where smaller eddies contribute significantly to the transport. There are some possibilities to achieve such improvements. In particular for water vapor measurements the average transmitted power can be increased significantly, the laser development is just at the beginning regarding this aspect. Also for the ozone system an increase in average power by increasing the repetition rate appears feasible. Another possibility is the use of bigger telescopes. In addition for a restricted height range better vertical resolution may be achieved by using a stronger absorption line. The combination of these actions will lead to a considerable expansion of the range of applicability of the eddy correlation technique in remote sensing.

Routine operation of water vapor DIAL measurements in the whole troposphere require an improved reliability of laser performance. In principle this is possible with the system presently used, since only long-life laser material is used, and since the resonator construction has proven to be very stable. Presently problems are encountered with the pump chamber of the pulsed amplifier, with the cooling system, and with the argon ion laser used for pumping the cw master laser. The latter will soon be replaced by a solid state laser for which high reliability has been demonstrated. The other problems are mainly of technical nature and should be fixed in the near future. A very reliable operation is expected when these improvements are incorporated.

The ultimate restriction for the achievable accuracy in water vapor measurements using the standard DIAL technique is caused by a residual uncertainty of the Rayleigh-Doppler-correction in regions of inhomogeneous aerosol distribution. To solve this problem it is suggested to use a very narrowband filter in the receiver optics, which reduces the receiver band width to those values which have already been reached for the laser transmitter. Then the Rayleigh-Doppler-correction becomes obsolete, which will significantly increase the accuracy of the measurements and significantly decrease the complexity of the data evaluation.

This suggested HSRD-method (High Spectral Resolution DIAL) will also make it possible to perform high resolution temperature measurements using the temperature dependence of oxygen absorption in the A-band in the near infrared. Only if the detection bandwidth is restricted to about 60 MHz this method, which has been in the discussion for a long time already, will yield accurate results.

As a special variant of the HSRD it is suggested to use heterodyne detection as a narrowband filter in the receiver. Besides many advantages with respect to the detector this technique also has disadvantages, mainly due to the different signal statistics. A detailed study is needed to assess the relative merits of heterodyne detection, but certainly the possibility of obtaining simultaneous measurements of water vapor or temperature as well as vertical wind speed, which is facilitated by simultaneous measurements of amplitude and frequency of the backscattered field, makes this technique very attractive. But detailed studies will have to be performed before this method will be ready for application.

Acknowledgements

First I would like to thank Prof. Dr. H. Hinzpeter for initiating and continuously supporting this work, and for providing the freedom necessary to perform such a long term development. In succession of Prof. Hinzpeter Prof. Dr. H. Graßl has continued to support this work, which is gratefully acknowledged.

I am particularly grateful to my family for the patience they have shown during the time when this work was performed, and for the important support, without which it would not have been completed.

The important contributions to the development of lidar techniques made by a number of coworkers and by students during their scientific education is very much appreciated. Special thanks go to the colleagues in the mechanical and electronic workshops, who made the complex lidar systems really existent by their independent and judicious work. In particular the development and operation of the special data acquisition systems and evaluation programs by Holger Linné is gratefully acknowledged.

Parts of this work have been supported by the Deutsche Forschungsgemeinschaft and by the Bundesminister für Forschung und Technologie. Other parts of the work were performed in the frame of the European program EUROTRAC within the subprojects TOR and TESLAS. Particular thanks go to the colleagues of TESLAS, whose works I had the pleasure to coordinate for the last couple of years, for providing me with numerous hints and stimulations evolving from their work before making them public to a wider community.

In the preparation of the figures the programs GMT-system (Wessel and Smith, 1991) and Gnuplot (copyright (c) 1986-1995 Thomas Williams, Colin Kelly and many others) have been used. Thanks go to their authors for providing these programs free of charge.

Last but not least the careful preparation of this manuscript by B. Zinecker and N. Bente is gratefully acknowledged.

J. References

Ancellet, G. (1995): Personal communication.

Ansmann, A. (1984): Fehleranalyse der Differential-Absorption-Lidartechnik zur Ermittlung des troposphärischen Wasserdampfes anhand von Modellsimulationen. Diplomarbeit, Universität Hamburg.

Ansmann, A. (1985): Errors in ground-based water-vapor DIAL-measurements due to Doppler-broadened Rayleigh Backscattering. *Appl. Optics*, 24, 3476-4380.

Ansmann, A. (1989): Bodengebundene DIAL-Wasserdampfmessung: Berücksichtigung der Dopplerverbreiterung der Laserlinie durch Rayleighrückstreuung. Dissertation, Universität Hamburg.

Ansmann, A. and J. Bösenberg (1987): Correction scheme of spectral broadening by Rayleigh scattering in differential absorption lidar measurements of water vapor in the troposphere. *Appl. Optics*, 26, 3026-2032.

Ansmann, A., M. Riebesell, U. Wandinger, C. Weitkamp, E. Voss, W. Lahmann, and W. Michaelis (1992a): Combined Raman elastic-backscatter lidar for vertical profiling of moisture, aerosol extinction, backscatter, and lidar ratio. *Appl. Phys.*, B, 55, 18-28.

Ansmann, A., U. Wandinger, M. Riebesell, C. Weitkamp, and W. Michaelis (1992b): Independent measurement of extinction and backscatter profiles in cirrus clouds by using a combined Raman elastic-backscatter lidar. *Appl. Optics*, 31, 7113-7131.

Baker, P.W. (1983): Atmospheric water vapor differential absorption measurements on vertical paths with a CO_2 lidar. *Appl. Optics*, 22, 2257-2264.

Bass, A.M., A.E. Ledford, and A.H. Lauffer (1976): Extinction coefficients of NO_2 and N_2O_4. *J. Res. Nat. Bur. Stand*, A, 80, 143.

Bissonnette, L.R., P. Bruscaglioni, A. Ismaelli, G. Zaccanti, A. Cohen, Y. Benayahu, M. Kleiman, S. Egert, C. Flesia, P. Schwendimann, A.V. Starkov, M. Noormohammadian, U.G. Oppel, D.M. Winker, E.P. Zege, I.L. Katsev, and I.N. Polonsky (1995): Lidar multiple scattering from clouds. *Appl. Physics*, B, 60, 355.

Bohren, C.F., and D.R. Huffman (1983): Absorption and Scattering of Light by Small Particles. John Wiley & Sons, New York.

Born, M. and E. Wolf (1993): Principles of Optics. Pergamon, Oxford, 6th edition.

Bösenberg, J. (1985): Measurements of the pressure shift of water vapor absorption lines by simultaneous photoacoustic spectroscopy. *Appl. Optics*, 24, 3531-3534.

Bösenberg, J. (1987): A DIAL system for high resolution water vapor measurements in the troposphere. In: Topical Meeting on Laser and Optical Remote Sensing, North Falmoth, Vol. 18 of Technical Digest,22-25, Opt. Soc. Amer.

Bösenberg, J. (1991): A differential absorption lidar system for high resolution water vapor measurements in the troposphere. Report 71, Max-Planck-Institut für Meteorologie, Hamburg.

Bösenberg, J. (1994): In: Cvitas, T. and D. Kley (editors): The TOR Network, Garmisch-Partenkirchen.

Bösenberg, J., G. Ancellet, A. Apituley, R. Barbini, E. Durieux, H. Edner, L. Fiorani, A. Papayannis, T. Trickl, C. Weitkamp, and V. Zuev (1995): TESLAS, Tropospheric Environmental Studies by Laser Sounding. in: J. Bösenberg, G. Brassington, and P. Simon (editors) Instrument Development. in press, Springer-Verlag, Berlin.

Bösenberg, J., G. Ancellet, A. Apituley, H. Bergwerff, G. von Cossart, H. Edner, J. Fiedler, B. Galle, C.N. de Jonge, J. Mellquist, V. Mitev, T. Schaberl, G. Sonnemann, J. Spakman, D.J.P. Swart, and E. Wallinder (1993): Tropospheric ozone lidar intercomparison experiment. TROLIX '91, Field Phase Report, Report 102, Max-Planck-Institut für Meteorologie, Hamburg.

Bösenberg, J., A. Ansmann, and F. Theopold (1989): Hochauflösende Feuchtemessungen mit einem Zwei-Frequenz-Lidar. *Ann. Meteorologie*, 26, 57-58.

Bösenberg, J., and H. Hinzpeter (1986): Entwicklung und Erprobung eines LIDAR-Systems zur Messung des Wasserdampfkonzentrationsprofiles in der Troposphäre mit hoher Genauigkeit sowie zeitlicher und räumlicher Auflösung. Abschlußbericht KF 10056, Max-Planck-Institut für Meteorologie, Hamburg.

Brassington, D.J. (1981):Sulphur dioxide absorption cross section measurements from 290 nm to 317 nm. *Appl. Optics*, 20, 3774-3779.

Browell, E.V. (1983): Remote sensing of tropospheric gases and aerosols with an airborne DIAL system. in: D.K. Killinger and A. Mooradian (editors) Optical and Laser Remote Sensing, 138-147, Springer-Verlag, Berlin.

Browel, E.V. (1989): Differential Absorption Lidar Sensing of Ozone. Proceedings IEEE, 77, 419-432.

Browell, E.V., A.K. Goroch, T.D. Wilkerson, S. Ismail, and R. Markson (1984): Airborne DIAL water vapor and measurements over the gulf stream. In: 12th International Laser Conference.

Browell, E.V., S. Ismail, and S.T. Shipley (1985): Ultraviolet DIAL measurements of O_3 profiles in regions of spatially inhomogeneous Aerosols. *Appl. Optics*, 24, 2827-2836.

Browell, E.V., T.D. Wilkerson, and T.J. McIlrath (1979): Water vapor differential absorption lidar development and evaluation. *Appl. Optics*, 18, 3474-3483.

Bruneau, D., T.A. des Lions, P. Quaglia, and J. Pelon (1994): Injection-seeded pulsed alexandrite laser for differential absorption lidar application. *Appl. Optics*, 33, 3941-3950.

Cahen, C. and G. Mégie (1981): A spectral limitation of the range resolved differential absorption LIDAR technique. *J. Quant. Spectrosc. Radiative Transfer*, 25, 151.

Cahen, C., G. Mégie, and P. Flamant (1982): Lidar monitoring of the water vapor cycle in the troposphere, *J. Appl. Meteorology*, 21, 1506-1515.

Cann, M.W.P., J.B. Shinn, and R.W. Nicholls (1984): Oxygen absorption in the spectral range 180-300 nm for temperatures to 3000 K and pressures to 50 atm. *Canadian Journal of Physics*, 62, 1738.

Collis, R.T.H., and P.B. Russell (1976): Lidar measurement of particles and gases by elastic backscattering and differential absorption. In: E.D. Hinkley (editor) Laser monitoring of the atmosphere. Springer Verlag, Berlin.

Crutzen, P.J. (1979): The role of NO and NO_2 in the chemistry of the troposphere and stratosphere. *Ann. Rev. Earth Planet. Sci.*, 7, 443-472.

Davenport, W.M. and W.L. Root (1958): Random Signals and Noise. McGraw-Hill, New York.

deBacker, H., E.P. Visser, D. deMuer, and D.P.J. Swart (1994): Potential for meteorological bias in lidar ozone data sets resulting from the restricted frequency of measurement due to cloud cover. *J. Geophys. Res.*, 99 (D1), 1395-1401.

deMuer, D. (1995): Personal communication.

deMuer, D., R. Heylen, and H. deBacker (1990): Vertical profiles of ozone and meteorological parameters at Uccle (Belgium) obtained with free balloons and a tethered balloon. Annual report, part 9, Tropospheric Ozone Research, EUROTRAC, Garmisch-Partenkirchen.

Edner, H., K. Fredriksson, A. Sunesson, S. Svanberg, L. Uneus, and W. Wendt (1987): Mobile remote sensing system for atmospheric monitoring. *Appl. Optics*, 26, 4330-4338.

Ehret, G., C. Kiemle, W. Renger, and G. Simmet (1993): Airborne remote sensing of tropospheric water vapor with a near-infrared differential absorption lidar system. *Appl. Optics*, 32, 4534-4551.

Eichinger, W.E., D.I. Cooper, F.L. Archuletta, D. Hof, D.B. Holtkamp, R.R. Karl, C.D. Quick, and J.Tie (1994): Development of a scanning solar-blind, water Raman lidar. *Appl. Optics*, 33, 3923-3932.

Eng, R.S., P.L. Kelley, A. Mooradian, A.R. Calawa, and T.C. Harman (1973): Tunable laser measurements of water vapor transitions in the vicinity of 5 μm. *Chem. Phys. Lett.*, 19, 524-528.

Eng. R.S., P.L. Kelley, A.R. Calawa, T.C. Harman, and K.W. Nill (1974): Tunable diode laser measurements of water vapour absorption line parameters. *Mol. Phys.*, 28, 653-664.

Feltz, W.F. (1994): Meteorological applications of the atmospheric emitted radiance interferometer (AERI). PhD thesis, University of Wisconsin, Madison,

Fernald, F.G. (1984):Analysis of atmospheric lidar observations: some comments. Appl. Optics, 23, 652-653.

Fukuda, T., Y. Matsuura, and T. Mori (1984): Sensitivity of coherent range-resolved differential absorption lidar. *Appl. Optics*, 23, 2026-2032.

Gast, E. (1991): Messung des Linearitätsverhaltens von Photomultipliern und Untersuchung der zeitabhängigen Nachwirkungen kurzer hoher Lichtimpulse. Diplomarbeit, Fachhochschule Wedel.

Goldsmith, J.E.M. and S.E. Bisson (1995): Raman lidar profiling of atmospheric water vapor. in: Combined Optical-Microwave Earth and Atmospheric Sensing, Conference Proceedings, 106-108.

Goldsmith, J.E.M., S.E. Bisson, R.A. Ferrare, K.D. Evans, D.N. Whiteman, and S.H. Melfi (1994): Raman lidar profiling of atmospheric water vapor simultaneous measurements with two collocated systems. *Bull. Am. Meteorol. Soc.*, 75, 975-982.

Goodman, J.W. (1965): Some effects of target-induced scintillation on optical radar performance. Proc. IEEE, 53, 1688-1700.

Grabbe, G.C. (1995): Untersuchungen troposphärischen Ozons mit DIAL. Dissertation, Universität Hamburg.

Grabbe, G.C., J. Bösenberg, H. Dier, U. Görsdorf, V. Matthias, G. Peters, T. Schaberl, and C. Senff (1996): Intercomparison of ozone measurements between lidar and ECC-sondes. *Contr. Atm. Physics*, 69, 189-203.

Grant, W.B., A.M. Brothers, and J.R. Bogan (1988): Differential absorption lidar averaging. *Appl. Optics*, 27, 1934-1938.

Grant, W.B., J.S. Margolis, A.M. Brothers, and D.M. Tratt (1987): CO_2 DIAL measurements of water vapor. *Appl. Optics*, 26, 3033-3042.

Grossmann, B. and E.V. Browell (1989): Spectroscopy of water vapor in the 720 nm wavelength region: line strengths, self-induced pressure broadenings and shifts, and temperature dependence of linewidths and shifts. *J. Mol. Spectrosc.*, 136, 264-294.

Hardesty, R.M. (1984): Coherent DIAL measurement of range-resolved water vapor concentration. *Appl. Optics*, 23, 2545-2553.

Hardesty, R.M., R.J. Keeler, M.J. Post, and R.A. Richter (1981): Characteristics of coherent lidar returns from calibration targets and aerosols. *Appl. Optics*, 20, 3763.

Harms, J. (1979): Lidar return signals for coaxial and noncoaxial systems with central obstruction. *Appl. Optics*, 18, 1559-1566.

Herzberg, G. (1950): Molecular Spectra and Molecular Structure. van Nostrand Reinhold, Cincinnati, 2nd edition.

Iikura, Y. N. Sugimoto, Y. Sasano, and H. Shimizu (1987): Improvement on lidar data processing for stratospheric aerosol measurements. *Appl. Optics*, 26, 5299.

Ismail, S. and E.V. Browell (1989): Airborne and spaceborne lidar measurements of water vapor profiles: a sensitivity analysis. *Appl. Optics*, 28, 3603-3615.

Jakeman, E., C.J. Oliver, and E.R. Pike (1975): Optical homodyne detection. *Adv. Phys.*, 24, 349-405.

Kempfer, U., W. Carnuth, R. Lotz, and T. Trickl (1994): A wide-range ultraviolet lidar system for tropospheric ozone measurements - development and application. *Review of Scientific Instruments*, 65(10), 3145-3164.

Killinger, D.K. and N. Menyuk (1987): Laser remote sensing of the atmosphere. *Science*, 235, 37-45.

Klett, J.D. (1981): Stable analytical inversion solution for processing lidar returns. *Appl. Optics*, 20, 211-220.

Korb, C.L. and C.Y. Weng (1979): A two-wavelength LIDAR technique for measurement of atmospheric temperature profiles. in: Proc. Ninth Int. Laser Radar Conf., Munich 185-186. Amer. Meteor. Soc.

Korb, C.L. and C.Y. Weng (1982): A theoretical study of a two-wavelength LIDAR technique for the measurement of atmospheric temperature profiles. *J. Appl. Meteor.*, 21, 1346-1355.

Lamport, L. (1985): LaTeX, A Document Preparation System. Addison Wesley, Reading, Ma.

Langmann, B. (1995): Einbindung der regionalen troposphärischen Chemie in die Hamburger Klimamodellumgebung: Modellrechnungen und Vergleich mit Beobachtungsdaten. Dissertation, Universität Hamburg.

Lehmann, S. (1994): Empfangssystem für Lidarsignale mit erweitertem Meßbereich. Diplomarbeit, Universität Hamburg.

Lenschow, D.H., J. Mann, and L. Kristensen (1994): How long is long enough when measuring fluxes and other turbulence statistics? *J. Atm. Oceanic Techn.*, 11, 661-673.

Lenschow, D.H. and B.B. Stankov (1986): Length scales in the convective boundary layer. *J. Atm. Sciences*, 43, 1198-1209.

Long. D.A. (1977): Raman Spectroscopy. McGraw-Hill, New York.

Macke, A. (1993): Scattering of light by polyhedral ice crystals. *Appl. Optics*, 32, 2780-2788.

Malicet, J., D. Daumont, J. Charbonnier, C. Parisse, A. Chakir, and J. Brion (1995): Ozone UV spectroscopy. II: Absorption cross-sections and temperature dependence. *J. Atm. Chem.*, 21, 263-273.

Mason, J.B. (1975): LIDAR measurements of temperature: A new approach. *Appl. Optics*, 14, 76-78.

Matthias, V. (1993): Messung der atmosphärischen Ramanstreuung mit Hilfe eines UV-LIDAR-Systems. Diplomarbeit, Universität Hamburg.

Matthias, V., J. Bösenberg, and V. Wulfmeyer (1994): Improvement of ozone DIAL by using an additional Raman channel. In: Proceedings EUROTRAC Symposium '94, 326-329, Garmisch-Partenkirchen.

McDermid, I.S., S.M. Godin, and D.T. Walsh (1990): Lidar measurements of stratospheric ozone and intercomparisons and validation. *Appl. Optics*, 29, 4914-4923.

McGee, T.J., M.R. Gross, R.A. Ferrare, W.S. Heaps, and U.N. Sing (1993): Raman lidar measurements of stratospheric ozone in the presence of volcanic aerosols. *Geophys. Res. Lett.*, 20, 955-958.

Measures, R.M. (1984): Laser Remote Sensing. John Wiley & Sons, New York

Mégie, G. (1980): Mesure de la pression et de la température atmosphériques par absorption différentielle lidar: Influence de la largeur d'émission laser. *Appl. Optics*, 19, 34-43.

Mie, G. (1908): Beiträge zur Optik trüber Medien, speziell kolloidaler Metallösungen. *Ann. Physik*, 25, 377-455.

Milton, M.J.T. and P.T. Woods (1987): Pulse averaging methods for a laser remote monitoring system using atmospheric backscatter. *Appl. Optics*, 23, 2026.

Molina, L.T. and M.J. Molina (1986): Absolute absorption cross sections of ozone in the 185- and 350-nm wavelength range. *Journal of Geophysical Research*, 91, 14501-14508.

Murray, E. (1978): Remote measurement of gases using differential-absorption lidar. *Opt. Eng.*, 17, 30-38.

Murray, E.R., R.D. Hake, J.E.v. der Laan, and J.G. Hawley (1976): Atmospheric water vapor measurements with a 10 micrometer DIAL system. *Appl. Phys. Lett.*, 28, 542-543.

Papayannis, A., G. Ancellet, J. Pelon, and G. Mégie (1990): Multiwavelength lidar for ozone measurements in the troposphere and the lower stratosphere. *Appl. Optics*, 29, 467-476.

Peters, G., D. Hasselmann, and S. Pang (1988): Radio acoustic sounding of the atmosphere using a FM-CW radar. *Radio Sci.*, 23, 640-646.

Peters, G. and H.J. Kirtzel (1994): Measurement of momentum flux in the boundary layer by RASS. *J. Atmos. Oceanic Technol.*, 11, 63-75.

Ponsardin, P., N.S. Higdon, B.E. Grossmann, and E.V. Browell (1994): Spectral control of an alexandrite laser for an airborne water-vapor differential absorption lidar system. *Appl. Optics*, 33, 6439.

Remsberg, E.E. and L.L. Gordley (1978): Analysis of differential absorption lidar from the space shuttle. *Appl. Optics*, 17, 624-630.

Ritter, K.J. (1986): A high resolution spectroscopy study of absorption line profiles in the A-band of molecular oxygen. PhD thesis, University of Maryland.

Ritter, K.J. and T.D. Wilkerson (1987): High-resolution spectroscopy of the oxygen A-band. *J. Mol. Spectrosc.*, 121, 1-19.

Rothe, K.W. (1980): Monitoring of various atmospheric constituents using a cw chemical hydrogen/deuterium laser and a pulsed carbon dioxide laser. *Radio Electron. Eng.*, 50, 567-574.

Russell, P.B., B.M. Morley, J.M. Livingston, G.W. Grams, and E.M. Patterson (1982): Orbiting lidar simulations. 1: Aerosol and cloud measurements by an independent-wavelength technique. *Appl. Optics*, 21, 1541-1553.

Sasano, Y., E.V. Browell, and S. Ismail (1985): Error caused by using a constant extinction/backscattering ration in the lidar solution. *Appl. Optics*, 24, 3929-3932.

Schaberl, T. (1990): Aufbau und Erprobung der Sende- und Empfangsoptik für ein Ozon-LIDAR unter Benutzung der stimulierten Raman-Streuung. Diplomarbeit, Universität Hamburg.

Schaberl, T. (1995): Messung des Ozonflusses in der unteren Troposphäre mit einem neuen Ozon-DIAL-System und einem Radar-Rass. Dissertation, Universität Hamburg.

Schlüssel, P. (1995): Passive Fernerkundung der unteren Atmosphäre und der Meeresoberfläche aus dem Weltraum. Berichte aus dem Zentrum für Meeres- und Klimaforschung, A20, Hamburg.

Schotland, R.D. (1966): Some observations of the vertical profile of water vapor by means of a ground based optical radar. in: Proc. Fourth Symposium on Remote Sensing of the Environment, University of Michigan, 271-273.

Schotland R.M. (1974): Errors in the lidar measurements of atmospheric gases by differential absorption. *J. Appl. Meteor.*, 13, 71-77.

Schwemmer, G.K. and T.D. Wilkerson (1979): LIDAR temperature profiling: Performance simulation of Mason's method. *Appl. Optics*, 18, 3539-3541.

Seiler, W. and J. Fishman (1981): The distribution of carbon monoxide and ozone in the free troposphere. *J. Geophys. Res.*, 86, 7255-7265.

Senff, C. (1993): Messung des Wasserdampfflusses in der konvektiven Grenzschicht mit DIAL und RADAR-RASS. Dissertation, Universität Hamburg.

Senff, C., J. Bösenberg, and G. Peters (1994): Measurement of water vapor flux profiles in the convective boundary layer with Lidar and Radar-RASS. *J. Atm. Oceanic Technology*, 11, 85-93.

Senff, C., J. Bösenberg, G. Peters, and T. Schaberl (1996): Remote sensing of turbulent ozone fluxes and the ozone budget in the convective boundary layer with DIAL and RADAR-RASS: a case study. *Contr. Atm. Physics*, 69, 161-177.

Staehr, W., W. Lahmann, and C. Weitkamp (1985): Range-resolved differential absorption lidar: Optimization of Range and Sensitivity. *Appl. Optics*, 24, 1950-1956.

Strutt, J.W. (1871): On the light from the sky, its polarization and colour. *Phil. Mag.*, 41, 107-120.

Stull, R. (1988): An Introduction to Boundary Layer Meteorology. Kluwer, Dordrecht.

Takano, Y. and K.-N. Liou (1989): Solar radiative transfer in cirrus clouds. Part I: Single-scattering and optical properties of hexagonal ice crystals. *J. Atmos. Sci.*, 46, 3-19.

Takano, Y. and K.-N. Liou (1995): Radiative transfer in cirrus clouds. Part III: Light scattering by irregular ice crystals. *J. Atmos. Sci.*, 52, 818-837.

Tennekes, H. and J.L. Lumley (1972): A First Course in Turbulence. MIT Press, Cambridge, Massachusetts.

Theopold, F.A. (1990): Bestimmung des Temperaturprofils der Troposphäre mit einem Zwei-Frequenz-Lidar. Dissertation, Universität Hamburg.

Theopold, F.A., C. Weitkamp, and W. Michaelis (1992): BELINDA: Broadband Emission Lidar with Narrowband Determination of Absorption. A new concept for measuring water vapor and temperature profiles. In: 16. International Laser Radar Conference, 671.

Theopold, F.A. and J. Bösenberg (1993): Differential absorption lidar measurements of atmospheric temperature profiles: Theory and experiment. *J. Atm. Oceanic Technology*, 10, 165-179.

USSA (1976): US Standard Atmosphere. Technical Report, NOAA, NASA, USAF, Washington, D.C.

van de Hulst, H.C. (1981): Light Scattering by Small Particles. Dover Publ., New York.

Völger, P. (1993): Optische Eigenschaften von Aerosolpartikeln und deren Auswirkungen auf Ozonmessungen mit einem LIDAR. Diplomarbeit, Universität Hamburg.

Völger, P., J. Bösenberg, and I. Schult (1996): Scattering properties of selected model aerosols calculated at UV-wavelengths: implications for DIAL measurements of tropospheric ozone. *Contr. Atm. Physics*, 69, 177-187.

Wandinger, U. (1994): Theoretische und experimentelle Studien zur Messung stratosphärischen Aerosols sowie zum Einfluß der Mehrfachstreuung auf Wolkenmessungen mit einem Polarisations-Raman-Lidar. Dissertation, Universität Hamburg.

WCRP-5 (1988): Concept of the global energy and water cycle experiment. WMO/TD-215, WCRP-Report 215, WMO, Geneva, Switzerland.

Wendling, P., R. Wendling, and H.K. Weickmann (1979): Scattering of solar radiation by hexagonal ice crystals. *Appl. Optics*, 18, 2663-2671.

Werner, C. and H. Herrmann (1981): Lidar measurements of the vertical humidity distribution in the boundary layer. *J. Appl. Meteorol.*, 20, 476-481.

Wessel, P. and W.H.F. Smith (1991): Free software helps map and display data. *EOS Transactions Am. Geophys. Union*, 72, 441-446.

Whiteman, D.N., S.H. Melfi, and R.A. Ferrare (1992): Raman lidar system for the measurement of water vapor and aerosols in the Earth's atmosphere. *Appl. Optics*, 31, 3068-3082.

Wulfmeyer, V. (1995): DIAL-Messungen von vertikalen Wasserdampfverteilungen. Ein Lasersystem für Wasserdampf- und Temperaturmessungen in der Troposphäre. Dissertation, Universität Hamburg.

Wulfmeyer, V., J. Bösenberg, S. Lehmann, C. Senff, and S. Schmitz (1995): Injection seeded Alexandrite ring laser: performance and application in a water vapor DIAL system. *Optics Letters*, 20, 638-640.

Wyngaard, J.C. (1991): On the maintenance and measurement of scalar fluxes: in: T. Schmugge and J.-C. André (editors) Land Surface Evaporation: Measurement and Parameterization, 199-229, Springer-Verlag, New York.

Yariv, A. (1985): Optical Electronics. Holt, Rinehart, and Winston, New York.

Yip, S. and M. Nelkin (1964): Application of a kinetic model to time-dependent density correlations in fluids. *Phys. Rev.*, A 135, 1241-1247.

Yura, H.T. (1979): Signal-to-noise ratio of heterodyne lidar systems in the presence of atmospheric turbulence. *Optica Acta*, 26, 627-644.

Zhao, Y., R.M. Hardesty, and M.J. Post (1992): Multibeam transmitter for signal dynamic range reduction in incoherent lidar systems. *Appl. Optics*, 31, 7623-7632.

Zuev, V.E., Y.S. Makushkin, V.N. Marichev, A.A. Mitsel, and V.V. Zuev (1983a): Lidar differential absorption and scattering technique: theory. *Appl. Optics*, 22, 3733-3741.

Zuev, V.V., V.E. Zuev, Y.S. Makushkin, V.N. Marichev, and A.A. Mitsel (1983b): Laser sounding of atmospheric humidity: experiment. *Appl. Optics*, 22, 3742-3746.

K.1 Appendix

List of Symbols and abbreviations

A	receiver area
A_{het}	effective receiver area for heterodyne detection
A_T, A_R	area of a "speckle" element
A_ρ	area of a "speckle" element due to scintillation
B	molecule constant describing rotational levels
B_{het}	bandwidth in heterodyne detection
C_{abs}	absorption cross section
C_{ext}	extinction cross section
C_{sca}	scattering cross section
C_n^2	structure constant of atmospheric refractive index fluctuations
D_S	gradient of the range corrected signal, $D_S = d/dR \ln (P \cdot R^2)$
$\vec{E}$	vector of an electric field
I	intensity
$I^{\perp}_s$	intensity of scattered light polarized perpendicular to the plane of incidence
$I^{\parallel}_s$	intensity of scattered light polarized parallel to the plane of incidence
J	rotational quantum number
K_S	scattering ratio, $K_S = \beta/(\beta_m + \beta_p)$
K_δ	factor accounting for depolarization of molecular scattering
M_L	mean molecular mass of air
M_{O_3}	molecular mass of ozone
N	particle density
$N(a)$	size distribution
N_T, N_R	Fresnel numbers
P	power of radiation
P_L	laser power
P_0	apparatus constant, $P_0 = P_L \frac{c \cdot \tau_L \cdot A}{2}$
R	distance
$S(p, T)$	absorption line strength
S_L	lidar ratio, $S_L = \alpha/\beta$
S_K	inverse scattering ratio, $S_L = 1/K_S$
S_{O_3}	source term of ozone
T	temperature
T_0	temperature for standard conditions
$T(\nu)$	transmission at wavenumber ν
T_a	transmission due to molecular and particular scattering
T_g	transmission due to gaseous absorption
T_u	transmission for the path from the laser to the scattering volume
T_d	transmission for the path from the scattering volume to the receiver

a	particle radius
a_m	mean polarizibility of a molecule
a_R	change of mean polarizibility for Raman scattering
a_{H_2O}	scale height of the water vapor profile in a standard atmosphere
a_V	parameter of the Voigt-function
b_L	halfwidth of the laser radiation
b_R	halfwidth of Rayleigh-scattering
b_R^*	corrected halfwidth of Rayleigh-scattering
b_T, b_R	Gaussian beam radii of transmitted and reference beams
b_c	halfwidth of an absorption line due to collison broadening
b_d	halfwidth of an absorption line due to Doppler broadening
c	speed of light
c_B	correction factor for Brillouin scattering
f	frequency
f_V	parameter of the Voigt-function
$g(\nu)$	normalized distribution of spectral density
$g_R(\nu)$	spectral density of Rayleigh backscatter
$h(\nu - \nu', R)$	spectral density of total backscatter
i	unit of the imaginary part of complex number
$\vec{k}$	wave vector
k	wave number
k_B	Boltzmann's constant
k_α	Ångström-coefficient for the wavelength dependence of α_β
k_β	Ångström-coefficient for the wavelength dependence of β_p
l	exponent of the temperature dependence of the absorption line strength
$l(\nu)$	spectral density of laser radiation
m	exponent of the temperature dependence of collision broadening of absorotion lines
n^*	complex index of refraction
p	pressure
p_0	pressure under standard conditions
$p(\Theta, \Phi)$	phase function
q	mixing ratio
t	time
$\vec{u}$	velocity vector
v	velocity
v	vibration quantum number
v_S	speed of sound
v_{th}	thermal velocity
w	vertical wind
w	complex error function

Abbreviations

ASE	**A**mplified **S**pontaneous **E**mission
BELINDA	**B**roadband **E**mission **L**idar with **N**arrowband **D**etermination of **A**bsorption
CNR	**C**arrier to **N**oise **R**atio
DIAL	**D**ifferential **A**bsorption **L**idar
EUROTRAC	European Experiment on the Transport of Transformation of Environmentally Relevant Trace Constituents over Europe
EZ	**E**ntrainment **Z**one
FWHM	**F**ull **W**idth at **H**alf **M**aximum
GEWEX	**G**lobal **E**nergy and **W**ater Cycle **Ex**periment
HSR-DIAL	**H**igh **S**pectral **R**esolution DIAL
HWHM	**H**alf **W**idth at **H**alf **M**aximum
Lidar	**Li**ght **D**etection **a**nd **R**anging
LFT	**L**ower **F**ree **T**roposphere
MOPA	**M**aster **O**scillator - **P**ower **A**mplifier
PBL	**P**lanetary **B**oundary **L**ayer
RASS	**R**adio **A**coustic **S**ounding **S**ystem
SLM	**S**ingle **L**ongitudinal **M**ode
SNR	**S**ignal to **N**oise **R**atio
TESLAS	**T**ropospheric **E**nvironmental **S**tudies by **L**aser **A**tmospheric **S**ounding
TOR	**T**ropospheric **O**zone **R**esearch
UFT	**U**pper **F**ree **T**roposphere
UT	**U**niversal **T**ime
WCRP	**W**orld **C**limate **R**esearch **P**rogramme
WMO	**W**orld **M**eteorological **O**rganization

α	extinction coefficient
α_{sca}	scattering coefficient
α_{abs}	absorption coefficient
α_g	absorption coefficient of a gas
α_m	extinction coefficient due to molecular scattering
α_p	extinction coefficient due to particle scattering
α_R	extinction coefficient due to Raman-scattering
β	backscatter coefficient
β_m	backscatter coefficient of molecular scattering
β_p	backscatter coefficient of particle scattering
β_R	backscatter coefficient of Raman-scattering
γ	temperature coefficient of the absorption cross section
γ_m	anisotropy of molecular polarizibility
γ_R	change of anisotropy of molecular polarizibility for Raman-scattering
δ	standard deviation
ε	energy of a molecular state
η	efficiency
η_{ant}	antenna loss factor
ν	wavenumber
ν_0	wavenumber of transmitted light
ν_s	wavenumber of scattered light
ν_R	wavenumber of a Raman-transition
ζ_V	parameter of the Voigt-function
λ	wavelength
ρ_n	number density
σ	absorption cross section
τ_L	laser pulse length
τ	optical depth
Δ	difference operator
Λ	ratio of wavelengths, $\Lambda = \lambda_1/\lambda_2$
$\Lambda(\nu, p, T)$	absorption line form
Ξ	correction term for the temperature dependence of absorption lines
Θ	angle in the scattering plane
Φ	azimuthal scattering angle
Ω	solid angle
$\Re$	real part of a complex number
$\mathcal{F}$	fraction of explained variance
$\mathcal{P}$	correlation coefficient

K.2 Appendix A

Derivation of the approximation for differential backscatter. The correction term for differential backscatter in equation (H.1) reads

$$[4] = \frac{1}{2\Delta\sigma}\frac{d}{dR}\ln\left(\frac{\beta_1}{\beta_2}\right) \tag{K.1}$$

$$= \frac{1}{2\Delta\sigma}\frac{d}{dR}\ln\left(\frac{\beta_{m,1}+\beta_{p,1}}{\beta_{m,2}+\beta_{p,2}}\right) \tag{K.2}$$

Using the abbreviations $\Lambda = \lambda_1/\lambda_2$ and assuming a power law with the Ångström coefficient k_β for the wavelength dependence of particle scattering we have:

$$\beta_{m,1} = \beta_{m,2}\cdot\Lambda^{-4} \qquad \beta_{p,1} = \beta_{p,2}\cdot\Lambda^{k_\beta}, \tag{K.3}$$

and hence

$$[4] = \frac{1}{2\Delta\sigma}\frac{d}{dR}\ln\left(\frac{\beta_{m,2}\cdot\Lambda^{-4}+\beta_{p,2}\cdot\Lambda^{k_\beta}}{\beta_{m,2}+\beta_{p,2}}\right), \tag{K.4}$$

$$= \frac{1}{2\Delta\sigma}\frac{d}{dR}\ln\left(\Lambda^{-4}\frac{\beta_{m,2}+\beta_{p,2}\cdot\Lambda^{4+k}}{\beta_{m,2}+\beta_{p,2}}\right), \tag{K.5}$$

$$= \frac{1}{2\Delta\sigma}\frac{d}{dR}\ln(S_{K,2}+(1-S_{K,2})\cdot\Lambda^{4+k_\beta}) \ . \tag{K.6}$$

For the wavelengths typically used we have $\Delta\lambda = \lambda_1 - \lambda_2 \ll \lambda_2$, and hence

$$\Lambda^{4+k_\beta} \approx 1+(4+k_\beta)\cdot\frac{\Delta\lambda}{\lambda_2}, \tag{K.7}$$

$$[4] \approx \frac{1}{2\Delta\sigma}\frac{d}{dR}\ln\left(S_{K,2}+(1-S_{K,2})\cdot\left(1+(4+k_\beta)\cdot\frac{\Delta\lambda}{\lambda_2}\right)\right) \ , \tag{K.8}$$

$$\approx \frac{1}{2\Delta\sigma}\frac{d}{dR}\ln\left(1+(4+k_\beta)\cdot\frac{\Delta\lambda}{\lambda_2}\cdot(1-S_{K,2})\right) \tag{K.9}$$

Since $(4 + k_\beta)\,\Delta\lambda/\lambda_2\,(1 - S_{K,2}) \ll 1$ and $\ln(1 + x) \approx x$ for $x \ll 1$ we have

$$[4] \approx \frac{1}{2\Delta\sigma}\frac{d}{dR}\ln\left(1 + (4 + k_\beta)\cdot\frac{\Delta\lambda}{\lambda_2}\right)\cdot(1 - S_{K,2}) \tag{K.10}$$

$$\approx \frac{1}{2\Delta\sigma}\frac{\Delta\lambda}{\lambda_2}(4 + k_\beta)\frac{d}{dR}S_{K,2} \tag{K.11}$$

This is the final expression for the approximation of the differential backscatter term in equation (H.1), which is very important for the evaluation of ozone lidar measurements.